Universität für Bodenkultur Wien
University of Natural Resources and Life Sciences, Vienna

Master Thesis

PROTOCOL DEVELOPMENT FOR THE PRODUCTION OF CELL-DERIVED CD4+, CCR5+ AND CXCR4+ T-CELL MIMICS

University of Natural Resources and Life Sciences, Vienna
Department of Nanobiotechnology
Institute for Synthetic Bioarchitectures
Head of Institute: Prof. Dr. Eva-Kathrin Ehmoser

Supervised by
Prof. Dr. Eva-Kathrin Ehmoser
Dr. Cherng-Wen Darren Tan

Submitted by
Yasmin Weiss

Vienna, March 2018

Acknowledgements

Darren, I want to thank you for your warm welcome at the department, for sharing your knowledge, skills and your fascination for science with me. I also want to thank Eva-Kathrin Ehmoser who made it possible to be part of the Synthetic Bioarchitectures group and Dietmar Pum who trained me at the TEM.

Thanks to all the people who made my time at the department special. Tanja, you have been an important study buddy and friend to me, kicking my ass whenever necessary.

Many thanks to my family, which is always there for me. Papa, thanks for your financial support that allowed me to focus on my studies. Also, without your suggestion I would have never thought of becoming a biotechnologist.

Patrick, without you the layout would have cost a lot of nerves and time. Thank you for being there whenever your help was needed.

Zu guter Letzt möchte ich Anni und Karli danken. Ihr seid in den letzten Jahren ein wichtiger Teil meines Lebens geworden. Immer interessiert und auf das Wohlergehen anderer bedacht. Anni, du hast für mein leibliches Wohl gesorgt und stehst mir auch sonst immer mit Rat und Tat zur Seite. Und Karli, dein Gesang am Morgen ist besser als jeder Wecker, um mit einem Lächeln in den Tag zu starten.

Kurzfassung

HIV infiziert menschliche Immunzellen um sich darin zu reproduzieren. Neue Viren können dann wiederum andere Zellen infizieren. Als Folge reduziert sich die Zahl der Immunzellen, die zur Bekämpfung von Pathogenen zur Verfügung stehen und die Entstehung von Sekundärinfektionen wird begünstigt. Dank antiretroviraler Medikamente ist HIV heute von einer tödlichen zu einer chronischen Erkrankung geworden. Trotzdem werden neue Therapiemethoden benötigt, da HIV rasch mutiert. Viren und HIV infizierte Zellen könnten jedoch zerstört werden, indem man mit Arzneimittel gefüllte Vesikel nutzt, die die primären Zielzellen von HIV – die T-Zellen – imitieren.

Im Rahmen dieser Arbeit wurden zwei Methoden untersucht um CD4+, CCR5+ und CXCR4+ T-Zell Modelle herzustellen. Die Detektion dieser Proteine erfolgte mittels Immunfärbung und Durchflusszytometrie. Es zeigte sich, dass die humane lymphoide Zelllinie A3R5.7 für meine Zwecke gut geeignet ist, da CD4, CCR5 und CXCR4 nachgewiesen wurden. Aus A3R5.7 Zellen wurden dann mittels Homogenisation und Extrusion 1-2 µm große Liposomen produziert und mit einem Transmissionselektronenmikroskop analysiert. Die Liposomen waren jedoch von uneinheitlicher Größe und in zu geringen Mengen vorhanden. Die Verwendung verschiedener Extruder oder Extrusionsmembranen konnte das Ergebnis nicht positiv beeinflussen. Weiters konnten CD4, CCR5 und CXCR4 in den von mir hergestellten Membranvesikeln nicht nachgewiesen werden. Aus diesen Gründen wurde eine alternative Methode getestet um T-Zell Modelle herzustellen, die osmotische Lyse. MilliQ-PI war ein geeigneter Lysepuffer, um 10-15 µm große lysierte Zellen zu produzieren und die Zielproteine CD4, CCR5 und CXCR4 konnten nachgewiesen werden.

Zukünftig könnten komplett synthetische T-Zell Modelle eingesetzt werden, um die Virenlast in infizierten Individuen zu reduzieren, wodurch das Immunsystem seine Funktion wieder aufnehmen könnte. Opportunistische Pathogene würden bekämpft und ein Ausbrechen der Krankheit könnte verhindert werden.

Schlüsselwörter: HIV, Liposom, T-Zell Modell, osmotische Lyse, CD4, CCR5, CXCR4

Abstract

HIV infects human immune cells in which it replicates. Newly synthesized virions are released and spread to infect other cells. That way, HIV infection reduces the amount of immune cells available to destroy pathogens. This promotes the occurrence of secondary infections that will lead to death at some point. Current antiretroviral therapeutics make HIV a manageable chronic disease. However, new therapeutic methods are needed as HIV mutates quickly. In this thesis, it is proposed to use mimics of HIV's main target cells – T-cells – as targeted drug delivery vesicles to destroy virions and HIV infected cells.

Two methods were investigated for the production of cell-derived CD4+, CCR5+ and CXCR4+ T-cell mimics. Detection of these proteins was performed using immunostaining and flow cytometry. It was demonstrated that the human lymphoid cell line A3R5.7 was well-suited for the production of T-cell mimics as 81% of the cells were tested positive for CD4, 56% for CCR5 and 100% for CXCR4. Two kinds of T-cell mimics, liposomes and ghost cells, were fabricated from A3R5.7 cells. Homogenization and extrusion were used for the production of 1-2 µm A3R5.7-derived liposomes. TEM characterization of these samples showed that liposomes were present but only in low amounts and not of uniform size. The use of different extruders or extrusion membranes did not alter the result. Furthermore, CD4, CCR5 and CXCR4 could not be detected in these liposomes. Thus, the approach was changed and ghost cells were produced *via* osmotic cell lysis instead. Osmotic lysis was observed using a fluorescence microscope along with Calcein-AM staining of the A3R5.7 cytoplasm. MilliQ-PI seemed to be a suitable lysis buffer, as ghost cells of 10-15 µm were obtained. Surface protein CD4 was detected in 36% of A3R5.7 ghost cells, CCR5 in 35% and CXCR4 in 73%.

In future, fully synthetic T-cell mimics could be used to reduce the viral load and allow the immune system to restore its functions. In this way, opportunistic pathogens could be effectively combated and a progress to AIDS might be prevented.

Keywords: HIV, liposome, T-cell mimic, osmotic lysis, CD4, CCR5, CXCR4

Contents

1 Introduction

Viruses are not able to replicate by themselves. Instead, they infect host cells and use their replication machinery. CD4, CCR5 and CXCR4 are surface membrane proteins that can be found in human immune cells. Human immunodeficiency virus (HIV), the virus that causes the acquired immune deficiency syndrome (AIDS), uses these receptors to invade the human immune system. This invasion leads to a decline in CD4+ T-cells, resulting in a weakened immune system. This promotes secondary infections that might lead to death. Antiretroviral treatment for HIV infections is available but can cause severe side effects. Furthermore, the highly mutable HIV would eventually develop resistance to such treatment. This necessitates the development of new HIV therapeutics. This thesis deals with the possibility to treat HIV infection using proteoliposomes loaded with HIV-destroying compounds. These should decrease the viral load and help the immune system to recover and withstand opportunistic pathogens.

1.1 The host membrane proteins CD4, CCR5 and CXCR4 are used for HIV entry

CD4, CCR5 and CXCR4 are transmembrane proteins (see Fig. 1). CD4 (cluster of differentiation 4) is a member of the immunoglobulin superfamily. It spans the membrane once and has four immunoglobulin domains on the extracellular side. These immunoglobulin domains allow interaction with MHC class II molecules that are present on antigen-presenting cells. This interaction is necessary for CD4+ T-cells to be activated by antigen presenting cells, e.g. dendritic cells (Alberts *et al.*, 2015, p. 1338).

However, HIV makes use of CD4 as the primary receptor to infect CD4+ cells. Along with CD4, a co-receptor is needed by HIV that can either be CCR5 or CXCR4 (Fig. 1).

CXCR4 (CXC chemokine receptor type 4) and CCR5 (CC chemokine receptor type 5) belong to the superfamily of seven-transmembrane-domain G-protein coupled receptors. Their task is to detect external signals and transmit them into the cell. G-protein coupled receptors are usually activated by chemokines, low molecular weight proteins. Chemokine binding leads to a conformational change of the receptor and allows it to activate an intracellular G-protein by the exchange of its GDP to GTP. The GTP-bound protein is then able to transmit extracellular signals into the cell by activating or inhibiting other proteins (Alkhatib, 2009). Rottman et al. demonstrated that CCR5 is expressed by bone-marrow-derived cells, including monocytes, macrophages and a subpopulation of lymphocytes (Rottman *et al.*, 1997). CXCR4 is expressed on different leukocyte subsets, hematopoietic progenitor cells and also on non-hematopoietic cells (Murdoch, 2000).

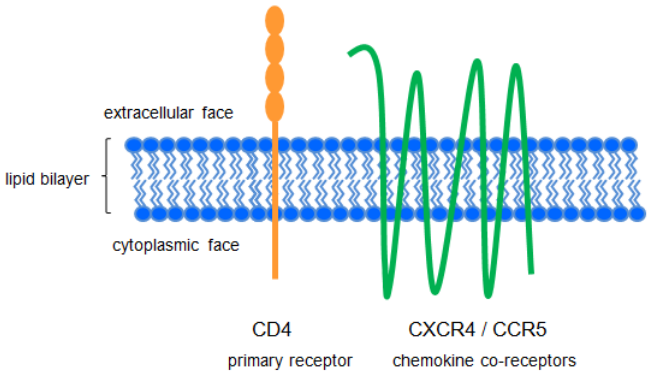

Fig. 1: HIV uses CD4 as the main entry receptor along with one of the two chemokine receptors, CCR5 and CXCR4. CD4, CCR5 and CXCR4 are embedded in the lipid bilayer membrane that forms the cell boundary.

1.2 HIV virion structure

As shown in Fig. 2, the mature HIV virion, as it is found in the blood of infected individuals, consists of two single-stranded RNA molecules that are protected by a protein shell. This cone-shaped protein shell, or capsid, is made up of capsid proteins (CA or p24 proteins). In addition to the viral genome, the capsid shelters all proteins necessary for genome replication, e.g. reverse transcriptase (RT), viral protease, integrase and nucleocapsid proteins (NC or p7 proteins). The capsid itself is surrounded by matrix proteins (MA or p17 proteins) that are associated with the inner side of a lipid membrane. This lipid bilayer membrane originates from the host cell. Therefore, it includes host cell proteins as well as the viral envelope proteins gp41 and gp120 that are essential for the infection of new CD4+ host cells (Sierra, Kupfer and Kaiser, 2005).

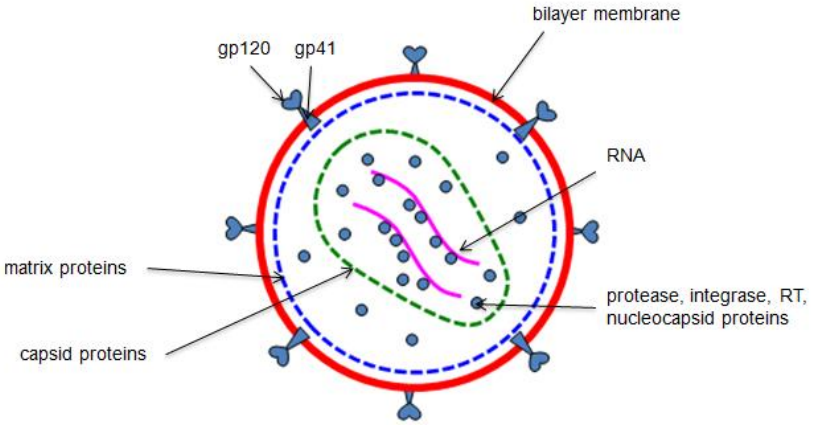

Fig. 2: Schematic representation of HIV virion. The virion consists of a lipid bilayer derived from its host cell. Beside host cell proteins, the viral envelope protein gp120/41 is present in this membrane. Virion structure is maintained by matrix and capsid proteins. The capsid

houses the viral RNA and proteins for viral replication. RT: reverse transcriptase. Drawing kindly provided by Dr. Cherng-Wen Darren Tan.

1.3 HIV life cycle

1.3.1 HIV enters a host cell

As shown in Fig. 3 (step 1-4), virus entry into host cells is mediated by viral surface proteins and host cell receptors. In case of HIV, the gp120 domain of HIV's envelope protein interacts with the host CD4 surface receptor. This binding event causes a conformational change in gp120, exposing the viral chemokine receptor binding domain that can bind either CXCR4 or CCR5 on host cells. Binding of the appropriate receptor and co-receptor initiates the fusion of viral and cellular membranes. The capsid is released into the cytoplasm. Cellular factors are involved in capsid disassembly to expose the viral genome and its associated proteins (Sierra, Kupfer and Kaiser, 2005).

1.3.2 HIV genome inserts into host cell DNA

Immediately the viral single-stranded RNA genome is reverse transcribed into proviral double-stranded DNA by the viral reverse transcriptase. Viral DNA is transported into the host cell nucleus and inserted into the host genome by the viral integrase enzyme (Sierra, Kupfer and Kaiser, 2005) (Fig. 3, step 5-6).

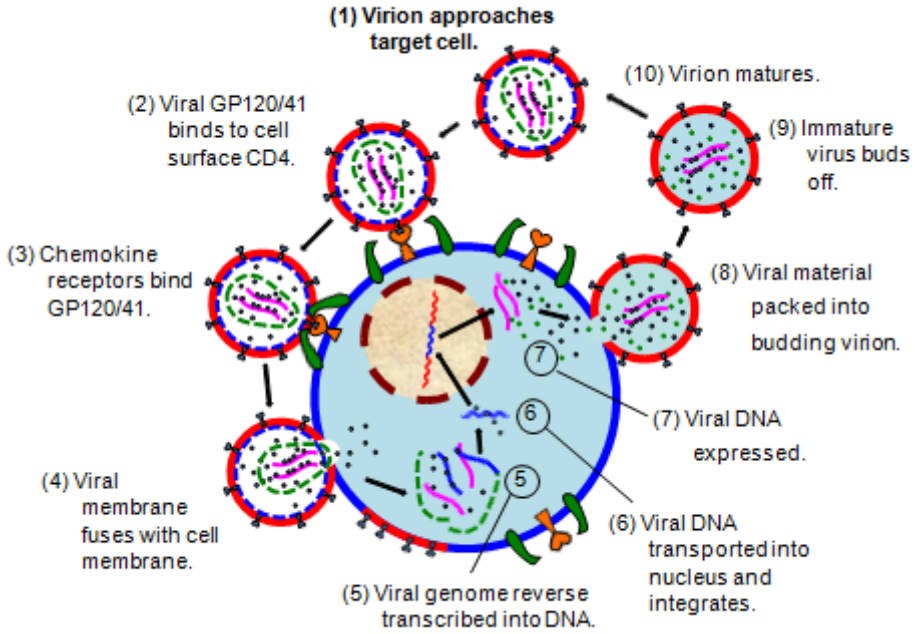

Fig. 3: The HIV life cycle starts with the fusion of virus and target cell and ends with the release of new virions. Drawing kindly provided by Dr. Cherng-Wen Darren Tan.

1.3.3 Viral gene expression and virion production

When activated, cellular gene expression machinery is used to transcribe the integrated proviral DNA into one long pre-mRNA strand (Sierra, Kupfer and Kaiser, 2005). The viral pre-mRNA needs to be further modified by splicing as only fully spliced mRNAs, without introns, can pass through the nuclear pores. This is due to the cellular quality control system that allows only completely processed mRNAs to leave the nucleus, but degrades damaged or incompletely processed mRNAs and introns locally using exonucleases.

HIV now faces a problem. Completely spliced mRNAs are translated into regulatory proteins but not into structural or envelope proteins, which are translated from incompletely spliced mRNAs. In addition, unspliced intact RNA is used as viral genomic RNA and is needed for the production of new virions. Thus, HIV needs to overcome the cellular quality control system to enable the transport of intron-containing RNA to the cytoplasm. This is achieved by the viral “rev protein”. “Rev” is one of the early translated viral regulatory proteins. When sufficient amounts of “rev” have accumulated, it binds to a certain intron sequence on the mRNA and guides the intron-including mRNA through the nuclear pore. This allows the transport of incompletely spliced mRNAs into the cytoplasm and the subsequent translation of all HIV proteins (Alberts *et al.*, 2015, p. 419-421) *(*Fig. 3, step 7).

1.3.3.1 Viral envelope glycoprotein

HIV mRNAs encoding the 160 kDa envelope glycoprotein (gp160) are first translated at the rough endoplasmatic reticulum and then glycosylated in the golgi apparatus following the standard cellular pathway of membrane protein synthesis. After glycosylation, gp160 is cleaved into the gp41 transmembrane protein and the soluble gp120 protein by cellular proteases. Both proteins are transported to the plasma membrane using vesicular transport and stay bound via non-covalent interactions.

1.3.3.2 Structural proteins and viral enzymes

The viral “group-specific antigen” (*gag*) mRNA is translated by free ribosomes in the cytoplasm into the 55 kDa long precursor “gag” polyprotein (p55). “Gag-pol” polyprotein results from a (-1) shift of the ribosome during translation. Thereby, the stop codon ending the “gag” sequence is omitted and the “gag-pol” fusion protein is generated (see Fig. 4). The “gag” polyprotein codes for the structural matrix, capsid and nucleocapsid proteins, whereas the “pol” polyprotein codes for viral enzymes, such as protease, integrase and reverse transcriptase.

After translation, “gag” and “gag-pol” polyptroteins are attached to specialized microdomains at the plasma membrane, using their myristoylated amino-terminal domains as lipid anchors.

In this way, matrix proteins are coupled to the inside of the plasma membrane. In addition to interactions between matrix proteins, interactions between capsid proteins also develop to form a robust bud structure. Nucleocapsid proteins then capture intron-containing RNA molecules that will function as the viral genome in prospective virions (Sundquist and Kräusslich, 2012).

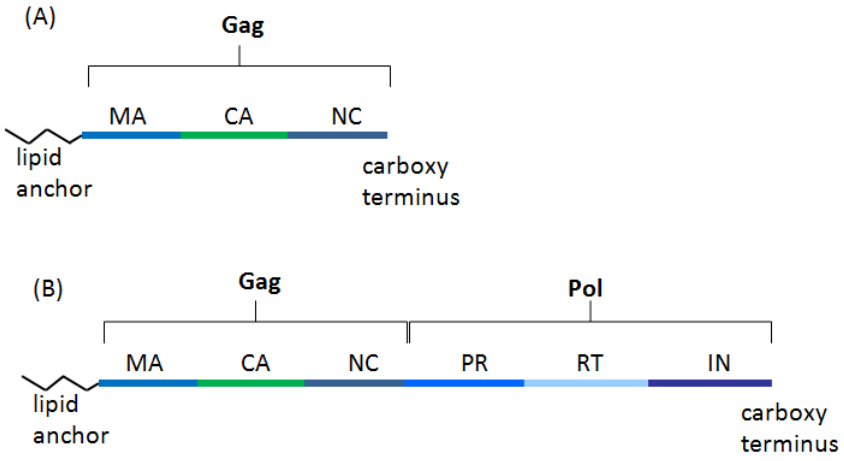

Fig. 4: (A) "Gag" polyprotein codes for structural proteins that form the virus core: matrix protein (MA), capsid protein (CA) and nucleocapsid protein (NC). (B) "Pol" polyprotein codes for viral enzymes: protease (PR), reverse transcriptase (RT) and integrase (IN).

1.3.4 Viral components are packed and virus is released

Now that all viral components are assembled, the immature virus is released from the host cell. Budding activates the viral protease that starts to cleave "gag" and "gag-pol" polyproteins into single proteins. Protease activity initiates the rearrangement of proteins and capsid formation. As soon as the virion finishes its rearrangement it becomes a mature virion and is ready to infect new host cells (Sundquist and Kräusslich, 2012) *(*Fig. 3, step 8-10*)*.

1.4 HIV infects CD4+ cells

HIV uses CD4 as the primary receptor to infect host cells. T-cells, dendritic cells and macrophages are typical cells that get infected by HIV. Early in infection, mainly CCR5-using strains infect macrophages that are commonly found in mucosal tissues. These strains are known as R5-tropic or M-tropic HIV strains. Later in infection, CXCR4 is used as the main co-receptor instead. These strains are called X4 strains or T-tropic because they preferably infect T-cells. Dual-tropic (R5X4) viruses can use both receptors. Tropism is caused by differences in the HIV gp120 sequence, as this sequence is responsible for co-receptor binding (Dimmock, Easton and Leppard, 2016, p 338-339).

1.5 CD4+ cells and the human immune system

All CD4+ cells that also express at least one of the two chemokine receptors, CCR5 and CXCR4, can serve as HIV targets. These cells are found in the human immune system.

All human immune cells are generated in the bone marrow from a common pluripotent stem cell. This precursor cell divides and differentiates into cells with different functions. Red blood cells are responsible for the transport of oxygen and carbon dioxide in the blood. In contrast, white blood cells, also called leukocytes, are able to leave the blood vessels to destroy pathogens and remove aged or degenerated cells and cellular debris in the human body. Leukocytes can be divided into three groups: granulocytes, monocytes and lymphocytes.

Granulocytes and monocytes produce the innate cellular immune response. They are phagocytes and they mediate inflammatory reactions through the release of cytokines. Granulocytes unspecifically destroy microorganisms like bacteria, and larger organisms like parasites, through phagocytosis or through the secretion of toxic substances. Monocytes develop into macrophages when they leave the blood vessels. Monocyte precursors can also give rise to dendritic cells. Dendritic cells are also capable of phagocytosis but their major function is the uptake of foreign antigens and their presentation to lymphocytes (Alberts *et al.*, 2015, p. 1239-1240).

Lymphocytes give adaptive immune responses. While humoral immunity is mediated by antibody-secreting B lymphocytes, cellular immunity is maintained by T lymphocytes, also called T-cells.

After T-cell activation by antigen presenting cells, such as dendritic cells, macrophages or B cells in the lymph nodes, T-cells differentiate into either CD4+ helper T-cells, or CD8+ cytotoxic T-cells. CD8+ T-cells directly destroy infected cells. In contrast, CD4+ helper T-cells stimulate and coordinate other immune cells *via* the secretion of cytokines (Luckheeram *et al.*, 2012). In this way, helper T-cells do not directly eliminate invading microorganisms but they activate those cells that are capable of defending the body. For example, CD4+ helper T-cell cytokines promote antibody secretion by activating B cells. At the same time, they activate cells of the innate immune system, like macrophages, and stimulate them to destroy captured pathogens. Cytokines also activate cytotoxic T-cells to kill infected target cells and stimulate non-immune cells to produce pro-inflammatory cytokines (Alberts *et al.*, 2015, p. 1326, 1335-1336).

1.6 Dendritic cells serve as HIV transport vehicles

Immature dendritic cells constantly scan their environment for pathogens or their antigens. Dendritic cells can be found in the blood and in mucosal membranes such as the vagina. It is for this reason, that dendritic cells are the first cells of the immune system that encounters

HIV, as HIV can be transmitted through sexual contact or blood (Maartens, Celum and Lewin, 2014).

When a dendritic cell recognises a pathogen via its pattern recognition receptor, the pathogen is endocytosed. The loaded dendritic cell then undergoes a series of maturation events and migrates toward lymphoid tissues. The internalized pathogen is degraded into peptides that are transported to the cell surface of the dendritic cell and presented as peptide-MHC Class II complexes to CD4+ T-cells waiting in the lymph nodes. Binding of the T-cell receptor and the T-cell's co-receptor, CD4, to the peptide-MHC Class II complex activates the T-cell and initiates adaptive immune responses directed against the presented antigen fragment (McDonald, 2010).

Dendritic cells express the primary HIV receptor, CD4, and both CCR5 and CXCR4 chemokine co-receptors in low levels. Thus, HIV is able to enter and replicate in dendritic cells and to produce new virions that are released to infect other cells (*cis*-infection). But the replication-dependent *cis*-infection is inefficient compared to HIV infection of macrophages or CD4+ T-cells (Coleman, St Gelais and Wu, 2013).

Instead, HIV uses dendritic cells as transport vehicles that carry it to the lymph nodes where it can easily infect CD4+ T-cells. For that purpose, HIV is packed into intracellular compartments that stay close to the dendritic cell surface (McDonald, 2010).

That way, HIV escapes the degradation pathway and can instead be: i) directly transferred via a virological synapse into a CD4+ T-cell in very close contact with the infected dendritic cell; or ii) released into the extracellular environment via the exosome secretion pathway, where it may infect adjacent cells (Coleman, St Gelais and Wu, 2013). As these infection modes are replication-independent, they are called *trans*-infections (McDonald, 2010).

1.7 Effect of the loss of CD4+ helper T-cells

Helper T-cells are CD4+, CCR5+ and CXCR4+ and the major targets of HIV infection. Infection of helper T-cells results in massive T-cell loss because cells are lysed in the course of new virion production. Infected cells may also be attacked by phagocytes or cytotoxic T-cells (Maartens, Celum and Lewin, 2014). Usually, syncytia are formed from infected cells. Syncytia form when adjacent cells fuse into one giant cell that contains multiple nuclei. HIV can induce syncytia formation because infected cells display the HIV gp120 protein on their surface. These interact with CD4 on other T-cells resulting in cell fusion. These giant cells then lyse and further decrease the T-cell count (Cann, 2012, p. 217-219). HIV infection reduces the amount of immune cells that can fight HIV and other pathogens, which finally leads to death if left untreated.

1.8 Untreated HIV infection progresses to AIDS

HIV can be transmitted from person to person through blood and other body fluids, or from mother to child. The acute HIV infection may last for days or months and can be accompanied by flu-like symptoms.

This stage is followed by an asymptomatic chronic HIV infection. Co-infections can also occur when immune cells release pro-inflammatory cytokines upon coming across pathogens. This allows other viruses to invade the human body by enhancing the permeability of the affected tissue (Maartens, Celum and Lewin, 2014). Arising co-infections also need to be combated. Years to decades later, the body may start to suffer from opportunistic infections that result in rapid weight loss or chronic diarrhea. This is when the third, and final, stage is reached. Diagnosis of acquired immune deficiency syndrome (AIDS) indicates that the HIV infection has already reached this last stage.

If this stage is left untreated, death within a couple of years is unavoidable because the immune system is overwhelmed by infections eventually (U.S. Department of Health and Human Services, 2016).

1.9 Antiretroviral therapeutics and their limits

Current antiviral therapy makes HIV a manageable chronic disease. Highly active anti-retroviral therapy (HAART) is a combination of three different compounds that attack at least two different processes in the HIV life cycle. The objective of HAART is to reduce the viral load in human plasma to an undetectable level and to restore immune functions. Nevertheless, HIV cannot be completely removed as it hides, as proviral DNA, in resting memory T-cells or other immune cells where it forms reservoirs of latent viruses.

HAART drugs aim at blocking receptors necessary for virus entry or inhibiting viral enzymes. HAART drugs currently used include reverse transcriptase inhibitors that inhibit virus replication. An example is azidothymidine (AZT), the first anti-HIV drug that was approved for human treatment. Azidothymidine has a high affinity to the reverse transcriptase that reverse-transcribes the viral RNA into pro-viral DNA. The incorporation of azidothymidine, a nucleoside analogue that lacks a hydroxyl group for phosphodiester bond formation, terminates the growing DNA chain.

Entry inhibitors target the cell receptors. The CCR5 inhibitor Maraviroc, for example, binds to CCR5 and thus blocks the co-receptor for HIV binding. Integrase or protease inhibitors are also available that inhibit proviral DNA integration into the host genome, and the formation of new virions, respectively (Danial and Klok, 2015).

Although HAART is available, not all people can afford it as it is very expensive. Application is also difficult as some drugs need to be applied subcutaneously. Furthermore, HAART can have severe side effects. Organs or nerves could be damaged and diabetes or heart diseases may develop. Also long-term effects are insufficiently studied (Danial and Klok, 2015). When HAART therapeutics are not taken according to instructions, new viruses can be produced from the reservoirs that might be resistant to the drugs. Furthermore, anti-retroviral drugs need to be taken for one's entire life. This means, that therapy can be needed for decades, giving HIV time to develop drug resistant mutants (Dimmock, Easton and Leppard, 2016, p. 343-345). Drug-resistant pathogens are an everlasting problem and new drugs are desperately needed.

A vaccine against HIV has not yet been developed as HIV mutates very quickly. A possible vaccine might be developed from the viral envelope protein gp120/41. However, due to the high error rate of the reverse transcriptase, the gp120 antigen is constantly changing. This means that any antibody raised against the vaccine might not recognise the mutated envelope protein (Dimmock, Easton and Leppard, 2016, p. 343-345).

1.10 New therapeutic methods are needed

This thesis deals with the application of T-cell mimics targeted against the viral envelope protein gp120/41. In this way, T-cell mimics would compete with actual T-cells for interaction with HIV virions. These T-cell mimics should also be able to fuse with HIV virions, just as T-cells and macrophages would. Upon fusion, HIV will not be able to replicate in T-cell mimics as the cell machinery necessary for replication is missing. Furthermore, T-cell mimics could be filled with enzymes, such as proteases and nucleases that would degrade the viral components (Fig. 5). T-cell mimics could continue to fuse with HIV virions until the accumulation of degradation products results in mimic lysis. Although, degraded viral components would be released into the blood, these nucleic and amino acids should not be infectious any more as they are no longer protected by the virion structure. Instead, nucleic and amino acids could serve as nutrients for the body. Released nucleases should not cause any harm, as nucleases are always present in the blood. However, released proteases might be a cause of concern as they might also degrade human proteins. To protect human proteins from being degraded by released proteases, the protease trypsin could be used, because trypsin would be inactivated by the trypsin inhibitor α-antitrypsin that is present in the blood plasma.

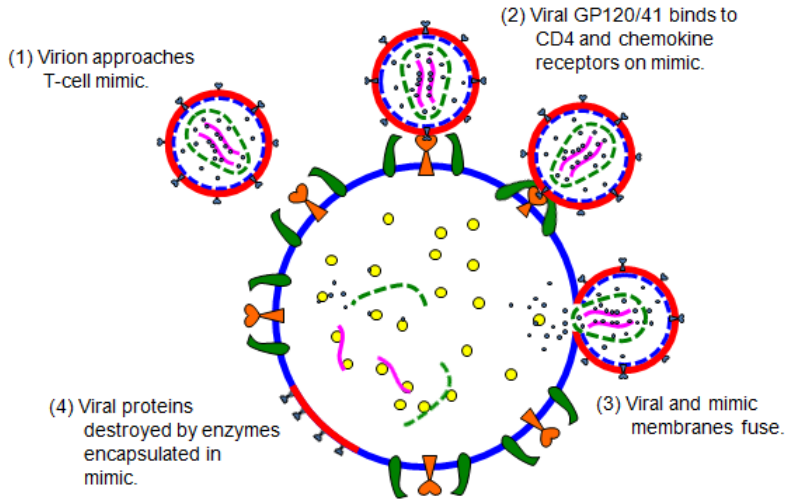

Fig. 5: CD4+, CCR5+ and CXCR4+ T-cell mimics should be able to fuse with HIV and destroy it. Drawing kindly provided by Dr. Cherng-Wen Darren Tan.

This mechanism can also be applied to infected cells, as they also present viral proteins on their cell surface. This is especially so immediately following HIV entry and during the assembly of new virions. Again, viral gp120/41 will serve as the fusion partner for T-cell mimics. After fusion, the nucleases and proteases entrapped in the T-cell mimic would destroy cellular DNA and proteins, leading to cell death (Fig. 6).

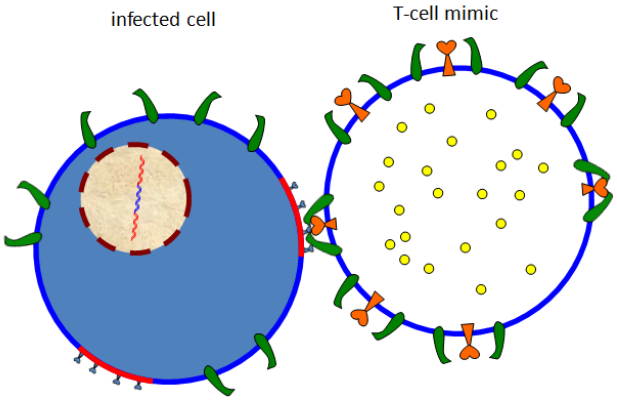

Fig. 6: A T-cell mimic might also capture and fuse with an infected cell via the latter's surface gp120/41. Drawing kindly provided by Dr. Cherng-Wen Darren Tan.

This would reduce the viral load in infected individuals and allow recovery of the human immune system. As a consequence, this would lower the occurrence of secondary infections and the HIV infection would less likely develop into AIDS.

1.10.1 T-cell mimics need to have similar properties as T-cells

T-cells consist of a bilayered membrane that separates the cell interior from the exterior. The membrane is mainly made out of phospholipids, amphiphilic molecules that can self-assemble into different structures, such as micelles, liposomes or layers (Alberts *et al.*, 2015, p. 9) (Fig. 7).

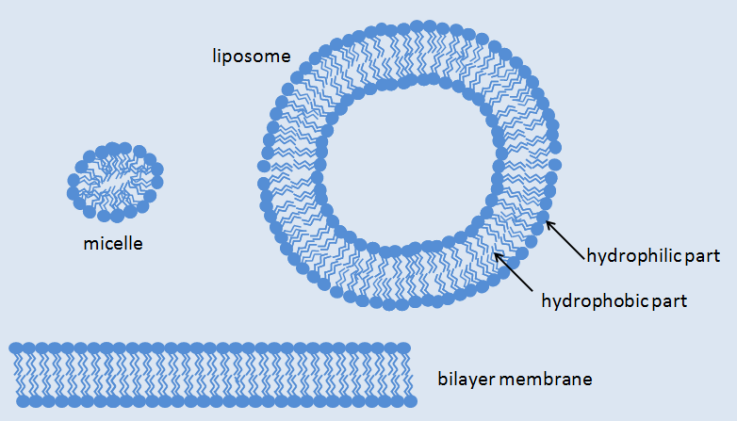

Fig. 7: Schematic drawing of lipid structures in an aqueous solution. Lipids self-assemble into micelles, liposomes or bilayers. Self-assembly in aqueous solutions is caused by the amphiphilic character of phospholipids. Each molecule consists of a hydrophilic and a hydrophobic part.

Proteins are embedded in or attached to this lipid bilayer. These proteins are, for example, responsible for cell communication or nutrient transport. In case of T-cells, the membrane-spanning CD4 receptor is needed for T-cell activation, and the chemokine receptors for signal transmission.

The aim was to generate T-cell mimics that are able to fuse with HIV virions or infected cells. The fusion is based on an interaction between the viral gp120/41 molecule and the T-cell receptors CD4, CCR5 and/or CXCR4. Therefore the T-cell mimic needs, at least, to consist of a lipid bilayer membrane that mimics the T-cell membrane, supplemented with the necessary proteins, CD4, CCR5 and CXCR4.

1.10.2 Producing T-cell mimics synthetically

T-cell mimics suitable for gp120/41 fusion can be produced from lipid vesicles, or liposomes, carrying the T-cell surface markers, CD4, CCR5 and CXCR4 on their surface. Liposomes with incorporated proteins are called proteoliposomes. CD4+ proteoliposomes could be made synthetically using a cell-free extract-based protein synthesis system to synthesize CD4, in the presence of an artificial membrane for protein insertion (Kalender, 2016).

However, cell-free protein synthesis and membrane integration of the resultant protein is not trivial. Reliable protocols for synthesizing and detecting proteins need to be developed. Besides, correct membrane protein folding is a complex process that will only take place in the presence of a membrane. Furthermore, membrane insertion might result in proteins which are wrongly oriented, where intracellular domains face outwards. Liposomes with wrongly oriented proteins would not be able to fuse with their target cells.

1.10.3 Producing T-cell mimics from cells

An attractive alternative is to produce CD4+, CCR5+ and CXCR4+ liposomes from appropriate cells. These liposomes can then be tested in assays to see if they will fuse with an appropriate target. There are several possibilities for the production of liposomes from live cells, such as homogenization and extrusion, osmotic cell lysis, cytochalasin B treatment or the use of optical tweezers.

Bronshtein *et al.* demonstrated the effectiveness of homogenization and extrusion for the production of small cell-derived liposomes. They homogenized cells with high shear forces, separated the membrane fragments and extruded them to produce liposomes of about 100-200 nm (Bronshtein *et al.*, 2011). Structures of 10 – 20 µm can be obtained by osmotic cytolysis. When cells are brought into contact with ultrapure water the cell membrane ruptures because it cannot withstand the osmotic pressure. The cell content is released into the environment, leaving the cell membrane behind that might reseal into a ghost cell (Alberts *et al.*, 2004, p. 725-726). In contrast to the treatment with ultrapure water that causes osmotic cell lysis, Grasso *et al.* treated cells with the mycotoxin cytochalasin B to destabilize the interaction between the cytoskeleton and the plasma membrane. This resulted in the formation of vesicle-like structures on the cell surface that could be sheared off by vortex-mixing or could be pulled off with an optical tweezer (Grasso *et al.*, 2013).

1.11 Developing a robust and reliable T-cell mimic production protocol

The objective of this master's thesis is the development of a robust and reliable protocol for the production, characterization and purification of CD4+, CCR5+ and CXCR4+ cell-derived proteoliposomes, to serve as T-cell mimics. The aim is for these mimics, possibly loaded with drugs or other substances, to be able to fuse with TF228.1.16 cells. TF228.1.16 express the uncleaved gp120/41 protein (gp160) necessary for gp120/CD4 interactions, and will be a model for HIV in my work. In addition, gp120/41+ liposomes will be produced that will serve as a negative control in experiments.

The selected working material had to be carefully characterized before the proteoliposome production could start. To do this, the characterization of cell lines, and the proteoliposomes

produced from them, was carried out using imaging techniques as well as immunostaining and flow cytometry.

Initial attempts at proteoliposome fabrication were based on cell homogenization and extrusion, as a promising protocol had already been developed for this in our laboratory. As the proteoliposomes produced this way were difficult to purify and characterize, an alternative fabrication technique involving osmotic cell lysis was developed.

In the process of developing these protocols, assays were developed for quality control following critical steps during T-cell mimic fabrication. This allowed the tracking of all important processes and to eliminate errors quickly.

1.11.1 Selection of materials

The methods of T-cell mimic production explored in this thesis use cells as a starting material. As such, it was critical that the cells were of the required quality. To ensure this, quality tests, including optical methods like phase contrast microscopy as well as analytical techniques like immunostaining and flow cytometry for the detection of surface proteins in their native conformation, were an essential part of each protocol.

For the production of CD4+, CCR5+ and CXCR4+ liposomes, two human lymphoid cell lines were investigated for the presence of these proteins. MOLT4/CCR5 cells purportedly express CD4 (Baba *et al.*, 2000) while A3R5.7 expresses CD4 and CXCR4 (McLinden *et al.*, 2013). Both cell lines are also engineered to express CCR5 under geneticin (G418) selection.

Based on immunostaining and flow cytometry results, I decided to use A3R5.7 cells for the production of T-cell mimics, as they were tested positive for CD4, CCR5 and CXCR4. This result could not be achieved with MOLT4/CCR5 cells, as the expression of CD4 and CCR5 was non-existent in these cells.

For the production of gp160+ liposomes, the CHO-WT cell line was investigated, The CHO-WT cell line purportedly expresses HIV gp160 on its surface but does not express CD4, CCR5 or CXCR4. However, CHO-WT cells grow as adherent monolayers while A3R5.7 cells grow in suspension culture. Therefore, TF2289.1.16 cells were tested as an appropriate alternative to CHO-WT cells, as TF228.1.16 cells also grow in suspension culture. The TF228.1.16 cell line is a Burkitt's lymphoma cell line that was genetically modified in 1993 to stably express the entire uncleaved HIV-1 envelope protein gp160. TF228.1.16 was used as a model for HIV, as well as a reference for A3R5.7 and MOLT4/CCR5 in all my experiments. In this way, TF228.1.16 serves as virus-free system that allowed for investigation of the HIV envelope protein and its interactions with other cells (Jonak *et al.*, 1993).

1.11.2 T-cell mimic fabrication - homogenization and extrusion

A paper from Bronshtein *et al.* that described the fabrication of cell-derived liposomes from non-human CD4+ CCR5+ Cf2Th/CCR5(C9) cells, using homogenization and extrusion, suggested that this might be a suitable method for producing my T-cell mimics.

Bronshtein *et al.* demonstrated that CD4+ CCR5+ liposomes produced this way, and filled with EDTA, were able to fuse with gp120+ target cells. Fusion led to the release of cytotoxic EDTA into the targets, leading finally to cell death. They also pointed out that these liposomes could be used as targeted drug delivery systems for HIV-infected cells (Bronshtein *et al.*, 2011).

When I produced liposomes, homogenization and extrusion did not result in a high liposome yield, but in the formation of aggregates. Furthermore, liposome purification was difficult, altnough necessary for the detection of target surface proteins by immunostaining and flow cytometry. Centrifugation, bead encapsulation and Exo-spin^{TM} Exosome Purification Kit treatment were used to harvest the liposomes. The Exo-spin^{TM} Exosome Purification Kit recovered most of the membrane material compared to the other methods and was thus used for immunostaining. But, components of the kit caused the fluorescently-labelled anti-CD4 antibodies, that were used for immunostaining, to bind non-specifically to the liposomes. Moreover, aggregation of membrane material could not be reduced by applying higher extrusion forces. As a consequence, mainly aggregates were subject to immunostaining and not liposomes, resulting in misleading data.

Because this method did not produce sufficient liposomes for subsequent immunostaining, enrichment and further processing, it was decided to explore an alternative method of T-cell mimic production. Hence, osmotic cell lysis was employed.

1.11.3 T-cell mimic fabrication - osmotic cytolysis

Osmotic cell lysis, a method of emptying cells of cytoplasmic material, has proven successful for the production of ghost cells from red blood cells. The results are an empty sac comprising the red blood cell membrane with its membrane proteins intact - essentially a proteoliposome. Although red and white blood cells have different physical characteristics, I thought that osmotic cytolysis of white blood cells may be able to provide us with similar proteoliposomes.

Cytolysis occurs when cells are exposed to media with a low salt concentration, such as deionized water. As the salt concentration inside and outside the cells differ, the cells would actively pump ions from the inside to the outside to re-establish the salt concentration balance. In addition, water diffuses into the cells, whereupon they swell and finally burst, releasing their content into the environment. The ruptured plasma membrane then appears

to reassemble, resulting in cell-like structures described as ghost cells. Such ghost cells retain their cell surface proteins (Alberts *et al.*, 2004, p. 725-726).

I lysed A3R5.7 and TF228.1.16 cells by exposing them to ultrapure water (MilliQ). To minimise the loss of membrane proteins caused by endogenous proteases released during lysis, the ultrapure water was supplemented with protease inhibitors (PI) to reduce protease activity. This MilliQ-PI lysis buffer was used in all of my experiments. I tested different lysis conditions, such as stationary lysis or gentle agitation by shaking or stirring. Successful lysis was determined using phase contrast microscopy. Live cells were smaller compared to ghost cells, had a better contrast against the background and a peripheral glow, while ghost cells looked dark and flat and were bigger.

The development of the lysis protocol was challenging, because aggregate formation and, as a consequence, the loss of ghost cells was observed during lysis. Aggregate formation was observed during stationary as well as during agitated lysis. However, aggregate formation could be reduced by the addition of FBS to a final concentration of 5% (v/v) FBS in MilliQ-PI lysis buffer directly after lysis was performed. It was concluded that the ghost cells tended to collapse upon prolonged exposure to MIlliQ-PI lysis buffer. Therefore, it was decided that a stirred lysis, directly followed by the addition of FBS, worked best compared to stationary lysis or the use of a shaker. Immunostaining and flow cytometry of the ghost cells demonstrated the presence of CD4, CCR5 and CXCR4, confirming that the cell surface proteins could be retained during osmotic cell lysis.

To summarise, osmotic cytolysis appears to be a promising method for producing T-cell mimics. The lysed cells have proven easy to handle and much easier to characterize than liposomes, due to their greater size. Future work will focus on the optimization of the osmotic cytolysis protocol.

2 Material and Methods

2.1 Cultivation of cells

The human lymphoid cell lines A3R5.7, MOLT4/CCR5 and TF228.1.16 were provided by the NIH AIDS Reagent Program. This program offers reagents, free of material charge, to registered researchers working on AIDS therapeutics and vaccine development. The A3R5.7 cell line was obtained from the NIH AIDS Reagent Program, Division of AIDS, NIAID, NIH: Cat#12386, A3R5.7 from Dr. Robert McLinden (McLinden *et al.*, 2013). The MOLT4/CCR5 cell line was obtained from the NIH AIDS Reagent Program, NIAID, NIH: MOLT-4/CCR5 from Dr. Masanori Baba, Dr. Hiroshi Miyake, Dr. Yuji Iizawa (Baba *et al.*, 2000).

A3R5.7 and MOLT4/CCR5 cells were cultured in Roswell Park Memorial Institute (RPMI) 1640 Medium supplemented with 10% fetal bovine serum (FBS), 1% L-Glutamine, and optionally with 1 mg/mL G418 (geneticin). The cells were cultured in suspension in T-75 flasks at a maximum volume of 20 mL and subcultured every three to four days at a ratio of 1:20.

The TF228.1.16 cell line was obtained from the NIH AIDS Reagent Program, Division of AIDS, NIAID, NIH: TF228.1.16 from Drs. Zdenka Jonak and Steve Trulli (Jonak *et al.*, 1993). The cells were cultured in Dulbecco's Modified Eagle's Medium (DMEM) supplemented with 10% FBS and 1% L-Glutamine. These cells were similarly cultured in suspension in T-75 flasks and subcultured every three to four days at a ratio of 1:20.

The mammalian chinese hamster ovary (CHO) cell lines, CHO-WT and CHO-EE, were cultured and kindly provided by Belinda Angjeli. CHO-WT expresses HIV gp160 on its surface, while CHO-EE does not, making them appropriate references or alternatives to TF228.1.16. Neither cell line expresses CD4, CCR5 nor CXCR4.

All cell lines were cultured at 37°C, 95% humidity and 5% CO_2 in a Heraeus BBD 6220 CO_2 Incubator.

RPMI 1640 Medium (Ref. 11875-093, Lot 1674912, Lot 1748058), DMEM (Ref. 41965-039, Lot 1667145), DPBS (Ref. 14190-144, Lot 1672863, Lot 1682691), L-Glutamine (200 mM, Ref. 25030-081, Lot 1748058) and fetal bovine serum (FBS) (Cat. No. 10437028) were purchased from Gibco®, Life Technologies™. Geneticin (G418 disulfate salt solution, G8168, Lot # SLBJ9876V) was purchased from Sigma-Aldrich®.

I monitored the quality of my cells by checking the culture density, colour of the growth media, and cell morphology. Checks were performed before every experiment to ensure that contaminated cells were not used. Immunostaining of surface markers followed by flow cytometry was used to ensure that the proteins of interest were expressed and detectable on

the appropriate cells. Besides flow cytometry, phase contrast microscopy was used to image the cells before they were used for the production of liposomes or ghost cells.

2.2 Production of liposomes

Bronshtein's method for liposome fabrication (Bronshtein *et al.*, 2011) was adapted to my needs and the available equipment by Alvaro Dominguez Baquero (Baquero, 2015). The production of my CD4+, CCR5+ and CXCR4+ cell-derived liposomes was similarly based on cell homogenization and subsequent extrusion.

Homogenization exposed the cell suspension to high shear forces that ruptured cell membranes. Nuclei were removed by centrifugation, leaving a homogenate of membrane aggregates behind. Complete nuclei separation depended on the centrifugation speed that was used. This step was monitored by microscopy and further adapted if necessary.

During extrusion, the homogenate was forced through a membrane of defined pore size (50 – 1,000 nm). This process was intended to break up lipid aggregates and force them to reassemble into liposomes. According to Dua *et al.* disrupted cell membranes should spontaneously reassemble into monolayered, bilayered or multilayered structures (Dua, Rana and Bhandari, 2012).

After extrusion, the samples were characterized using transmission electron microscopy and probed for CD4 by immunostaining and flow cytometry.

2.2.1 Cell homogenization

For liposome fabrication, 10^8 cells per cell type were used. Centrifugation at 340 x *g*, for 10 min, at 4°C was used to pellet the cells. Each cell pellet was washed twice with 10 mL TM-buffer, pH 7.4 (10 mM Tris-HCL [Trizma® hydrochloride, T3253, Lot#SLBD8313V, Sigma-Aldrich®], 1 mM $MgCl_2$ [Magnesium chloride hexahydrate, 105833, Merck], pH adjusted with 1 M NaOH) before being resuspended in 10 mL TM-buffer, pH 7.4 supplemented with 1 Pierce™ Protease Inhibitor Tablet, EDTA free (Thermo Scientific). After incubation on ice for 5 min, the cell suspension was homogenized for one minute at maximum speed, using a T18 basic ULTRA-TURRAX homogenizer. Immediately, 1 mL of 1.25 M sucrose (Sigma-Aldrich®) in TM-buffer was added. The suspension was vortex-mixed and then centrifuged at 100 x *g*, for 30 min, at 4°C. The nuclei-containing pellet was discarded. The centrifugation speed needed to achieve this separation was determined by trial and observation of the pellet and supernatant using phase contrast microscopy. Phase contrast microscopy was performed using a Nikon ECLIPSE TE2000-S inverted microscope.

Subsequently, the supernatant was centrifuged at 3,270 x *g*, for 30 min, at 4°C to pellet the membrane fragments. The supernatant was discarded and the pellet was resuspended in 10

mL TM-buffer supplemented with 0.25 M Sucrose, pH 8.6. After a final centrifugation at 3,270 x *g*, for 30 min, at 4°C, the pellet was resuspended in 10 mL storage buffer (TM-buffer pH 8.6 supplemented with 0.25 M Sucrose and 1 Pierce™ Protease Inhibitor Tablet). All steps should be performed on ice and with buffers maintained at 4°C. Membrane fragment-containing samples were stored at 4°C.

2.2.2 Liposome extrusion

The samples were extruded in storage buffer using different extrusion membrane pore-sizes. Extrusion through 50 nm pore-sized membranes should break up all aggregates bigger than that and should give liposomes that are about 50 nm in diameter. Similarly, 200 nm pore-sized membranes should produce 200 nm liposomes and so on. In addition, extrusion was performed using three different methods - manual, pneumatic and pneumatic one-way extrusion. After extrusion, samples were imaged using transmission electron microscopy and compared with respect to liposome size and number, aiming to find the method that gave the highest number density of liposomes of uniform size. If liposomes of uniform shape and size were produced, subsequent immunostaining would be used for the detection of CD4, CCR5 and CXCR4. After extrusion, samples were stored at 4°C.

2.2.2.1 Manual extrusion

The LiposoFast Basic (LF-1, Avestin) is a manual extruder with a capacity of 1 mL (Fig. 8).

Fig. 8: The LiposoFast Basic (LF-1) is an easy-to-handle manual extruder for volumes up to 1 mL.

Samples were loaded into one syringe, then manually forced through a membrane - extruded - into the other syringe. This process was then repeated in the opposite direction. Extrusion was performed 21 times per sample, using membranes of different pore size (1,000, 800, 400, 200, 100 or 50 nm; Avestin Polycarbonate Membrane). One membrane was used to extrude 3 x 1 mL of each sample. The extruded sample aliquots were then combined and stored at 4 °C.

2.2.2.2 Pneumatic extrusion

The LiposoFast Pneumatic (LF-P, Avestin) can apply pressures up to 40 bar and has the capacity to accommodate 2 mL samples (Fig. 9).

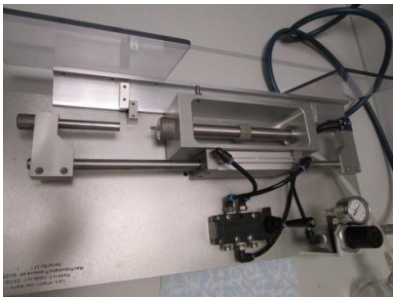

Fig. 9: The LiposoFast Pneumatic (LF-P) can be used to apply defined pressures up to 40 bar. Up to 2 mL of sample can be extruded at a time.

It was used to extrude each sample 21 times at 40 bar using membranes of pore size 1,000 nm (Whatman Nuclepore Track-Etched Membranes, diam. 25 mm, pore size 1 µm, polycarbonate, WHA110610, Sigma-Aldrich) or 2,000 nm (Whatman Nuclepore Track-Etched Membranes, diam. 25 mm, pore size 2 µm, polycarbonate, WHA110611, Sigma-Aldrich).

2.2.2.3 Pneumatic one-way extrusion

The LiposoFast LF-50 (LF-50, Avestin) is a one-way extruder that can handle a maximum sample size of 50 mL (Fig. 10). It was used 3 to 6 times per sample at 5 bar. LF-50 uses the same membranes as LF-P.

Fig. 10: The LiposoFast LF-50 (LF-50) has a capacity of 50 mL. In contrast to LF-1 and LF-P, LF-50 is a one-way extruder.

2.2.3 Liposome purification

Different methods were investigated regarding their ability to separate membrane fragments or liposomes from the surrounding medium. The ideal purification method was required to maintain target protein functionality and retain as much membrane material as possible.

Centrifugation was a promising method for precipitating the membrane fragments, but might be limited due to similar densities of membranes and medium. Another possibility was the use of an exosome purification kit. These kits were designed to improve the precipitation of exosomes – lipid vesicles similar to liposomes - from solution. The separation efficiency of centrifugation was compared to the efficiency of the Exo-spin™ Exosome Purification Kit. Because the possibility existed that components of the Exo-spin™ Exosome Purification Kit could interfere with my samples, I also tried to enhance the liposome density for effective centrifugation by bead encapsulation.

2.2.3.1 Centrifugation versus Exo-spin™ Exosome Purification Kit treatment

After homogenization of TF228.1.16 cells, the sample was split into two tubes. No extrusion was performed at that time, as only the ability of the Exo-spin™ Exosome Purification Kit for membrane material recovery was compared to that of centrifugation at high speed. The membrane fragments in one tube were pelleted by centrifugation at 3,270 x *g*, 30 min, 4°C. The supernatant was discarded and pellets were resuspended in 500 µL FACS solution (DPBS + 5% FBS).

Membranes in the other tube were purified using the Exo-spin™ Exosome Purification Kit (Cell Guidance Systems, USA, Cat. No. EX01-25). Buffer A from the Exo-spin™ Exosome Purification Kit was added to a volume of sample at a ratio of 1:2 (e.g. 2.5 mL Buffer A + 5 mL sample). The tube was inverted to mix the sample. Then it was incubated at 4°C for at least one hour or overnight. Centrifugation at 18,400 x *g*, for 60 min, at 4°C was then performed to pellet the membrane material. The supernatant was removed and discarded. The pellet was resuspended in 500 µL FACS solution.

Flow cytometry was used to compare the final material density of both samples, as represented by the number of events detected in the sample per second. This, in turn, represented the yield of membrane material from each purification method. Both samples had the same amount of starting membrane material and resulted in a final volume of 500 µL. A 30 µL aliquot of membrane material-containing sample from each method of purification was added to 1,000 µL of FACS solution. These were then analyzed by flow cytometry. The time needed by the flow cytometer to detect 10,000 events for each sample was compared. The sample that was richer in material needed less time to present 10,000 events.

2.2.3.2 Encapsulation of silicon dioxide beads

Membrane fragments were produced by cell homogenization. One milliliter of sample was then supplemented with 1 µL of 150 nm silicon dioxide particles (56799 Sigma, Micro particles based on silicon dioxide, size: 0.15 µm, Sigma Aldrich) and vortex-mixed. Then, manual extrusion using a 1,000 nm pore-sized membrane was performed 21 times per sample. My aim was to have the liposomes encapsulate the beads when self-assembling during extrusion. TEM samples were prepared from the resultant liposomes.

2.3 Production and characterization of ghost cells

Ghost cells were produced by exposing cells to a lysis buffer comprising ultrapure water supplemented with a protease inhibitor (MilliQ-PI). The protease inhibitor was included to minimise the loss of membrane proteins, due to endogenous protease activity during lysis. Because aggregate formation was observed during lysis, different lysis conditions were tested to reduce this problem. Aggregates seemed to be caused by long exposure to the MilliQ-PI lysis buffer. Thus, fetal bovine serum (FBS) was added directly after lysis to increase the salt concentration. This action reduced aggregate formation, but further optimisation will be needed.

2.3.1 Calcein-AM and Nile Red staining prior to osmotic cell lysis

Phase contrast microscopy was used to check for successful cell lysis. Because it was difficult to differentiate between live and ghost cells in bright field imaging, the cells were stained with Calcein-AM and Nile Red prior to osmotic cell lysis. Images were captured using a CCD camera fitted to a Nikon ECLIPSE TE2000-S inverted microscope with fluorescence capability.

Calcein-AM is a membrane-permeable non-fluorescent molecule that is converted to fluorescent calcein by hydrolysis once it has entered a cell. Calcein has limited membrane permeability and is thus entrapped in cells and vesicles. This property allows calcein to stain the cytoplasm and be used as an indicator for leakage of cytoplasmic material during cell lysis (Sigma-Aldrich, no date a). Under excitation with blue light (excitation filter wavelengths: 480/40 nm) and observation in the green channel (emission filter wavelengths: 535/50 nm), intact calcein-stained cells fluoresce, while lysed cells do not.

Nile Red is typically used to stain intracellular lipids and hydrophobic domains of proteins (Sigma-Aldrich, no date b).Under excitation with green light (excitation filter wavelengths: 540/25 nm, and observation in the red channel (emission filter wavelengths: 605/55 nm),

intact cells would fluoresce red with a high intensity while lysed cells fluoresce red with a lower intensity due to their loss of internal membranes.

The staining solution was prepared by adding 1 µL Nile Red (1 mg/mL, N3013 Sigma-Aldrich) and 0.5 µL Calcein-AM (4 mM in DMSO, 17783 Sigma-Aldrich) to 1 mL DPBS.

For each sample, 8 x 10^6 cells were harvested and pelleted by centrifugation at 340 x *g*, for 5 min, at 37°C. The supernatant was discarded. The cell pellet was washed twice using 0.5 mL DPBS (Ref. 14190-144 gibco® by life technologies™) each time.

The cell pellet was then resuspended in 1 mL of staining solution and incubated for 30 min at 37°C in the dark. Afterwards, the cells were washed twice using 0.5 mL DPBS each time. Then the cell pellet was resuspended in 1 mL DPBS and split into 2 aliquots of 0.5 mL each.

Stained cells were either directly used for phase contrast microscopy, or they were lysed into ghost cells. Note that the exposure time used for imaging of cells and ghost cells was kept the same, to allow a comparison of calcein and Nile Red fluorescence intensities.

2.3.2 Protocol 1 for osmotic cell lysis

The lysis buffer was made by dissolving one Pierce™ Protease Inhibitor Tablet (PI), EDTA free (Thermo Scientific) in 50 mL MilliQ by vortex-mixing.

Two cell aliquots that were stained with Calcein-AM and Nile Red according to the protocol described in paragraph 2.3.1 were used for osmotic cell lysis. The cells were pelleted by centrifugation at 340 x *g*, for 5 min, at 37°C and the supernatant was discarded. For osmotic cell lysis, the cell pellet of one aliquot was resuspended in 150 µL of 4°C MilliQ-PI lysis buffer, and incubated for 5 min with agitation at 1,000 rpm on a shaker in the dark. The ghost cells were then pelleted at 50 x *g*, for 5 min, at 4°C. The supernatant was discarded. Then MilliQ-PI lysis buffer was added to top the volume of sample up to 150 µL. The other cell aliquot was treated with 150 µL DPBS instead of MilliQ-PI lysis buffer and maintained at 37°C to serve as the negative control. Both samples were imaged using phase contrast microscopy.

2.3.3 Protocol 2 for osmotic cell lysis

For ghost cell production, 5 x 10^6 cells were harvested and pelleted by centrifugation at 340 x *g*, for 5 min, at 4°C using a 50 mL tube. The supernatant was discarded and the cell pellet was washed twice using 1 mL DPBS each time. The cells were then resuspended in 1 mL FACS solution. The sample was incubated at 4°C for at least 20 min. After incubation, the cells were centrifuged at 340 x *g*, for 5 min, at 4°C and the supernatant was discarded. The pellet was resuspended in 60 µL FACS solution and vortex-mixed. Then a magnetic stirrer and 6 mL of 4°C MilliQ-PI lysis buffer were added. The sample was stirred for 5 min at 300 -

500 rpm (a small vortex should be seen), at room temperature. Then the sample was imaged using phase contrast microscopy.

2.3.4 Extension of Protocol 2 for osmotic cell lysis

Osmotic cell lysis was performed according to Protocol 2 for osmotic cell lysis (2.3.3). After the final incubation step, 300 µL of FBS were quickly added to the sample while it was still stirring, to obtain a final concentration of 5% (v/v) FBS in MilliQ-PI lysis buffer. The stirrer was removed and the sample was visually checked for aggregate formation. If aggregates were visible, they were pelleted by pulse-spinning and the supernatant with the ghost cells was removed. The ghost cells were pelleted at 50 x *g*, for 5 min, at 4°C, and then washed twice with 0.5 mL FACS solution per wash. The ghost cells were stored at 4 °C in the dark in FACS solution.

2.4 Flow cytometry

2.4.1 Principle

Flow cytometry can be used for cell counting, for the identification of different cell populations in a sample, as well as for the detection of immunolabelled proteins. Immunolabelling was performed using fluorescent antibodies that were raised against the target proteins CD4, CCR5, CXCR4 or gp120/41 (gp160). These antibodies can only bind their targets if the target proteins are present in the sample and in their native conformation. The presence of target proteins was demonstrated by the fluorescence of captured antibody, using flow cytometry. The flow cytometer detects fluorescence resulting from immunostained samples. Unlabelled cells were used to determine the intensity of auto-fluorescence in each sample. Signals that are of higher intensity than the auto-fluorescence of unlabelled cells indicate the presence of the corresponding target protein.

Each sample consists of antibody-labelled or unlabelled cells in suspension, which are injected into the flow cytometer. The cells are transported by BD FACS Flow Buffer, which also serves to disperse the cells. This way, only one cell at a time passes, and scatters, the detector laser light (Fig. 11). The cells are also illuminated by light of wavelengths that would excite any fluorescent antibody present. The detector collects: (1) forward-scattering data (FSC) that provides information about the cell size; (2) side-scattering data (SSC) that informs about cell complexity; and (3) fluorescence data (ThermoFisher Sientific, no date).

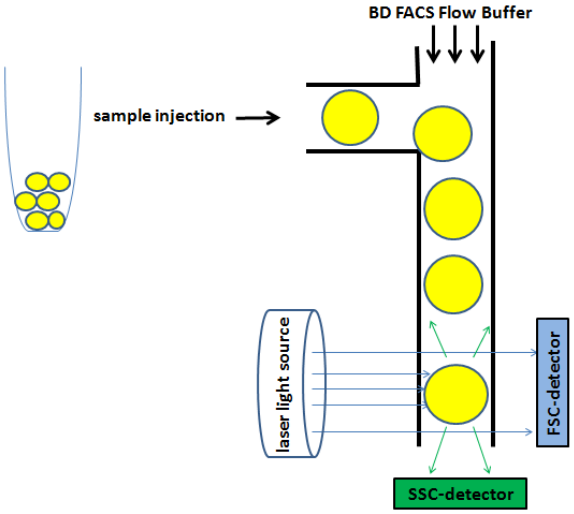

Fig. 11: Schematic drawing showing the principle of flow cytometry. The yellow beads represent the sample that is to be analyzed (e.g. cells). Inside the flow cytometer a buffer flows that transports the sample through the system, where it passes a laser beam. Scattered laser light and sample fluorescence is collected by detectors.

The BD FACS Canto^{TM}II flow cytometer was set to detect and analyze 10,000 events. Each event corresponds to a single entity detected by the flow cytometer in the samples. This data could then be displayed in a FSC/SSC-dot plot. Before the data was recorded, the detector voltage had to be adjusted using BD FACSDiva (TM) software v6.1.3 until all signals were within the detection limits of the detector. Voltages for the different fluorescence channels had to be adjusted one by one, by ensuring that auto-fluorescence signals lay within the detection range of the instrument (see Fig. 12). To set these parameters, unlabelled cell samples were used. The BD FACS Canto^{TM}II flow cytometer had three flow rate settings. Low flow rates of 10 µL/min or medium flow rates of 60 µL/min were used for measurements, while high flow rates of 120 µL/min were used for flushing the tubing.

2.4.2 Protocol to confirm correlation between particle size and forward scattering

The forward-scatter value (FSC) obtained in flow cytometry experiments, depends on the size of the object passing the laser beam at the time of measurement. Large objects should produce higher forward scattering values and small objects, lower forward scattering values. To determine the relationship between size and forward-scatter, beads of different sizes were analysed using the BD FACS Canto^{TM}II flow cytometer. Latex and silicon dioxide (SiO_2) beads with a size range from 100 – 3,000 nm (L3030, L4655, L3280, L9904, 66373, 81108, 56798, 56796, 56799, Sigma-Aldrich®) were used.

1 µL of bead suspension was added to 1 mL of FACS Flow Buffer (Cat. No. 342003, BD Biosciences). The suspension was vortex-mixed before being analyzed by flow cytometry at

a low flow rate. After every sample, the instrument was flushed for 2 minutes at high flow rate with FACS Flow Buffer to clean the instrument tubing of beads.

Beads of the largest size were used to set the detector voltage settings for forward- and side-scattering and to perform gating. FSC and SSC detector parameters were then kept the same for all bead samples.

2.4.3 Flow cytometric data analysis

Flow cytometry data were analyzed using *Flowing Software* version 2.5.1 (released 4.11.2013) created by Perttu Terho, Truku Centre for Biotechnology, University of Turku, Finland; In collaboration with Turku Bioimaging (Terho, 2013).

Gating of the data allows us to define the population of events that is most likely to include sample material (e.g. cells) and to exclude debris, as well as to analyze only the data belonging to such a population. SSC-FSC dot plots of unlabelled samples were used to manually perform gating. Cells that have similar size and complexity, and therefore show similarity in forward- and side-scatter, would appear as a focused collection of events (Fig. 12 (A)). This can then be defined as a single population by gating.

Next, a histogram is created displaying the number of events that show fluorescence in the chosen fluorescence channel. The fluorescence channel chosen corresponds to the wavelengths emitted by the sample fluorescence, which in turn is determined by the fluorophore used to label the antibodies used for immunostaining. The detector voltages had been set so that auto-fluorescence intensities lie within the limits of detection. By gating the auto-fluorescence signal peak, it can be distinguished from antibody-labelled cells that would show fluorescence of higher intensities (Fig. 12 (B)). This is best shown in an overlay histogram (Fig. 12 (C)).

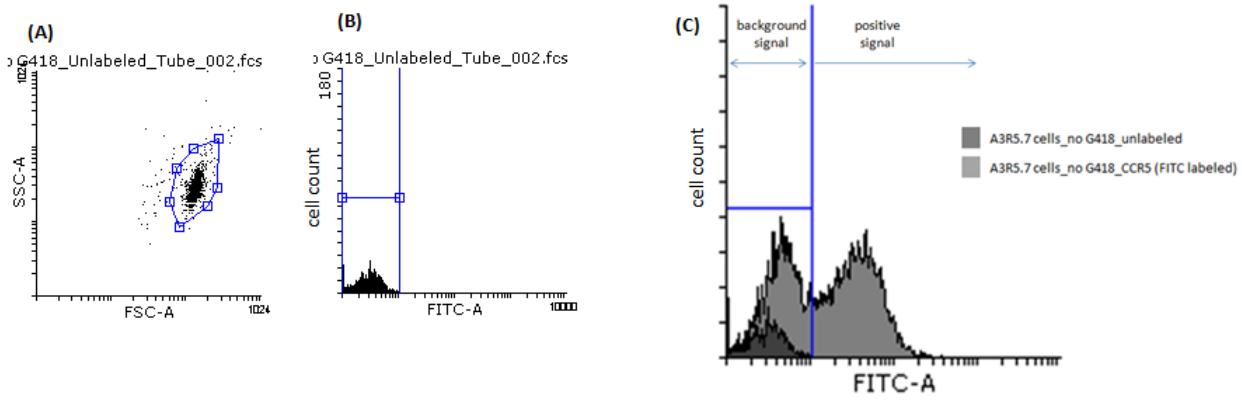

Fig. 12: The flow cytometer records 10,000 events. (A) All events are displayed inside the SSC-FSC dot plot. The blue circle gates the cell population and excludes debris. (B) Detector voltages are set so that the auto-fluorescence signal is located within the instrument detection

range. This signal is similarly gated using bracket-gates. Signals of intensity higher than that defined by the bracket-gates would indicate the presence of a sample (positive) signal. The channel displayed on this histogram was used to detect fluorescein (FITC)-labelled samples. (C) Overlay histogram of unlabelled sample and FITC-antibody-labelled sample.

Finally, the statistical display was used to determine the percentage of cells that showed higher mean fluorescence intensities than the auto-fluorescence signal. Since this fluorescence signal arises from labelled antibodies that are bound to their cell surface protein targets, the percentage of cells that show fluorescence represents the target protein-carrying cell population.

As the monitoring of cultured cell quality depends on the antibodies used, their affinity and specificity had to be ensured. To do this, a negative control was prepared for each sample, which the antibodies used were not supposed to bind to. A cell line not expressing the target protein, or an antibody that was not raised against the target protein, are suitable negative control samples. Results from various flow cytometry experiments are summarized in the form of graphs and displayed in section 3.

2.5 Immunostaining of sample surface markers

2.5.1 Immunostaining of cells

10^6 cells were used to prepare each sample. The cells were centrifuged at 340 x *g*, for 5 min, at 4°C. The supernatant was discarded and the cells were resuspended in 0.5 mL DPBS (Ref. 14190-144, gibco® by life technologies™) per sample. Each was then pelleted again by centrifugation at 340 x *g*, for 5 min, at 4°C, followed by another washing step using 500 µL FACS solution (DPBS + 5% FBS) per sample. The final supernatant was discarded and the cell pellet was resuspended in 80 µL FACS solution.

The manufacturer's recommended amount of antibodies was added to each sample: 20 µL **CD4-FITC** (Fluorescein isothiocyanate [FITC] Mouse Anti-Human CD4, Cat. 555346, Lot 4118723, BD Pharmingen™), 20 µL **CCR5-FITC** (FITC Mouse Anti Human CD195, Cat. 555992, Lot 4091664, BD Pharmingen™), 20 µL **CXCR4-APC** (Allopycocyanin [APC] Mouse Anti Human CD184, Cat. 555976, Lot 404820, BD Pharmingen™) or 1 µL **RbIgG-FITC** (Anti-Rabbit IgG [whole molecule]–FITC antibody produced in goat, F0382, Lot # SLBH5241V, Sigma-Aldrich®).

Different antibodies directed against gp160 were used: 2 µL **gp160 from Bioss** (HIV gp160 Polyclonal Antibody, FITC conjugated, Product No. bs-0786R-FITC, Lot AD112847, Bioss Antibodies), 1 µL **gp160 from Biorbyt** (HIV gp160 antibody, Product No. orb10821, Biorbyt) labelled with FITC, or 1 µL **gp160 from Abcam** (Anti-HIV gp160 antibody, Product No.

ab131729, Abcam) labelled with Peridinin-chlorophyll-protein complex (PerCP). The antibodies from Biorbyt and Abcam were fluorescently-labelled by Dr. Cherng-Wen Darren Tan, using the Lightning-Link system (Innova Biosciences).

FACS solution was then added to top the volume of sample up to 100 µL. The cells were incubated for one hour at 4°C in the dark for the antibodies to bind. After incubation, unbound antibodies were removed by washing three times, as described before, with 500 µL FACS solution per sample. Finally, each pellet was resuspended in 500 µL FACS solution and directly used for analysis in the BD FACS Canto™II flow cytometer at a medium flow rate.

For each experiment a negative control was needed. As negative control, either an antibody that will not interact with human proteins, e.g. 1 µL RbIgG-FITC, or another cell line that does not express the target proteins were used. When A3R5.7 cells were probed for CD4, CXCR4 or CCR5, TF228.1.16 cells served as the negative control and vice versa.

2.5.2 Immunostaining of liposomes

A3R5.7 liposomes were analyzed for the presence of CD4 using immunostaining. As the liposome labelling process needed to be optimized, only FITC-labelled anti-CD4 antibody was used in these experiments. TF228.1.16 liposomes were used as a negative control, since they are CD4 negative and should not be able to bind anti-CD4 antibody.

Normally, liposomes were kept in storage buffer (TM-buffer pH 8.6 supplemented with 0.25 M Sucrose and 1 Pierce™ Protease Inhibitor Tablet) until they were needed for experiments. However, the immunostaining of liposomes in storage buffer resulted in unspecific antibody binding which I tried to reduce by blocking the liposome surface prior to immunostaining. Surface blocking was performed by supplementing the storage buffer with 5% FBS.

I also wanted to find out, if Buffer A from the Exo-spin™ Exosome Purification Kit, which was used to harvest the liposomes, influenced the antibody binding process. Therefore, I incubated one sample with antibodies that had already been in contact with Buffer A. These antibodies were recycled from immunostaining experiments that were performed with liposomes in storage buffer.

2.5.2.1 Immunostaining of liposomes in storage buffer

As described in paragraph 2.2.1, 10^8 cells per cell type were homogenized and stored in 10 mL of storage buffer (TM-buffer pH 8.6 supplemented with 0.25 M Sucrose and 1 Pierce™ Protease Inhibitor Tablet) overnight. Then the samples were manually extruded 21 times through a 1,000 nm pore-sized membrane to produce liposomes. A3R5.7 and TF228.1.16 sample volumes were reduced by Exo-spin™ Exosome Purification Kit treatment (Cell Guidance Systems, USA, Cat. No. EX01-25). This was done by adding Buffer A at a ratio of

1:2 (5 mL of Buffer A + 10 mL of extruded sample) and incubation at 4°C overnight. Centrifugation at 18,400 x *g*, for 60 min, at 4°C was then used to pellet the liposomes. Almost all of the supernatant was discarded and the pellet was resuspended in the leftover liquid, yielding a total volume of about 1 mL. After volume reduction, A3R5.7 and TF228.1.16 samples were stored at 4°C until used for immunostaining.

One unlabelled sample was prepared per cell type, by adding 50 µL of FACS solution to 100 µL of extruded sample, yielding a total volume of 150 µL that was stored in the dark, at 4°C, until FACS measurement was performed.

Three samples were immunostained per cell type. To do so, 100 µL of extruded A3R5.7 or TF228.1.16 sample were incubated with 20 µL of fresh FITC-labelled anti-CD4 antibody, taken directly from the purchased antibody-containing vial, for one hour, in the dark, at 4°C. After incubation, excess antibody was removed using the Exo-spin™ Exosome Purification Kit: Buffer A was added to the sample at a ratio of 1:2 (60 µL Buffer A + 120 µL sample) followed by incubation for one hour, at 4°C, in the dark. Liposomes were then pelleted at 18,400 x *g*, for 60 min, at 4°C and the pellet was resuspended in 500 µL FACS solution. The supernatant was kept in a separate vial, containing excess antibodies that could be re-used as recycled antibodies. The three samples were then treated differently.

To thoroughly remove unbound antibodies, one sample was washed once, by incubating it with Buffer A at a ratio of 1:2 (250 µL Buffer A + 500 µL sample) for 1 hour at 4°C in the dark, followed again by centrifugation at 18,400 x *g*, for 60 min, at 4°C. The pellet was then resuspended in 150 µL FACS solution and stored in the dark, at 4°C, until flow cytometry was performed.

To another sample, a second washing step was added, performed as described above by adding Buffer A a second time at a ratio of 1:2, followed by incubation, centrifugation and resuspension of the pellet in 150 µL FACS solution.

The last sample was only washed once to remove unbound antibodies, by adding Buffer A at a ratio of 1:1 (500 µL Buffer A + 500 µL sample).

These samples were analyzed using the flow cytometer at a low or medium flow rate.

	Sample 1	Sample 2	Sample 3
Extrusion buffer	storage buffer	storage buffer	storage buffer
Volume reduction after extrusion	yes	yes	yes
CD4-FITC antibody	fresh	fresh	fresh
Purification method	Exo-spin™ Exosome Purification Kit treatment		
Number of washing steps	1	2	1
Ratio Buffer A : liposome sample	1:2	1:2	1:1

Fig. 13: Summary of the differences in sample preparation for the immunostaining of liposomes in storage buffer.

2.5.2.2 Immunostaining of liposomes in blocking buffer

From each cell type, A3R5.7 and TF228.1.16, 10^8 cells were homogenized (for preparation see 2.2.1) and kept in 10 mL blocking buffer (storage buffer supplemented with 5% FBS) overnight. Then each sample was manually extruded 21 times through a 1,000 nm pore-sized membrane to produce liposomes.

Two samples per cell type were immunostained, by adding FITC-labelled anti-CD4 antibody to 1 mL of liposome sample. One sample was incubated with 20 µL of fresh antibody. The other sample was incubated with 160 µL of FITC-labelled anti-CD4 antibodies that had been recycled from the previous staining experiment. The samples were incubated with the antibodies for 1 hour at 4°C in the dark. Then, unbound antibodies were removed by incubating every sample with 500 µL Buffer A for one hour, at 4°C, in the dark. This was followed by centrifugation at 18,400 x *g*, for 60 min, at 4°C. The excess antibody-containing supernatant was discarded and the pellet was resuspended in 500 µL FACS solution.

Next, every sample was washed once, by incubating it with Buffer A at a ratio of 1:2 (250 µL Buffer A + 500 µL sample) for 1 hour at 4°C in the dark, again followed by centrifugation at 18,400 x *g*, for 60 min, at 4°C. The pellet was resuspended in 150 µL FACS solution and stored in the dark, at 4°C, until flow cytometry was performed.

An unlabelled sample was produced in parallel with the labelled ones, where FACS solution was added instead of CD4-FITC antibody. The samples were analysed using the BD FACS Canto™II flow cytometer at a low or medium flow rate.

	Sample 4	Sample 5
Extrusion buffer	blocking buffer	blocking buffer
Volume reduction after extrusion	no	no
CD4-FITC antibody	fresh	recycled
Purification method	Exo-spin™ Exosome Purification Kit treatment	
Number of washing steps	1	1
Ratio Buffer A : liposome sample	1:2	1:2

Fig. 14: Summary of the differences in sample preparation for the immunostaining of liposomes in blocking buffer.

2.5.3 Immunostaining of ghost cells

Protocol 2 for osmotic cell lysis (2.3.3) was used to fabricate ghost cells. The ghost cells were pelleted at 50 x *g*, for 5 min, at 4°C. The ghost cells were then resuspended in 500 µL FACS solution (DPBS + 5% FBS). The sample was again pelleted at 50 x *g*, for 5 min, at 4°C. Then, either 20 µL CD4-FITC antibodies, or 20 µL CCR5-FITC antibodies, or 20 µL CXCR4-APC antibodies were added for labelling. FACS solution was added until a total volume of 100 µL was reached. The ghost cells were then incubated for one hour at 4°C in

the dark. After incubation, unbound antibodies were removed by washing three times, as described before, with 500 µL FACS solution per sample. Finally, the pellet was resuspended in 250 µL FACS solution and directly used for analysis in the BD FACS Canto^{TM}II flow cytometer at a medium flow rate.

Ghost cells that were incubated with FACS solution instead of antibodies were used as unlabelled sample.

2.6 Liposome analysis by transmission electron microscopy (TEM)

2.6.1.1 Preparation of pioloform- and carbon-coated copper grids for TEM samples

Copper grids of 300 mesh (Christine Gröpl, Electron Microscopy, Cat. No. G2430C) were rinsed three times with deionised water and three times with acetone before they were air-dried overnight with protection against dust. Clean glass slides were dipped into a 0.25% (w/v) pioloform in chloroform solution for 7 s, followed by 5 min of air-drying. Then the pioloform at the edge of the slide was scored on three sides using a surgical blade to create a small sheet of the polymer. The glass slide was plunged into a bowl of water to let the cut pioloform film lift off and float freely. The copper grids were placed on the pioloform sheet one by one, with the darker side of the grid facing downwards. A strip of parafilm was used to collect the pioloform sheet and the copper grids they carry. Finally, carbon was sputtered onto the pioloform on the grids, using a Leica EM SCD005 sputter coater. The coated grids were stored in a covered petri dish to protect them from dust.

2.6.1.2 Sample preparation for TEM

30 µL liposome suspension were dispensed onto a sheet of parafilm. A pioloform and carbon-coated copper grid was placed on top of the droplet, with the darker side facing downwards. A 10 min incubation at room temperature allowed the sample to adsorb onto the grid. Next, the grid was placed onto a 30 µL droplet of 25% glutaraldehyde, with the darker side facing downwards. After incubation for 10 min at room temperature, the grid was transferred to a 15 µL droplet of 1% uranyl acetate for negative staining, with the darker side facing downwards, for 10 min. The grid was finally rinsed three times with MilliQ water and then stored in a grid cassette to dry overnight before TEM imaging.

2.6.1.3 Transmission Electron Microscopy

Transmisson electron microscopy was used for imaging structures in the nanometer range, because of its higher resolution compared to light microscopy. Light microscopy worked well for cells but not for liposomes because extruded liposomes were expected to have sizes

between 50 nm and 2 µm, depending on the pore size of the extrusion membrane that was used. Therefore, all liposome samples were analyzed using the FEI Tecnai G^2 200 kV TEM.

2.7 Phase contrast microscopy and fluorescence microscopy of ghost cells

Cells and ghost cells have sizes of about 10 – 15 µm and were imaged using a Nikon ECLIPSE TE2000-S inverted microscope. However, it was difficult to differentiate between live cells and ghost cells in bright-field images. This differentiation was necessary to determine if the osmotic cell lysis was successful. Therefore, I fluorescently stained the cells with Calcein-AM and Nile Red prior to osmotic cell lysis. Fluorescently-labelled cells and ghost cells were then imaged using a CCD camera fitted to a Nikon ECLIPSE TE2000-S inverted microscope with fluorescence capability.

3 Results

3.1 Cell surface marker characterization

The aim of this thesis was the production of CD4+, CCR5+ and CXCR4+ cell-derived T-cell mimics. As the starting material for T-cell mimic production is cells, I needed to find cells that carried these proteins on their surfaces. Flow cytometry of cells immunostained with fluorescently-labelled antibodies is a suitable method for detecting different cell surface proteins. These antibodies needed to be quite specific. To test their specificity a negative control in the form of a cell line known not to express the target protein was used.

3.1.1 A3R5.7 cells were immunostained for CD4, CCR5 and CXCR4 proteins

Two cell lines were chosen to probe for CD4, CCR5 and CXCR4 expression: MOLT4/CCR5 and A3R5.7. Both cell lines were cultured with and without geneticin and then analyzed with flow cytometry to compare their protein expression levels. TF228.1.16 cells served as the negative control as they should not produce CD4, CXCR4 or CCR5.

Flow cytometric data was obtained by immunostaining these cells with antibodies directed against the surface antigens CD4, CCR5 or CXCR4 following the protocol for immunostaining described in section 2.5.1.

Both MOLT4/CCR5 and A3R5.7 cells express CD4 and CXCR4 constitutively. In addition, both are expected to express CCR5 under geneticin (G418) selection.

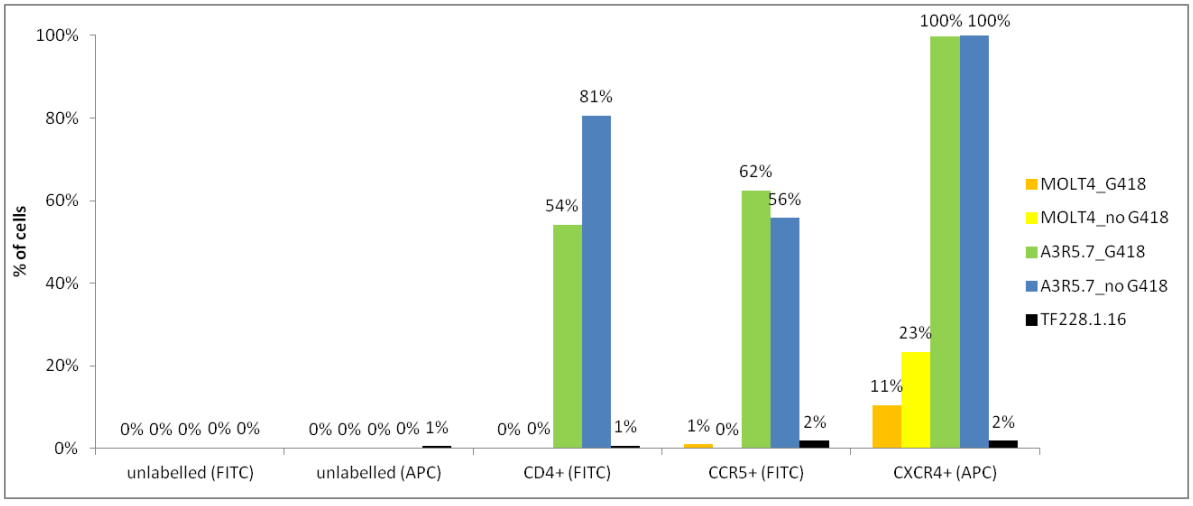

Fig. 15: Different cell types tested for the presence of CD4, CCR5 and CXCR4.

From the data in Fig. 15 it appears that MOLT4/CCR5 cells expressed neither CD4 nor CCR5. However, 11% of cells were immunostained with anti-CXCR4 antibody if cultured in

the presence of geneticin, while 23% were immunostained without geneticin supplementing the growth medium.

A3R5.7 data shows that 54% of cells grown in the presence of geneticin bound anti-CD4 antibody, 62% bound anti-CCR5 antibody and 100% bound anti-CXCR4 antibody. Without geneticin induction, 81% of A3R5.7 cells were immunostained with anti-CD4 antibody, 56% with anti-CCR5 antibody and 100% with anti-CXCR4 antibody. In contrast, fluorescence caused by anti-CD4, anti-CXCR4 and anti-CCR5 antibodies was detected at a maximal level of only 2% in TF228.1.16 cells.

Since A3R5.7 cells that were cultured without geneticin expressed all the desired proteins, they were chosen for the production of T-cell mimics. Detailed information on auto-fluorescence and fluorescence of immunostained cells is provided as supporting information in paragraph 8.1.

3.1.2 gp160 protein could not be detected in TF228.1.16 or CHO cells

Gp160+ cell lines such as TF228.1.16 or CHO-WT might serve as HIV models and possible fusion partners for CD4+/CCR5+ or CD4+/CXCR4+ liposomes. In the course of quality testing, it was essential to test the availability of gp160 surface protein on these cell surfaces. As flow cytometry worked well to show the presence of surface proteins for A3R5.7 cells, this method was also used on TF228.1.16 and CHO cells. The cells were labelled with antibodies from Bioss against gp160 following the protocol for immunostaining described in paragraph 2.5.1. A3R5.7 cells served as the negative control.

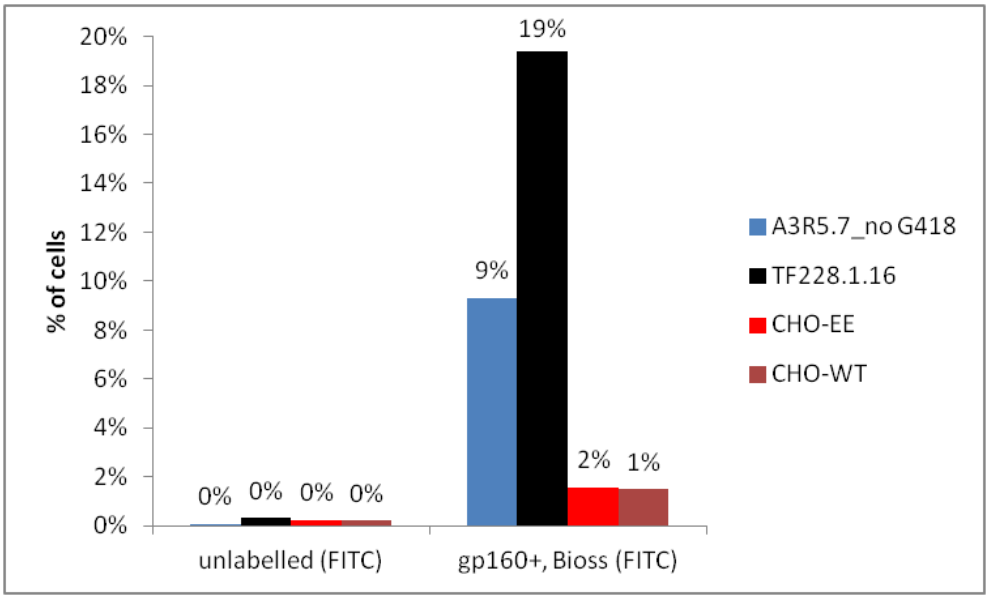

Fig. 16: Different cell types tested for the presence of gp160.

19% of the TF228.1.16 cells were demonstrated to be immunostained with anti-gp160 antibody. Despite A3R5.7 cells being known to be gp160 negative, 9% of cells had bound anti-gp160 antibody. Only 1% of CHO-WT cells but 2% of CHO-EE cells were immunostained with anti-gp160 antibody (Fig. 16). Additional information is provided as supporting information in section 8.2.

I decided to use TF228.1.16 cells for T-cell mimic production because they were easier to handle compared to CHO cells, as TF228.1.16 cells grew in suspension culture while CHO cells grew as adherent monolayers. Being a suspension culture also made TF228.1.16 the more appropriate reference cells for A3R5.7.

3.1.3 Determining reliability of surface marker characterisation

To determine the repeatability of my experiments and data, surface marker characterization was performed three times for A3R5.7 cells using unlabelled, CD4-FITC-labelled and CXCR4-APC-labelled antibodies.

The mean value of each triplicate sample was used to calculate the standard deviation. As shown in Fig. 17, standard deviations were below 2% for both signals.

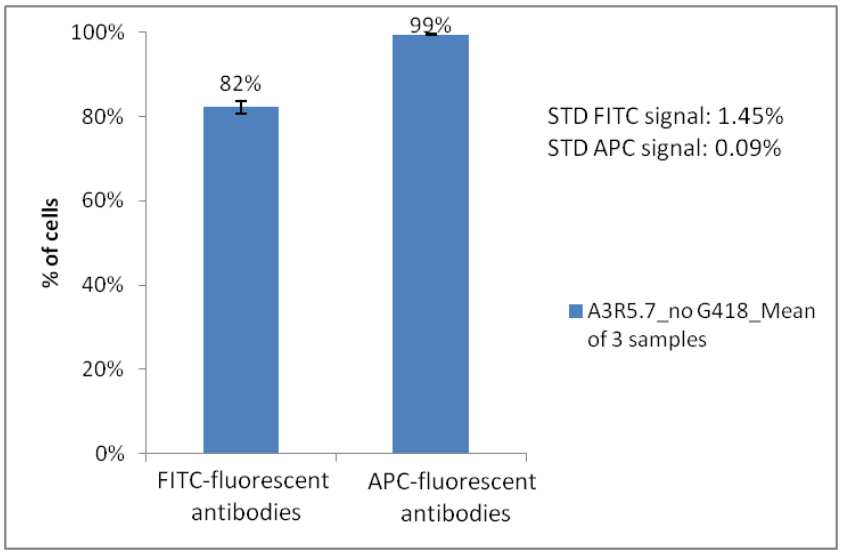

Fig. 17: Determining standard deviation for surface marker characterisation of immunostained A3R5.7 cells. The mean value of triplicate samples labelled with FITC-or APC-fluorescent antibodies is presented, along with the calculated standard deviation.

3.2 Liposomes

The aim was to produce CD4+/CCR5+/CXCR4+ liposomes of size about 1 - 2 µm from cells. To do this, A3R5.7 cells were homogenized and extruded. Every step was closely monitored using phase contrast microscopy for the separation of nuclear and membrane material after homogenization, and transmission electron microscopy for imaging liposomes that were produced by extrusion. Once liposomes were produced, they were immunostained and probed for CD4, CCR5 and CXCR4. However, the immunostaining protocol for cells, which was adapted for the immunostaining of liposomes, included several washing steps to remove unbound antibodies after the antibody-labelling process. Usually, excess antibody was removed by centrifugation, but centrifugation was likely to result in material loss due to the low density of the liposomes compared to the surrounding medium. Therefore, samples were treated using the Exo-spin^{TM} Exosome Purification Kit, aiming to overcome this problem. Alternatively, I tried to enhance the liposome density by bead encapsulation.

3.2.1 Cell homogenization disrupted cellular membranes

Using the protocol for cell homogenization (2.2.1), A3R5.7 cells were disrupted using a T18 basic ULTRA-TURRAX homogenizer. The result was a suspension containing membrane fragments, nuclei and other cell components.

Fig. 18 (A) shows material from the pellet after the first centrifugation at 100 x *g*. The sample contained predominantly nuclei and little membrane fragments. Fig. 18 (B) shows material from the pellet of the second centrifugation at 3,270 x *g*. It points out that not all nuclei were removed successfully by centrifugation at 100 x *g*, although membrane fragments were predominantly collected.

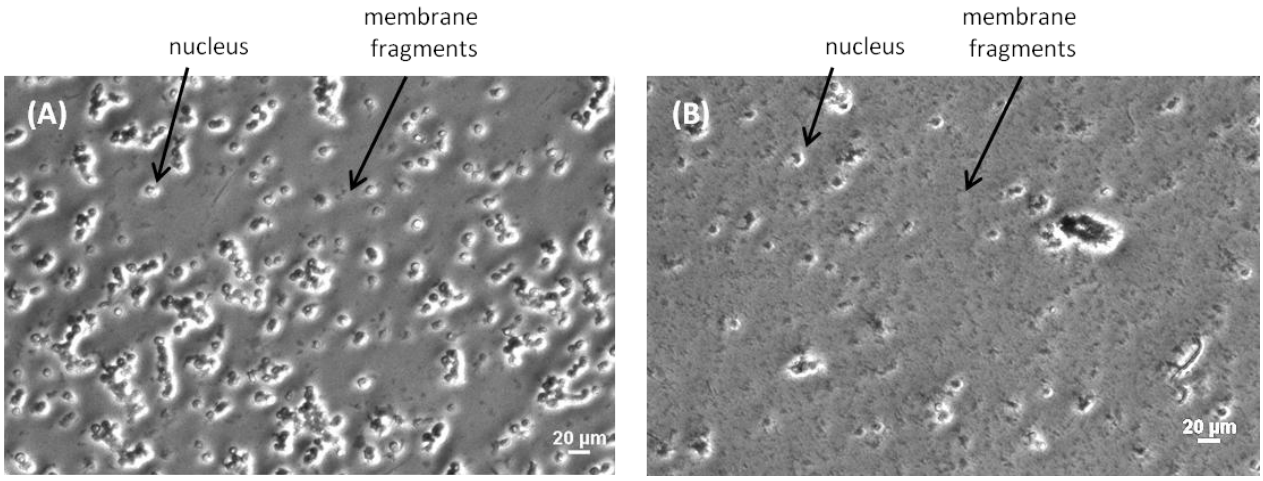

Fig. 18: After homogenization, the nuclear fraction (A) and the membrane fragment fraction (B) of disrupted A3R5.7 cells were separated by centrifugation and imaged using phase contrast microscopy.

3.2.2 Liposomes produced by extrusion

After cell homogenization and nuclei removal, the membrane fragments were stored in aqueous buffer at 4°C. This environment caused the membrane fragments to aggregate in the absence of a detergent because of the amphiphilic character of membrane lipids. Extrusion was used to break up these aggregates and to form liposomes of defined size, depending on the pore size of the extrusion membrane used (see 2.2.2). The liposomes were then morphologically characterized using transmission electron microscopy (see 2.6).

The following shows images of material produced using the three different methods of extrusion. Please note that the images are displayed in different scales.

Fig. 19 and Fig. 20 show that liposome-like structures as well as membrane aggregates were produced when manual extrusion was used.

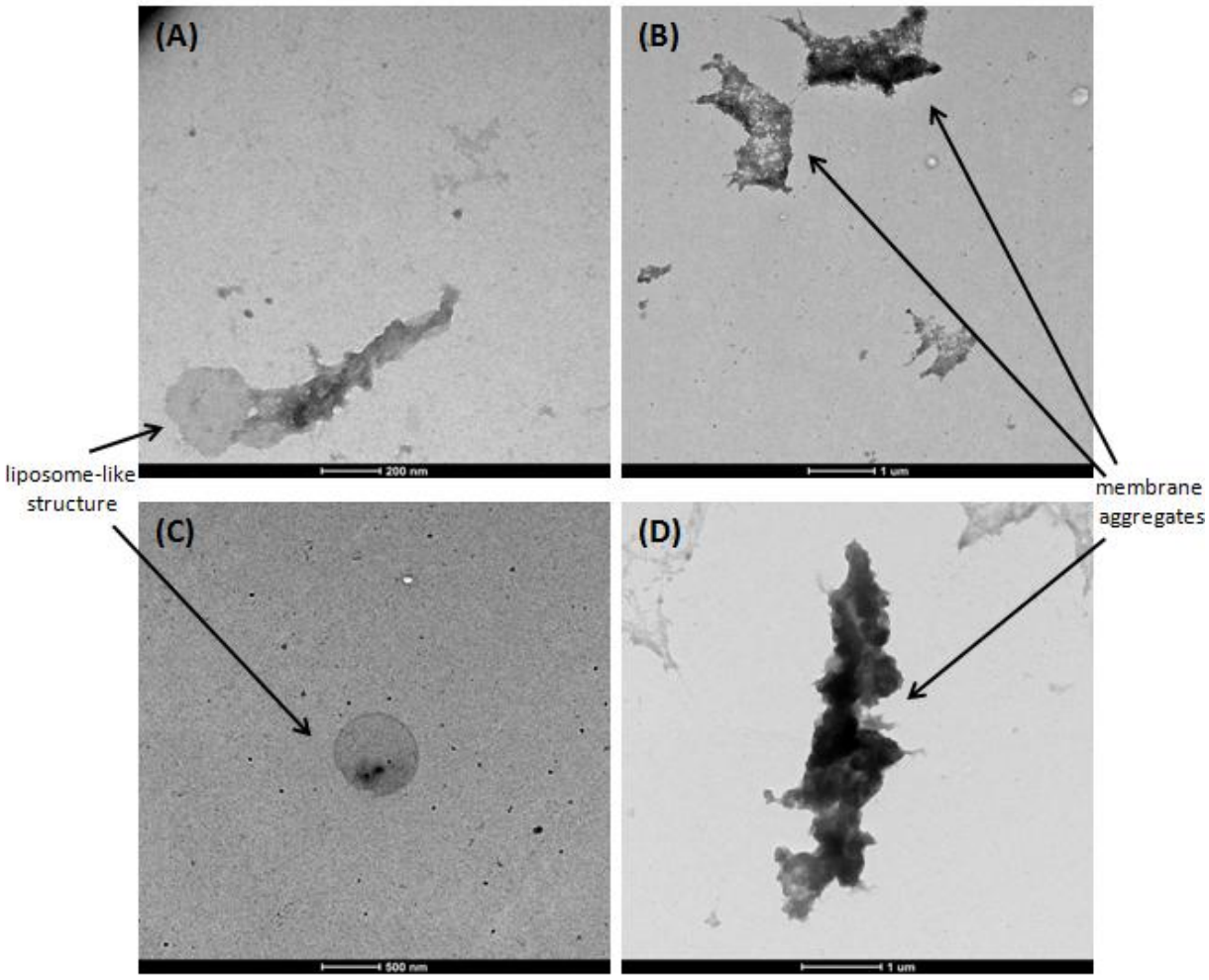

Fig. 19: Transmission electron microscopy images of A3R5.7 sample, manually extruded through a 50 nm pore-sized membrane (A & B) and TF228.1.16 sample manually extruded through membranes of 200 nm (C & D).

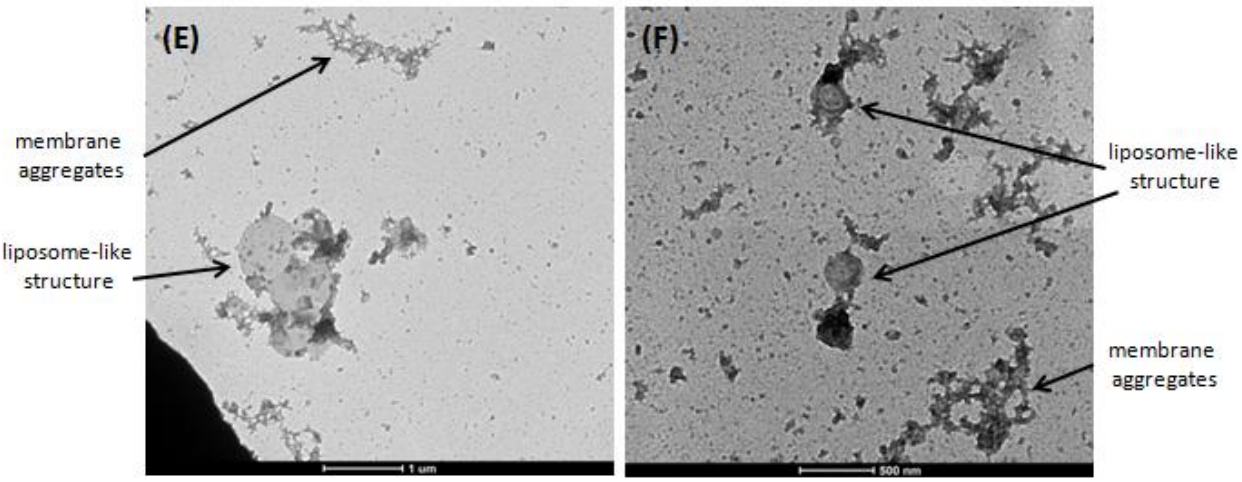

Fig. 20: Transmission electron microscopy images of TF228.1.16 sample manually extruded through membranes of pore-size 800 nm (E) and 1000 nm (F).

The pneumatic extruder LiposoFast Pneumatic (LF-P) was also used to produce liposomes from A3R5.7 cells. However, no liposomes could be found in the TEM samples analyzed.

After homogenization and extrusion of A3R5.7 cells, the pneumatic one-way extruder LiposoFast LF-50 (LF-50) was used to extrude the membrane fragments three times, using a 2,000 nm pore-sized membrane. The majority of the membrane fragments remained as aggregates, but some liposome-like structures could be seen when the LF-50 extruder was applied (Fig. 21).

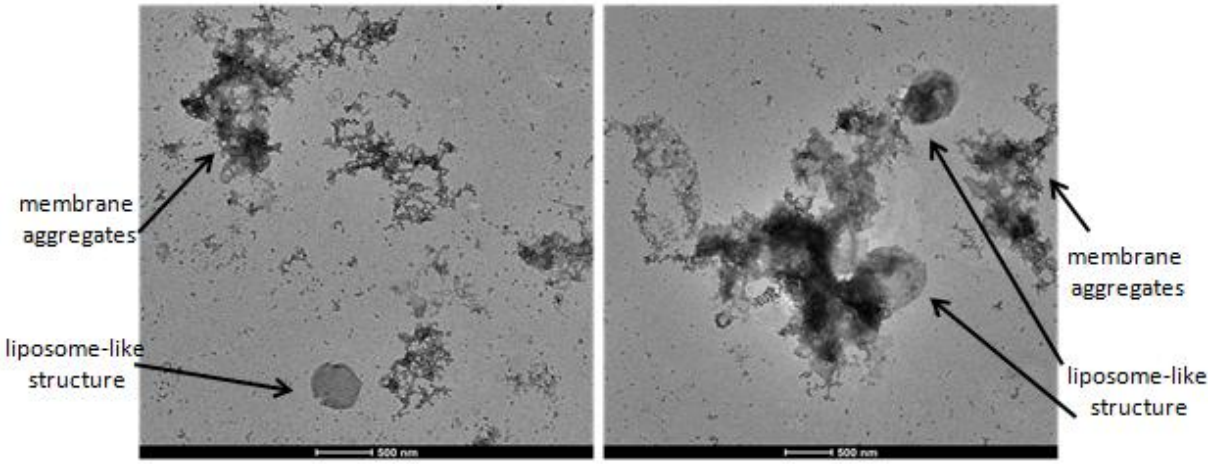

Fig. 21: Transmission electron microscopy images of A3R5.7 sample, extruded with the pneumatic one-way extruder LF-50, using a 2000 nm pore sized membrane.

3.2.3 Purification using the Exo-spin™ Exosome Purification Kit treatment improved membrane material recovery

As preparation for immunostaining experiments, different methods were tested to precipitate membrane material. After TF228.1.16 homogenization, flow cytometry was used to compare a membrane material sample that was purified by centrifugation with a membrane material sample that was treated with the Exo-spin™ Exosome Purification Kit (see 2.2.3.1). The material density was represented by the number of events detected in the sample per second and thus by the time needed to detect 10,000 events. It seemed that the time needed to count 10,000 events could be halved by using the Exo-spin™ Exosome Purification Kit (Fig. 22). That is, half of the membrane material was lost during centrifugation if the Exo-spin Exosome Purification Kit was not used. Therefore, in order to prevent membrane material loss I decided to use the Exo-spin™ Exosome Purification Kit whenever a reduction in liposome sample volume was needed or for removal of excess antibodies and washing during immunostaining.

	10,000 events [min:sec]
Liposome purification - centrifugation	07:30
Liposome purification - Exo-spin™ Exosome Purification Kit treatment	03:47

Fig. 22: Liposome samples after centrifugation or Exo-spin™ Exosome Purification Kit treatment were analyzed using flow cytometry. The times needed to count 10,000 events per sample were compared.

The results obtained with homogenized TF228.1.16 cells clearly demonstrated that more membrane material could be collected when the samples were treated with the Exo-spin™ Exosome Purification Kit. Therefore, this experiment was not repeated with material from A3R5.7 cells.

3.2.4 Beads were not encapsulated by liposomes

As an alternative to treatment with the Exo-spin™ Exosome Purification Kit, it was attempted to modify the density of the liposomes in order to improve their pelleting during centrifugation. Because centrifugation separates particles based on their density and because liposomes have almost the same density as the surrounding medium, I decided to encapsulate silicon dioxide beads in the liposomes in order to increase their density (see 2.2.3.2). Fig. 23 shows that the beads were not encapsulated into liposomes. In addition there were more membrane aggregates than liposomes.

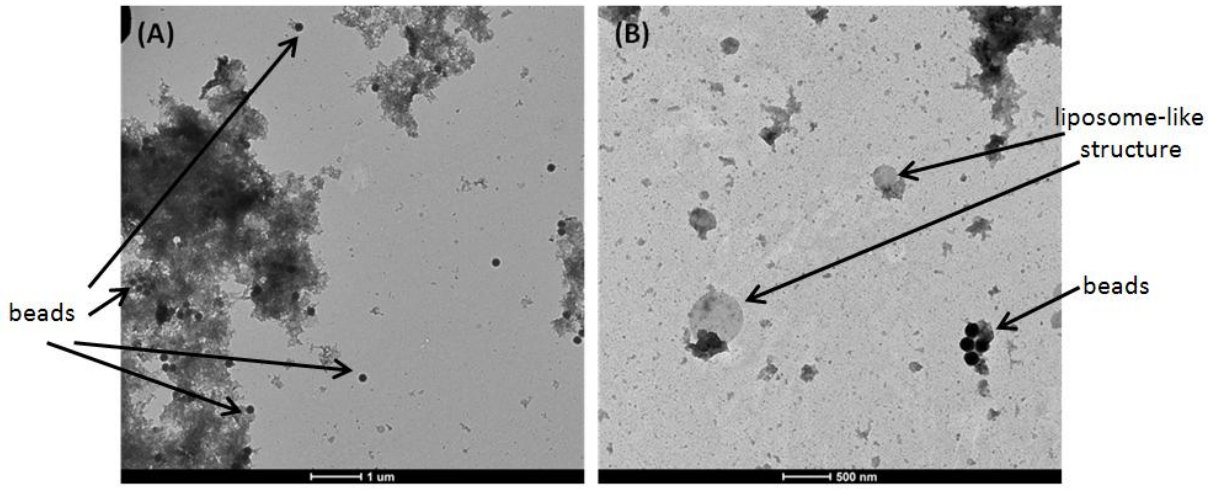

Fig. 23: Transmission electron microscopy images of A3R5.7 (A) and TF228.1.16 (B) liposomes prepared by extruding the respective cell homogenates in the presence of silicon dioxide beads.

3.2.5 No correlation between particle size and forward scattering was found

As seen in Fig. 19, Fig. 20 and Fig. 21, extrusion produced liposomes and aggregates of different sizes. It would be helpful if cells, liposomes and aggregates show different forward scattering values when analysed with the flow cytometer. For one thing, this would allow a distinction of the different populations present in the sample, based on their sizes and thus their forward-scatter values. On the other hand, the forward-scatter signal could also be used as indicator for extrusion efficiency, as successful extrusion would result in one population of reduced size and thus in one forward-scatter signal. The ability of the BD FACS Canto^{TM}II flow cytometer to differentiate between these sample types was tested with beads of different sizes.

Data from flow cytometry of silicon dioxide (SiO_2) and latex beads was collected following the protocol to confirm correlation between particle size and forward-scatter described in paragraph 2.4.2. From Fig. 24 (A) we can see that 150 and 500 nm SiO_2 beads were located at the lower range of values on the x-axis because they generated a smaller forward-scatter than 3,000 nm beads. The latter produced forward-scatter of highest values on the x-axis. 1,000 and 2,000 nm SiO_2 beads produced forward-scatter of values found in between.

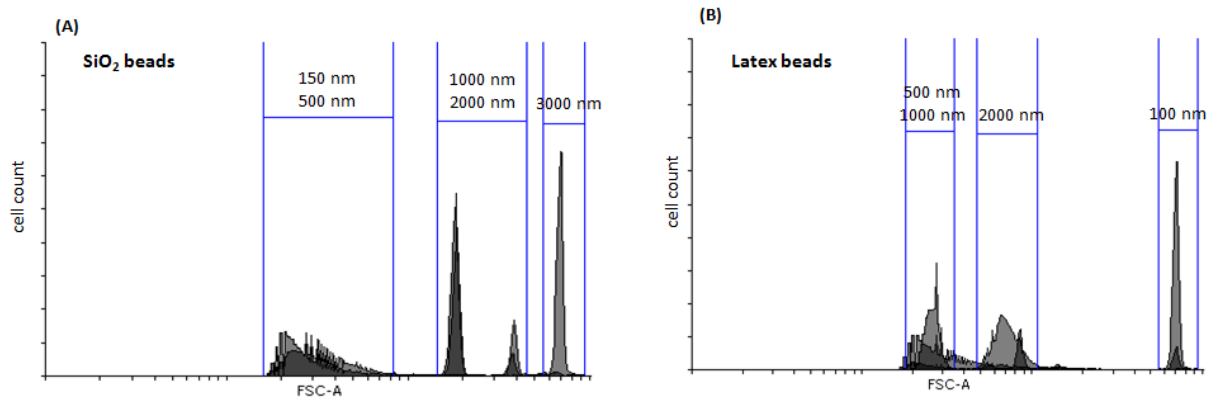

Fig. 24: Overlay histograms of (A) SiO_2 and (B) latex beads of different sizes. The forward-scatter value (FSC) should increase with bead size.

The distribution of latex beads looks different, with the smallest beads, 100 nm in diameter, yielding the highest forward-scatter values on the x-axis. 500 and 1,000 nm beads produced the same forward scattering values, followed by 2,000 nm beads that produced forward-scatter values in between (Fig. 24 (B)).

There does not appear to be a size-dependent change in forward scatter in my samples. As such the distinction between cells and liposomes based on their forward-scatter value does not seem to be feasible at this time.

3.2.6 CD4 antibody bound non-specifically to the liposomes

Surface marker detection was carried out using immunostaining and flow cytometry. The samples were prepared as described in paragraph 2.5.2 and Fig. 25. As I needed to optimize the liposome staining process before detailed surface marker characterization, only FITC-labelled anti-CD4 antibody was used in initial experiments. TF228.1.16 liposomes were used as a negative control.

A critical step during immunostaining was the removal of unbound antibodies. Usually, this was done by centrifugation. However, because liposomes have a low density, centrifugation might result in material loss. To reduce the loss of membrane material, the samples were treated with Buffer A from the Exo-spin™ Exosome Purification Kit that showed to reduce material loss in previous experiments.

	Sample 1	Sample 2	Sample 3	Sample 4	Sample 5
Extrusion buffer	storage buffer	storage buffer	storage buffer	blocking buffer	blocking buffer
Volume reduction after extrusion	yes	yes	yes	no	no
CD4-FITC antibody	fresh	fresh	fresh	fresh	recycled
Purification method	Exo-spin™ Exosome Purification Kit treatment				
Number of washing steps	1	2	1	1	1
Ratio Buffer A : liposome sample	1:2	1:2	1:1	1:2	1:2

Fig. 25: Summary of the differences in sample preparation for the immunostaining of liposomes in storage or blocking buffer.

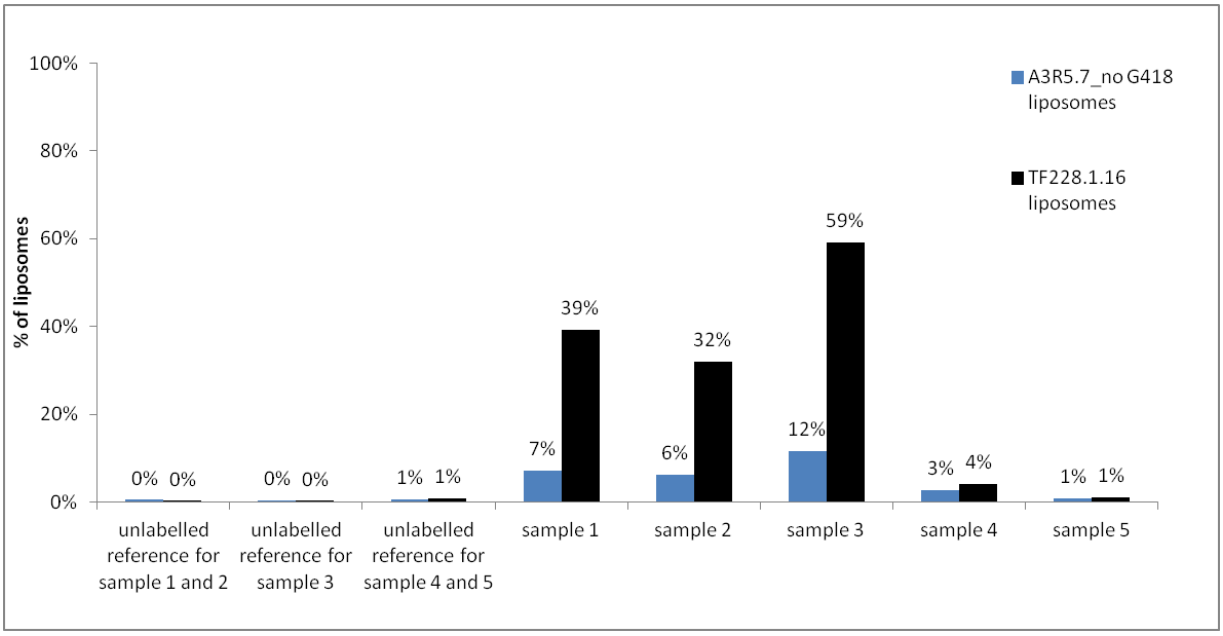

Fig. 26: Liposomes tested for the presence of CD4, using different immunostaining procedures. The data from three experiments is summarized in this diagram.

To improve the removal of unbound antibodies after immunostaining, different washing procedures were tested. However, neither the number of washing steps, nor the use of increased amounts of Buffer A seemed to reduce antibody binding to A3R5.7 or TF228.1.16 liposomes. Instead, flow cytometry data clearly showed, that if the liposome surface was not blocked before antibody labelling, five times more CD4-FITC antibody bound to TF228.1.16 liposomes than to A3R5.7 liposomes (Fig. 26, samples 1, 2 and 3). This indicated non-specific binding of the anti-CD4 antibody to TF228.1.16 liposomes. As shown in Fig. 26, sample 4, blocking the liposome surface prior to antibody labelling significantly reduced the amount of liposomes with bound CD4-FITC antibody to below 4%, but there was still non-specific binding.

As excess antibodies were usually collected for re-use after immunostaining, I needed to know if they would still have the same binding affinity for CD4 after they had came into contact with Buffer A from the Exo-spin™ Exosome Purification Kit. To determine if the presence of Buffer A interfered with the antibody binding process, anti-CD4 antibodies were

incubated in Buffer A before being used to immunostain liposomes. This resulted in a further reduction of target binding to 1% (Fig. 26, sample 5). As such, further probing for CD4, CCR5 or CXCR4 was not performed.

Based on the data from Fig. 26, the Exo-spin™ Exosome Purification method was abandoned as it was not suited for liposome pelleting during immunostaining. Buffer A influenced the antibody binding process and caused anti-CD4 antibody to bind non-specifically. Therefore, this method was not suited to probe liposomes for the presence of CD4 proteins.

3.3 Ghost cell production

I aimed for the osmotic cell lysis of A3R5.7 and TF228.1.16 cells by exposing them to ultrapure water supplemented with a protease inhibitor. Different fluorescent stains were used to trace the progress of osmotic cell lysis and microscopy was used to check for lysis efficiency. Different lysis protocols were used to enhance the lysis efficiency and to reduce aggregate formation during lysis. Immunostaining of the ghost cells with antibodies raised against CD4, CCR5 and CXCR4 was performed to ensure that these proteins were still retained in their native conformation.

3.3.1 Osmotic cell lysis using Protocol 1 produced ghost cells

TF228.1.16 cells were stained with Calcein-AM and Nile Red (see 2.3.1). They were then osmotically lysed, following Protocol 1 for osmotic cell lysis (see 2.3.2). Fluorescence microscopy was finally used to image the ghost cells (see 2.7).

Intact calcein-stained cells fluoresce when excited with blue light and observed in the green channel, while lysed cells do not. Under excitation with green light and observation in the red channel, intact Nile Red-stained cells would fluoresce red with a high intensity while lysed cells fluoresce red with a lower intensity due to their loss of internal membranes. Fig. 27 shows a mixture of live cells and ghost cells, resulting from partial cell lysis, viewed under bright field (A), green fluorescence (B) and red fluorescence (C). In bright field, live cells displayed their typical round shape and peripheral glow, while ghost cells looked darker and more flat. In addition, live cells showed intense green and red fluorescence, while lysed cells showed less intense green and red fluorescence.

From this result I concluded that only some of the cells were lysed successfully, and that the cell lysis protocol still needed further improvement.

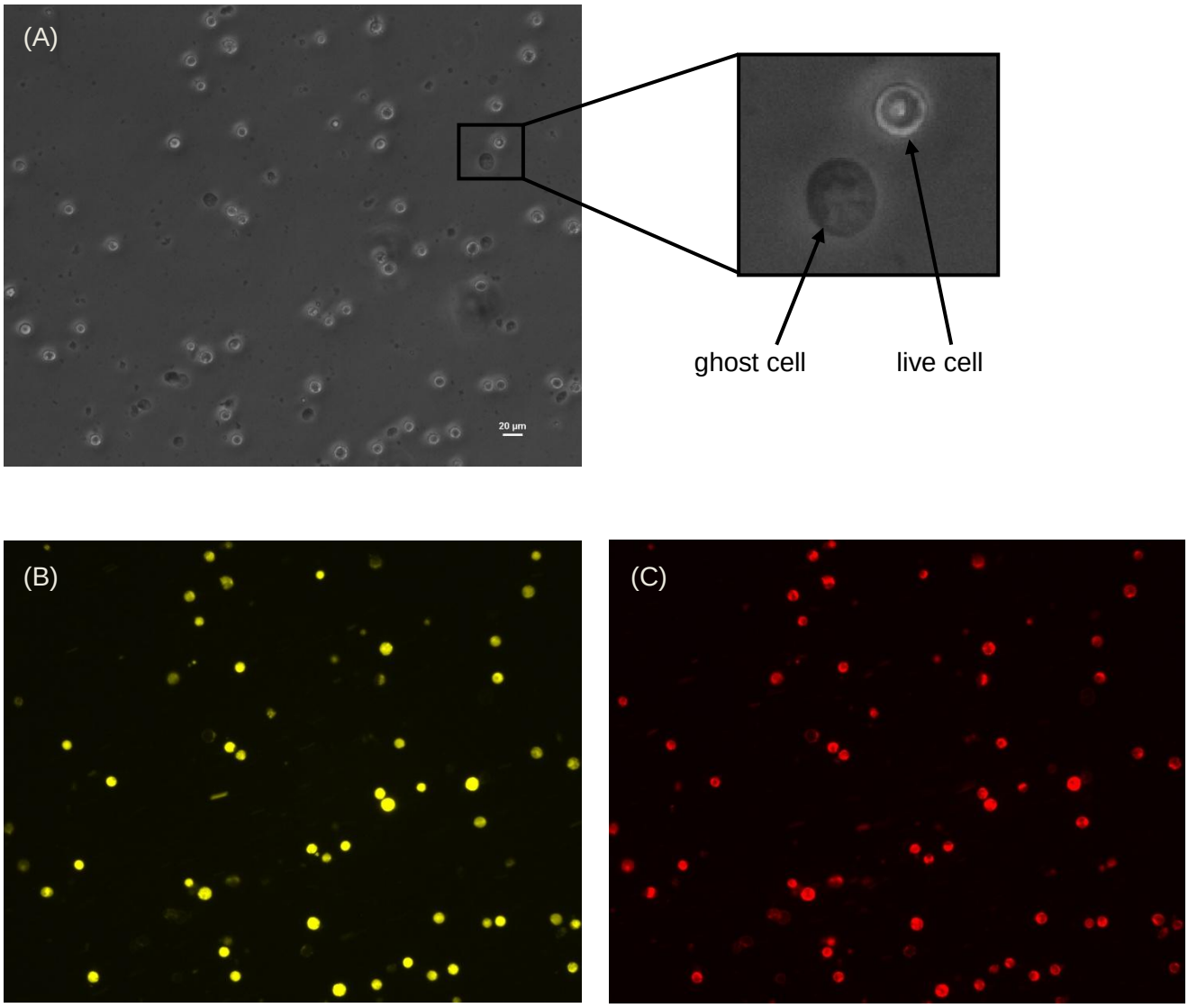

Fig. 27: Bright field (A), green fluorescence (B) and red fluorescence (C) images of TF228.1.16 cells lysed using Protocol 1 and fluorescence microscopy, showing live cells and ghost cells.

3.3.2 Efficiency of osmotic cell lysis using Protocol 2

To produce ghost cells, Protocol 2 for osmotic cell lysis (see 2.3.3) was followed. Unlike osmotic lysis using Protocol 1, the cells were resuspended in 60 µL FACS solution containing DPBS and 5% FBS prior to lysis. This cell suspension was then slowly added to 6 mL of MilliQ-PI lysis buffer while stirring at 300-500 rpm. Phase contrast microscopy images of the resultant ghost cells were taken immediately after the lysis was performed.

The difference between intact cells and ghost cells is shown in Fig. 28. Intact cells (A) were smaller, had a better contrast against the background, and a typical peripheral glow compared to ghost cells (B).

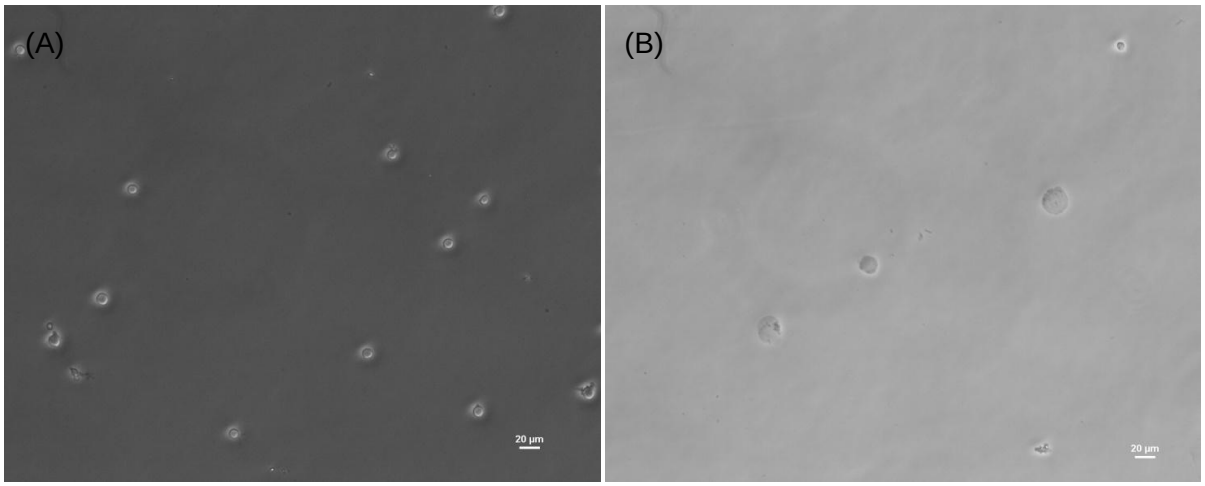

Fig. 28: : Phase contrast microscopy images of A3R5.7 cells in FACS solution (A) and A3R5.7 ghost cells produced by exposure to MilliQ-PI during osmotic cell lysis (B).

3.3.3 Aggregate formation during cell lysis

Following lysis using Protocol 1, large reddish aggregates were repeatedly visible by eye in the sample (Fig. 29). The reddish colour was due to the Nile Red staining of cellular membranes.

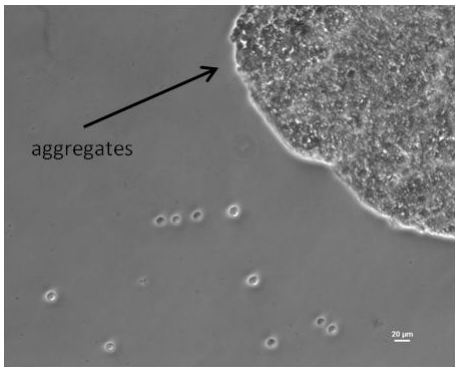

Fig. 29: Bright field image of a cell aggregate produced during osmotic cell lysis using Protocol 1 and phase contrast microscopy.

Under bright field illumination, these aggregates looked like large masses with indistinct internal features, and were seen in the majority of the experiments. If aggregates were visible by eye, they were removed by pulse-spinning or by centrifugation at 10 x *g,* for 5 min before ghost cells in the supernatant were pelleted for further application. Aggregates as depicted in Fig. 29 were also observed when Protocol 2 was used for osmotic cell lysis. From flow cytometry assays, I noticed that ghost cells were stabilized when they were resuspended in FACS solution (DPBS + 5% FBS) directly after lysis. Therefore, to reduce aggregate formation, Protocol 2 needed to be further modified by adding fetal bovine serum (FBS).

3.3.4 Aggregate formation was reduced by the addition of FBS after lysis

A3R5.7 cells were osmotically lysed using Protocol 2, described in paragraph 2.3.3. Immediately after that, 300 µL FBS were added according to the protocol described in paragraph 2.3.4, to stabilize the ghost cells and prevent aggregation. Samples before and after FBS addition were taken for imaging (Fig. 30).

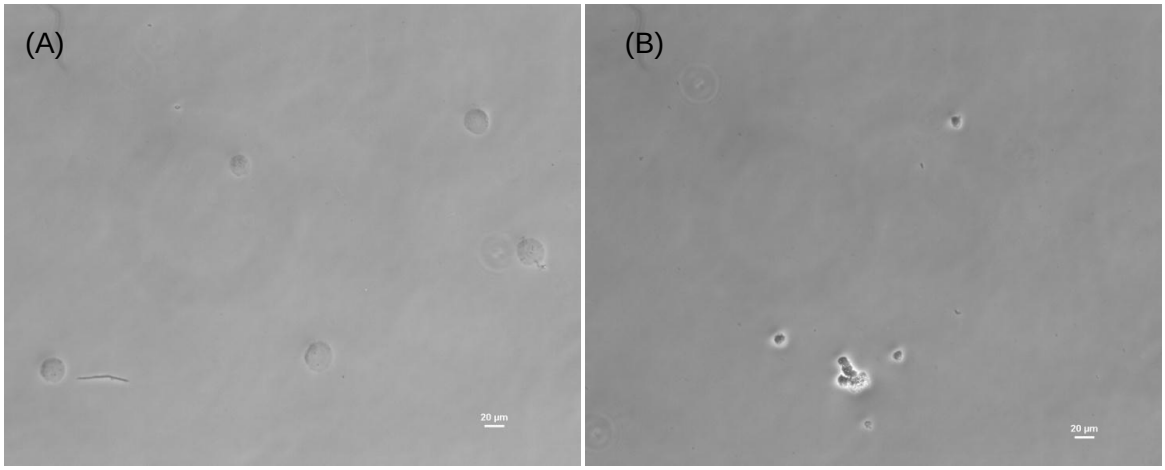

Fig. 30: Ghost cells produced using osmotic lysis Protocol 2 and imaged using phase contrast microscopy. FBS was added to the mixture directly after lysis. Image (A) shows the ghost cells before addition of FBS. Image (B) shows the ghost cells after addition of FBS.

To confirm that FBS was, indeed, necessary for ghost cell stabilization a sample from flow cytometry was modified and analyzed (for result and sample preparation see 3.3.5). This sample of TF228.1.16 ghost cells was suspended in FACS solution (DPBS supplemented with 5% FBS). The cells were washed twice with 1 mL DPBS using centrifugation at 50 x *g*, for 5 min, at 4°C to remove FBS. The ghost cells were finally suspended in 250 µL DPBS. Bright field images were taken before and after removal of FBS (Fig. 31).

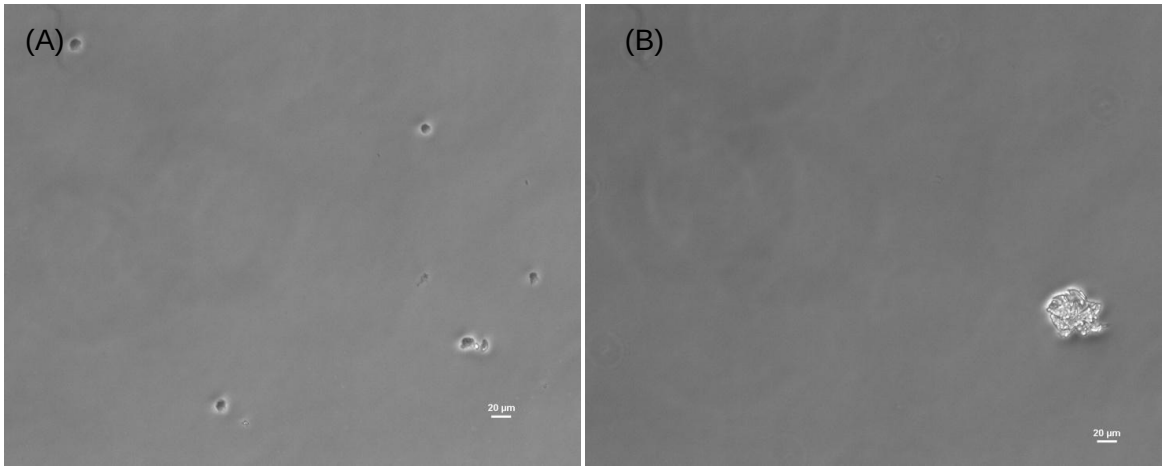

Fig. 31: Phase contrast microscopy images of ghost cells in FACS solution (A) and ghost cells in DPBS (B). If FBS was removed from the suspension buffer, the ghost cells aggregated.

From the images in Fig. 30 and Fig. 31 it seems that FBS helps the ghost cells to regain their three-dimensional structure. In addition, the ghost cells were still intact after multiple centrifugation steps at 50 x *g*, for 5min, at 4°C, if FBS was present. In contrast, they aggregated when FBS was removed. This supports the hypothesis that FBS helps to increase ghost cell stability in suspension.

3.3.5 CD4, CXCR4 and CCR5 were detected

Ghost cells were produced and labelled by immunostaining according to the Protocol for Immunostaining of ghost cells (see 2.5.3). Antibodies raised against CD4, CXCR4 and CCR5 were used. Live cells were also similarly immunolabelled to serve as a reference (see 2.5.1). TF228.1.16 cells and ghost cells were used as negative controls. All samples were analyzed by flow cytometry.

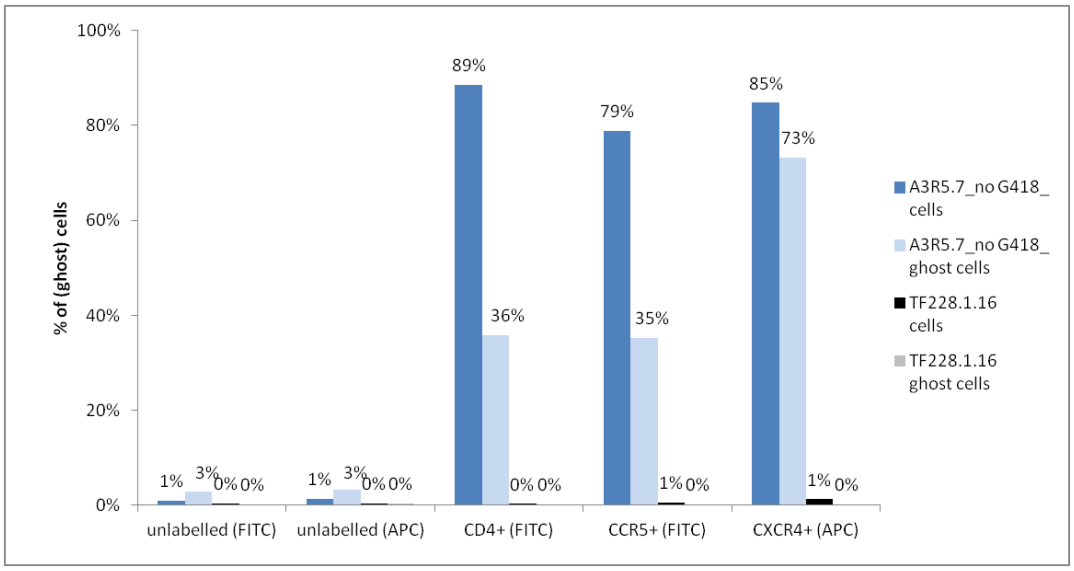

Fig. 32: Live and ghost cells probed for the presence of CD4, CCR5 and CXCR4.

Fig. 32 shows that 89% of A3R5.7 live cells bound anti-CD4 antibodies, 79% bound anti-CCR5 antibodies and 85% bound anti-CXCR4 antibodies. Of the A3R5.7 ghost cells, 36% bound anti-CD4 antibodies, 35% bound anti-CCR5 antibodies and 73% bound anti-CXCR4 antibodies. In contrast, TF228.1.16 live cells and ghost cells did not bind antibodies for all three target proteins.

3.3.6 Ghost cells were morphologically stable for up to 4 days

The samples from the immunostaining and flow cytometry experiment (result and sample preparation see 3.3.5) were stored at 4°C in the dark in FACS solution. The image in Fig. 33 (A) was taken directly after the immunostaining experiment. After four days, the bright field

image in Fig. 33 (B) was obtained, showing that the ghost cells had the same morphological structure as they had immediately following lysis using Protocol 2.

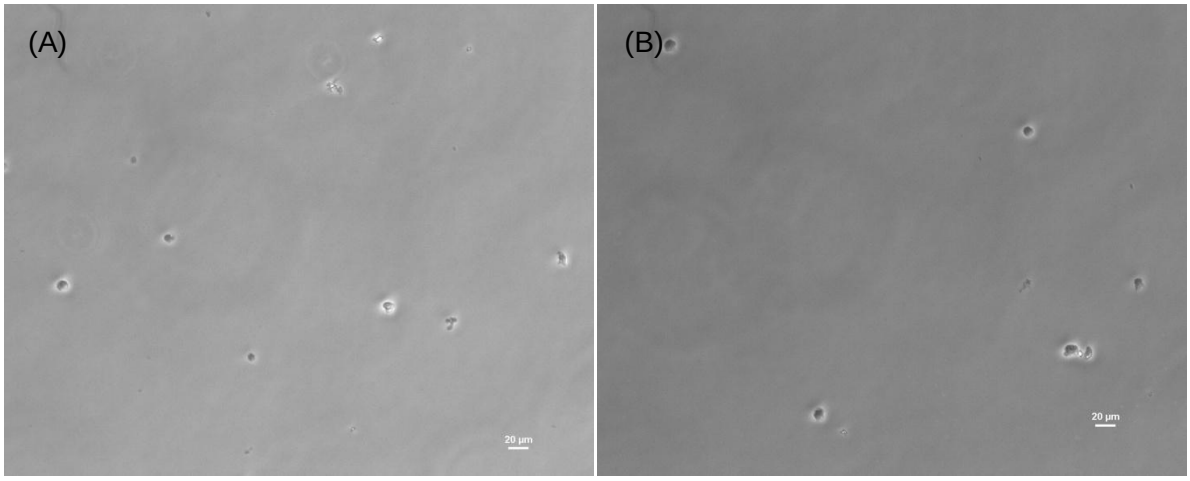

Fig. 33: Phase contrast microscopy images of ghost cells in FACS solution after lysis using Protocol 2 (A) and after four days of storage at 4°C (B).

4 Discussion

Initially, this thesis was focused on the enrichment of CD4+/CCR5+/CXCR4+ liposomes, produced from A3R5.7 cells using homogenization and extrusion. This promising protocol for liposome production was modified in our laboratory, but had not proven reliable. The production of liposomes in great quantities using this method turned out to be hardly possible. In addition, morphological characterization of the liposomes was based on transmission electron microscopy, a method that needed special training and time-consuming sample preparation. Therefore I decided to explore an alternative method of liposome production using a method I had never tried before: osmotic cell lysis.

Osmotic cell lysis produced liposomes that consisted of the membranes of empty cells, so-called ghost cells. Successful lysis could readily be confirmed with fresh samples using an easily handled phase contrast microscope, instead of a transmission electron microscope. Furthermore, purification by centrifugation of the larger ghost cells proved much easier than for liposomes. These advantages were decisive to investigate this method further. Thus, the project's objective was changed to the production of CD4+/CCR5+/CXCR4+ T-cell mimics produced by osmotic cell lysis instead of by cell homogenization and extrusion. I aimed for the development of an efficient, easy-to-handle cell lysis protocol that would generate reproducible results, and enable me to easily control the quality of all intermediate processes.

The problems I faced during liposome and ghost cell production will be discussed in this section.

4.1 Cell characterization

Before T-cell mimics were produced, the cell lines used were probed for the presence of the necessary proteins, CD4, CCR5 and CXCR4. From the cell immunostaining assays, I saw that the A3R5.7 cell line was well-suited for the production of T-cell mimics as CD4 and both chemokine receptors were expressed by this cell line. This CD4+/CXCR4+ cell line was genetically-modified to express CCR5 under geneticin selection (McLinden *et al.*, 2013). Surprisingly, A3R5.7 cells also expressed detectable amounts of CCR5 protein when cultured without geneticin. This could be explained by the fact that the working cell culture used consisted mainly of A3R5.7 cells carrying the CCR5 expression plasmid. Most probably, further culturing without geneticin as a selection pressure would result in CCR5 expression plasmid loss and reduction of CCR5 expression over time. However this trend was not observed during the time of my study.

Alternatively to the A3R5.7 cell line, MOLT4/CCR5 was characterized. However, CD4, CCR5 and CXCR4 expression was non-existent or very low in these cells. Perhaps there was an error during sample immunostaining, although this is unlikely since loss of CD4 expression by this cell line had also been reported by other users in our laboratory. However, the characterization assay was not repeated because A3R5.7 cells had fulfilled all my requirements.

The TF228.1.16 cell line was intended to be used as a potential fusion partner for the T-cell mimics, as TF228.1.16 cells were susceptible to T-tropic (CXCR4-using) HIV infection. This cell line was assumed to be gp120/41 positive, as gp160 envelope protein was expressed, and some might be cleaved into the gp41 transmembrane domain and the soluble gp120 domain (Jonak *et al.*, 1993). Furthermore, TF228.1.16 liposomes or ghost cells were used as references for A3R5.7 liposomes or ghost cells in flow cytometry assays.

However, I was not able to convincingly detect the gp120/41 surface protein on TF228.1.16 by immunostaining and flow cytometry. The antibodies available in our laboratory failed to bind the target protein. Antibodies raised against HIV gp160, using epitopes common to those on gp120, from three different companies – Abcam, Bioss and Biorbyt - were tested without success. Since the Bioss antibody was the only one that did not bind erratically, only this immunostaining data is reported here (see Fig. 16). Bioss antibodies were bound to A3R5.7 as well as TF228.1.16 cells. Therefore their specificity for gp120/41 was questioned.

To determine if antibody specificity was the problem and not a lack of expression of gp160 protein, the gp160+ CHO-WT cell line along with its negative control CHO-EE were tested. However, the CHO-WT cell population that was supposed to bind the Bioss anti-gp160 antibody did not show binding of any significant magnitude, when the assay standard deviation is considered. Nevertheless, I assumed TF228.1.16 and CHO-WT to be gp120/41 positive, despite the fact that this could not be confirmed by immunostaining at this stage.

4.2 Liposome production

Liposome production was carried out according to a protocol that was developed in our laboratory by Alvaro Dominguez Baquero (Baquero, 2015). His work was based on a paper that described the production of CD4+/CCR5+ cell-derived liposomes that can be used as a targeted drug-delivery system for HIV-infected cells (Bronshtein *et al.*, 2011). Because other cell lines and different equipment were available in our laboratory, the original protocol from Bronshtein *et al.* had to be modified by Mr Baquero. This modified protocol was used to produce A3R5.7- and TF228.1.16-derived liposomes by homogenization and extrusion. Cell homogenization resulted in membrane fragments, nuclei and other cellular components. For the production of proteoliposomes, only membrane fragments along with their embedded

membrane proteins were needed. Therefore nuclei were separated and discarded by centrifugation before the membrane fragments were pelleted at higher centrifugation speeds. The separation process needed constant monitoring as the centrifugation speed necessary for successful nuclei separation depended on the amount of starting material as well as on the cell type. Therefore the relative centrifugal force given in the protocol serves only as a guide. After every centrifugation step, supernatants and pellets were imaged. The first centrifugation was performed at low speed, aiming to pellet as many nuclei as possible. Otherwise, they would completely block the extrusion membranes later on. At the same time, the speed used should pellet as little of the membrane fragments as possible. The second centrifugation at high speed should pellet all the membrane fragments, along with any remaining nuclei, and should leave a clear supernatant. With centrifugation speeds below 100 x *g* only few nuclei were pelleted, but after centrifugation at 100 x *g*, no nuclei were visible in the supernatant when phase contrast microscopy was used. Instead, the pellet was rich in nuclear material. Phase contrast microscopy after the second centrifugation at 3,270 x *g* showed, that the pellet contained predominantly membrane fragments and only few nuclei. The supernatant was clear. Therefore, I used centrifugation at 100 x *g* for the separation of nuclei and membrane fragments in my experiments.

When the membrane fragments were collected, manual extrusion was used to produce liposomes of about 1,000 nm in size. These liposomes were imaged using transmission electron microscopy. The TEM images showed that liposomes were indeed produced, but only in low amounts. The majority of the material seemed to be membrane aggregates. Therefore I tested extrusion membranes of other pore sizes, 6 different ones in all ranging from 50 to 1,000 nm, aiming to find the pore size that produces the most liposomes. Unfortunately, the results were not significantly different, as few liposomes were produced using each of the different pore sizes, and aggregates were often visible, larger than expected considering the extrusion membrane pore-size.

The presence of aggregates after manual extrusion might be due to insufficient or inconsistent shear forces for the reorganization of the membrane fragments into liposomes. To overcome this problem I tried pneumatic extrusion, where shear forces were adjustable and of constant magnitude. However, samples produced with the LiposoFast Pneumatic (LF-P) and the LiposoFast LF-50 (LF-50) looked similar to the manually-produced ones. Also the amount of liposomes produced could not be increased.

From the TEM images it did not seem possible to produce liposomes of uniform size nor in useful amounts with this method. Because I was reliant on the flow cytometer for my sample analyses, I thought it would be interesting to find out if the flow cytometer could differentiate between the liposome or aggregate populations in my samples. The forward-scatter value could serve as indicator for extrusion efficiency. One forward-scatter signal peak would

indicate successful extrusion because then only liposomes of similar size would be present in the sample. Aggregates would have different sizes and would result in multiple forward-scatter signal peaks. This hypothesis was tested with beads of defined sizes. The BD FACS Canto™ II flow cytometer manual indicates that the magnitude of forward-scatter (FSC) should be proportional to the size of the sample particle. To confirm this relationship, two size experiments were carried out using latex or silicon dioxide beads ranging from 100 - 3,000 nm that represented cells or cell-derived liposomes. However, no correlation between these two parameters could be confirmed in my assay. Therefore the forward-scatter value was not used as markers of liposomes and aggregates, nor of cell or liposome size, in my samples.

Despite the problems with liposome aggregation, I started to develop an immunostaining protocol for liposomes, based on the staining protocol that was used for cells. For immunostaining, the sample was incubated with fluorescently-labelled antibodies. After incubation, excess antibodies were removed by washing the sample – sample material was pelleted and resuspended in antibody-free buffer – several times. The purification of liposomes from the extrusion buffer was a big challenge but necessary for further experiments, like immunostaining, that required multiple washing steps. The simplest method of liposome collection would be centrifugation. However, because the medium inside and outside of the liposome was the same, the density difference between the liposomes and surrounding medium was very little. In which case, high centrifugation speeds were necessary for liposome pelleting. However, centrifugation at high speed could destroy the liposomes. Thus, low speed centrifugation is preferable.

An alternative method of liposome purification is the use of an exosome purification kit. Exosomes would have similar densities as my liposomes. Exosomes are vesicles filled with cell content that bud from cells and are used as transport vehicles that transfer cellular components like proteins, lipids and mRNAs to recipient cells or to release cellular components into the environment. They consist of a cell-derived membrane, and with sizes from 30 – 150 nm, they are in the size range of small liposomes (Lane *et al.*, 2015). Different exosome purification kits are available, including the Invitrogen Total Exosome Isolation Kit (Life Technologies, USA) or the ExoQuick-TC Exosome Precipitation Kit (System Biosciences, California). These kits use reagents that sequester water molecules. As a result, membranes are forced out of solution and liposome recovery is improved. Membranes can then be collected by a short centrifugation at low speed (Zeringer *et al.*, 2015). However most of these kits require incubation overnight to precipitate exosomes from solution and thus are not useful for my purpose because I needed to perform multiple precipitation steps per day for one immunostaining experiment. I tested the Exo-spin™ Exosome Purification Kit (Cell Guidance Systems, USA) that used low centrifugation speeds and an incubation time of one hour for exosome purification. Lane et al. demonstrated this kit's ability to isolate other

cellular material along with exosomes (Lane *et al.*, 2015). As such, the Exo-spin™ Exosome Purification Kit might also be effective for purifying my cell-derived liposomes. I compared the efficiency of liposome purification using both the Exo-spin™ Exosome Purification Kit as well as merely centrifugating at 3,270 x *g.* The resultant samples were then analysed using flow cytometry. The data showed that more membrane material could indeed be collected if the Exo-spin™ Exosome Purification Kit was used.

Therefore, during immunostaining of the liposomes, the Exo-spin™ Exosome Purification Kit was used to remove unbound antibodies. At that time, the liposomes were only probed for the presence of CD4, as I was not yet sure if the Exo-spin™ Exosome Purification Kit had any influence on antibody binding. But indeed, flow cytometry data revealed that non-specific binding of anti-CD4 antibody was a problem. For unknown reasons, TF228.1.16 liposomes bound more anti-CD4 antibody than A3R5.7 liposomes did. It could be that in the process of liposome preparation membrane components that were usually not available for antibody binding were now exposed. These components might be capable of non-specific anti-CD4 antibody binding.

To test this hypothesis, the liposome surface was blocked with 5% FBS prior to immunostaining, just like it was done for the cells. In the case of the cells, the cell surface was blocked by FBS because they were resuspended in FACS solution (DPBS + 5% FBS) before immunostaining.

As a matter of fact, this additional step reduced the amount of anti-CD4 antibody binding by both A3R5.7 as well as TF228.1.16 liposomes. The amount of antibody bound was not significantly different between sample and reference. Furthermore, purification Buffer A seemed to interfere with antibody binding, because if immunostaining was performed in its presence, no antibody binding was observed. This also suggests that antibodies that have been in contact with Buffer A cannot be re-used and need to be disposed of.

To avoid the use of the Exo-spin™ Exosome Purification Kit, I also tried to increase liposome density by bead encapsulation. This was done by adding silicon dioxide beads to the cell homogenate before extrusion was performed. During extrusion, the membrane material would reorganize around the beads, producing membrane-coated beads. The beads used needed to be smaller than the pore size of the extrusion membrane, otherwise the membrane would be damaged during extrusion. This would increase liposome density and centrifugation at low speeds could then be used for pelleting. TEM analysis showed that bead encapsulation did not work, although the beads did not affect the extrusion process. As before, mainly membrane aggregates were found in the samples instead of liposomes.

The homogenization and extrusion protocols were well-suited to producing membrane fragments, but not to producing liposomes in useful quantities. Moreover, morphological characterization was difficult as sample preparation was time-consuming and special training

was needed to handle the TEM. Another difficulty emerged during immunostaining. Due to the lack of liposomes, mainly aggregates were produced that could not be labelled meaningfully. My concern was, that due to the dearth of liposomes in my samples, mainly aggregates were being analyzed during the immunostaining assays. This would make the data misleading and not relevant to my needs. As such, I decided to abandon the production of liposomes via homogenization and extrusion.

4.3 Ghost cell production

I decided to produce ghost cells from A3R5.7 cells as T-cell mimics instead, using osmotic cell lysis. Osmotic cell lysis occurs when cells are placed into a hypotonic solution like water. Water enters the cell by diffusion until the cell membrane can no longer withstand the rising internal pressure and bursts. The cellular content is released into the environment, leaving ghosts behind (Alberts *et al.*, 2004, p. 725-726). The first experiment I performed had a very simple setup. Cells were harvested and washed once with DPBS. One microliter of pelleted cells resuspended in leftover DPBS was added to a 20 µL droplet of ultrapure water that was placed onto a slide. This allowed me to directly observe the bursting event using a phase contrast microscope. However, it was difficult to differentiate between live and ghost cells in bright field imaging. Therefore, I repeated the experiment with the cell cytoplasm stained with Calcein-AM prior to imaging. Intact cells would fluoresce brightly while ghost cells, having lost their cytoplasmic content and calcein staining during the lysis, would not. With this experiment it was demonstrated that cytolysis could be performed successfully when ultrapure water was used as lysis buffer and that the stained cell content was at least partly released. In addition, cellular membranes were stained with Nile Red and a decrease in Nile Red fluorescence was noticed after lysis that could be due to a loss of internal membranes.

Furthermore, I tested ghost cell resealing by adding unmodified calcein to the lysis buffer in a 1:100 dilution. Unlike Calcein-AM, calcein cannot penetrate intact membranes. As such, if the ghost cell membranes reseal after lysis, calcein should be trapped within the ghost cells. Calcein encapsulation was, indeed, observed, but not reproducibly, at this time.

The development of the lysis protocol was challenging as such a protocol could not be found for leukocytes in the scientific literature. Although many protocols are available for the lysis and production of erythrocyte ghost cells, leukocytes have not been of as much interest in terms of ghost cell studies. From my first experiments it seemed that ultrapure water was a very effective and simple lysis medium. As such, it was decided to supplement it with protease inhibitors and to work at 4°C to minimise the loss of membrane proteins due to endogenous protease activity during lysis. After the lysis buffer was optimized, different lysis conditions were tested to improve the lysis efficiency. Lysis without agitation tended to generate precipitates. I first tried to reduce precipitate formation by shaking the samples

during lysis. However, sample volumes were limited by the shaker used and the small volumes could not be shaken effectively. This led to samples with many cells that were not lysed at all. Stirring with a magnetic stirrer allowed the use of bigger sample volumes, although aggregation still occurred, reducing the number of ghost cells produced.

From my flow cytometry assays, I noticed that ghost cells were stabilized when they were resuspended in FACS solution (DPBS + 5% FBS) directly after lysis. This suggested that prolonged exposure to MilliQ-PI had led to ghost cell collapse and aggregation. Supplementation of the MilliQ-PI lysis buffer, directly after lysis, with FBS to a final concentration of 5% FBS actually seemed to reduce aggregate formation. This effect could be reversed by resuspending the ghost cells in DPBS, resulting in ghost cell aggregation and precipitation. FBS addition also helped the ghost cells to recover their morphological structure. Therefore a lysis with stirring was preferred, followed directly by the addition of FBS for ghost cell stabilisation.

A3R5.7 ghost cells were able to bind antibodies raised against CD4, CCR5 and CXCR4, as determined by immunostaining and flow cytometry. But the results showed that a lower percentage of ghost cells bound the antibodies than did intact cells. Possibly, the presence of debris in the ghost cell samples could have diluted the signal density. It also needs to be considered, that the flow cytometer cannot distinguish between live cells and ghost cells. Therefore live cells also could contribute to the signal detected by the flow cytometer, in case the lysis was not successful. After analysis, the ghost cell samples could be stored at 4°C, in the dark, for up to four days without losing their morphological stability.

4.4 Future work

It is still a long way to go until the osmotic cell lysis protocol will be reliable and efficient. Microscopy showed that cell lysis was often only partly effective and that the cells somehow seemed to withstand the lysis buffer. However, complete lysis is of great importance as live cells cannot be used as T-cell mimics. This is especially so, for the purpose of using ghost cells as anti-HIV therapeutics one day. This highlights the need for a protocol that is able to evaluate the lysis efficiency.

Beside successful lysis, soluble proteins and genetic material should be completely removed or destroyed to ensure that the ghost cells are not able to replicate. Nevertheless, the membrane proteins that are necessary for future A3R5.7 ghost cell and TF228.1.16 live cell fusion need to be preserved. Also, appropriate antibodies that demonstrate the presence of gp120/41 surface proteins via immunostaining and flow cytometry need to be found.

After lysis, a change in membrane orientation might lead to a decrease in accessible membrane proteins as inside-out ghosts might occur. This needs to be addressed. Another

question deals with the resealing properties of the ghost cells. A method that successfully reseals ghost cells needs to be developed, because leaking ghosts cannot be used to encapsulate drugs, such as proteases or nucleases, or other substances. Once this is achieved, fusion of CD4+/CCR5+/CXCR4+ ghost cells with gp120/41+ ghosts or live cells will be studied.

In future, T-cell mimics could be loaded with protein- and DNA- degrading enzymes, and then directed against HIV or HIV-infected cells. Fusion would lead to the merging of the cellular cytoplasm and the T-cell mimic contents, leading to a degradation of viral or cellular proteins and DNA. This would inhibit HIV replication and might restore immune functions in patients. Of course, possible side-effects need to be identified and vigorously investigated. If this endeavour is successful, treatment with T-cell mimics might slow down or prevent the progression of HIV-infection to AIDS.

5 Conclusion

This project's objective was the development of a reliable protocol to fabricate CD4+/CCR5+/CXCR4+ T-cell mimics. I worked with A3R5.7 and TF228.1.16 cells, robust cell lines which grew in suspension cultures. Using these cells, I successfully developed a protocol for osmotic cell lysis as an alternative T-cell mimic production method. I demonstrated that MilliQ-PI was a suitable lysis buffer for producing ghost cells of size about 10 - 15 µm. These ghost cells were large enough to be easy to handle and to enable the use of phase contrast microscopy for observation. Aggregate formation during stirred lysis could be reduced by the addition of FBS directly after lysis. Furthermore, the necessary surface proteins were preserved in the A3R5.7 ghost cells and detectable by flow cytometry.

6 References

Alberts, B. *et al.* (2004): *Molekularbiologie der Zelle*. 4th edn. Weinheim: Wiley-VCH Verlag.

Alberts, B. *et al.* (2015): *Molecular biology of the cell*. 6th edn. New York: Garland Science.

Alkhatib, G. (2009): 'The biology of CCR5 and CXCR4', *Current opinion in HIV and AIDS*, 4(2), pp. 96–103. doi: 10.1097/COH.0b013e328324bbec.

Baba, M. *et al.* (2000): 'Establishment of a CCR5-expressing T-lymphoblastoid cell line highly susceptible to R5 HIV type 1', *AIDS Res Hum Retroviruses*, 16(10), pp. 935–941. doi: 10.1089/08892220050058344.

Baquero, A. D. (2015): *Fabrication and molecular characterization of CD4+, CCR5+ and CXCR4+ cell-derived proteoliposomes*. Fachhochschule Technikum Wien.

Bronshtein, T. *et al.* (2011): 'Cell derived liposomes expressing CCR5 as a new targeted drug-delivery system for HIV infected cells', *J Control Release*. 2011/02/26, 151(2), pp. 139–148. doi: 10.1016/j.jconrel.2011.02.023.

Cann, A. J. (2012): *Principles of molecular virology*. 5th edn. Amsterdam: Elsevier Acad. Press.

Coleman, C. M., St Gelais, C. and Wu, L. (2013): 'Cellular and Viral Mechanisms of HIV-1 Transmission Mediated by Dendritic Cells', *Advances in experimental medicine and biology*, 762, pp. 109–130. doi: 10.1007/978-1-4614-4433-6_4.

Danial, M. and Klok, H. A. (2015): 'Polymeric anti-HIV therapeutics', *Macromolecular Bioscience*, 15(1), pp. 9–35. doi: 10.1002/mabi.201400298.

Dimmock, N. J., Easton, A. J. and Leppard, K. N. (2016): *Introduction to modern virology*. 7th edn. Chichester: Wiley Blackwell.

Dua, J. S., Rana, A. C. and Bhandari, A. K. (2012): 'Liposome: Methods of preparation and applications', *International Journal of Pharmaceutical Studies and Research*, 3(2), pp. 14–20.

Grasso, L. *et al.* (2013): 'Downscaling the Analysis of Complex Transmembrane Signaling Cascades to Closed Attoliter Volumes', *PLoS ONE*, 8(8), p. e70929. doi: 10.1371/journal.pone.0070929.

Jonak, Z. L. *et al.* (1993): 'A human lymphoid recombinant cell line with functional human immunodeficiency virus type 1 envelope.', *AIDS research and human retroviruses*, 9(1), pp. 23–32. Available at: http://www.ncbi.nlm.nih.gov/pubmed/8094000.

Kalender, M. (2016): *Protein synthesis and detection in a wheat germ derived in vitro protein synthesis system*. Universität für Bodenkultur Wien.

Lane, R. E. *et al.* (2015): 'Analysis of exosome purification methods using a model liposome system and tunable-resistive pulse sensing', *Scientific Reports*, 5, p. 7639. doi: 10.1038/srep07639.

Luckheeram, R. V *et al.* (2012): '$CD4^+$ T cells: differentiation and functions', *Clin Dev Immunol*. 2012/03/14, 2012, p. 925135. doi: 10.1155/2012/925135.

Maartens, G., Celum, C. and Lewin, S. R. (2014): 'HIV infection: epidemiology, pathogenesis, treatment, and prevention', *The Lancet*, 384(9939), pp. 258–271. doi: http://dx.doi.org/10.1016/S0140-6736(14)60164-1.

McDonald, D. (2010): 'Dendritic Cells and HIV-1 Trans-Infection', *Viruses*, 2(8), pp. 1704–1717. doi: 10.3390/v2081704.

McLinden, R. J. *et al.* (2013): 'Detection of HIV-1 neutralizing antibodies in a human $CD4^+$/$CXCR4^+$/$CCR5^+$ T-lymphoblastoid cell assay system', *PLoS One*. 2013/11/28, 8(11), p. e77756. doi: 10.1371/journal.pone.0077756.

Murdoch, C. (2000): 'CXCR4: chemokine receptor extraordinaire', *Immunol Rev*. 2001/01/04. Division of Child Health, University of Sheffield, Sheffield Children's Hospital, UK. 177, pp. 175–184.

Rottman, J. B. *et al.* (1997): 'Cellular localization of the chemokine receptor CCR5. Correlation to cellular targets of HIV-1 infection', *Am J Pathol*. 1997/11/14. LeukoSite Inc., Cambridge, MA 02142, USA., 151(5), pp. 1341–1351.

U.S. Department of Health and Human Services (13.09.2016): 'AIDSinfo - Understanding HIV/AIDS'. online. Accessed 27.03.2017. Available at: https://aidsinfo.nih.gov/.

ThermoFisher Sientific (no date): 'Fluorescence Tutorials'. Accessed 18.08.2017. Available at: http://www.thermofisher.com/us/en/home/support/tutorials.html.

Sierra, S., Kupfer, B. and Kaiser, R. (2005): 'Basics of the virology of HIV-1 and its replication', *J Clin Virol*. 2005/09/29, 34(4), pp. 233–244. doi: 10.1016/j.jcv.2005.09.004.

Sigma-Aldrich (no date a): ‘17783 SIGMA, Calcein-AM’. Accessed 22.08.2017. Available at: http://www.sigmaaldrich.com/catalog/product/sigma/17783?lang=de&region=AT.

Sigma-Aldrich (no date b): ‘N3013 SIGMA, Nile Red’. Accessed 22.08.2017. Available at: http://www.sigmaaldrich.com/catalog/product/sigma/n3013?lang=de&region=AT.

Sundquist, W. I. and Kräusslich, H.-G. (2012): ‘HIV-1 Assembly, Budding, and Maturation’, *Cold Spring Harbor Perspectives in Medicine*, 2(7), p. a006924. doi: 10.1101/cshperspect.a006924.

Terho, P. (2013): ‘Flowing Software 2.5.1’, *http://flowingsoftware.btk.fi*. Accessed 01.09.2017. Available at: http://flowingsoftware.btk.fi.

Zeringer, E. *et al.* (2015): ‘Strategies for isolation of exosomes’, *Cold Spring Harb Protoc*. 2015/04/04. Thermo Fisher Scientific, Austin, Texas 78744., 2015(4), pp. 319–323. doi: 10.1101/pdb.top074476.

7 Figures

8 Supporting information

8.1 Flow cytometry data for A3R5.7, MOLT4/CCR5 and TF228.1.16 characterization (Fig. 15)

FITC and APC signals of the unlabelled sample were used to define the background signal. Cells were labelled with anti-CD4-FITC, anti-CCR5-FITC and anti-CXCR4-APC antibodies before being analyzed. TF228.1.16 cells and RbIgG-FITC antibodies were used as negative controls for A3R5.7 immunostaining.

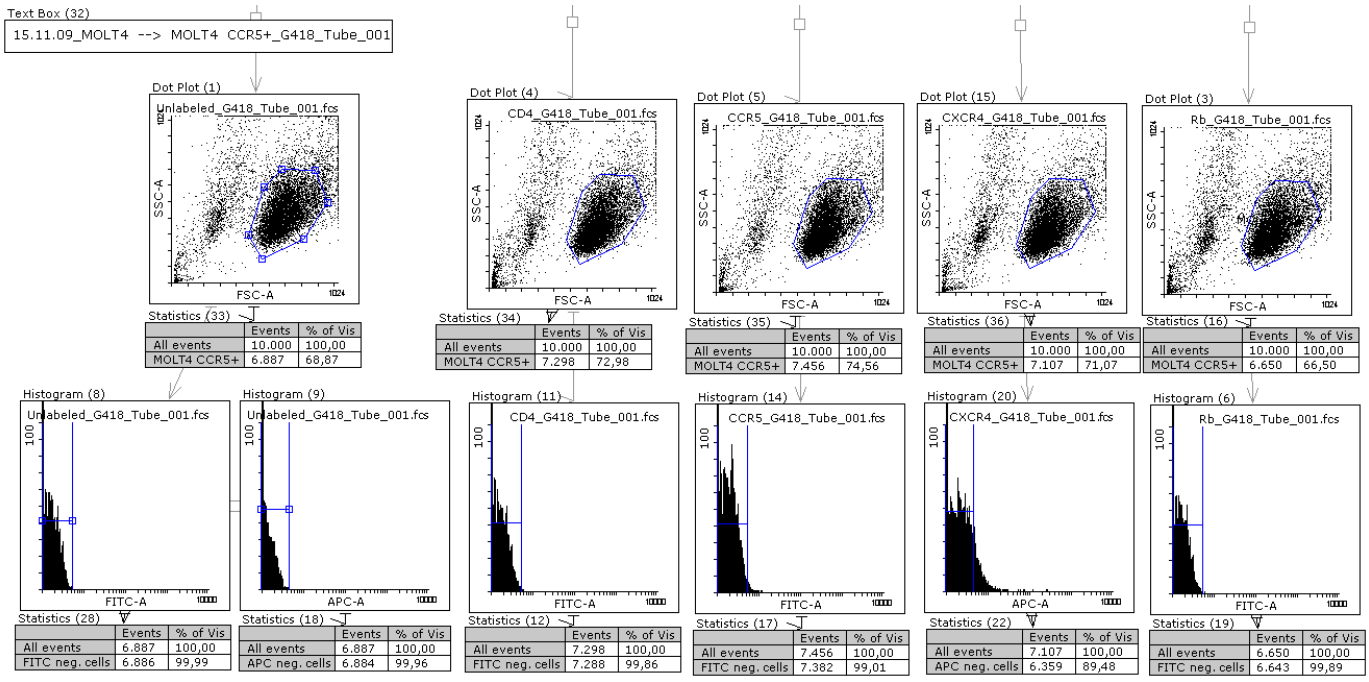

Figure 1: MOLT4/CCR5 cells, cultured in the presence of geneticin for CCR5 induction.

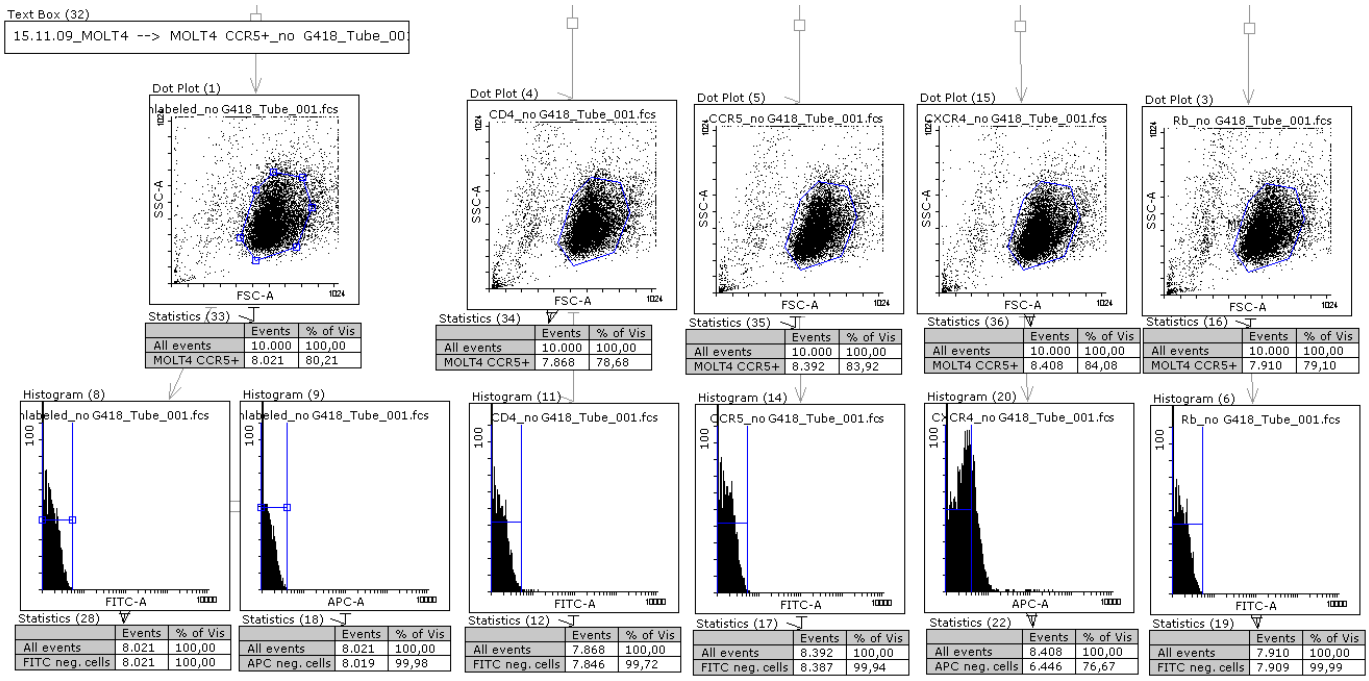

Figure 2: MOLT4/CCR5 cells, cultured without geneticin.

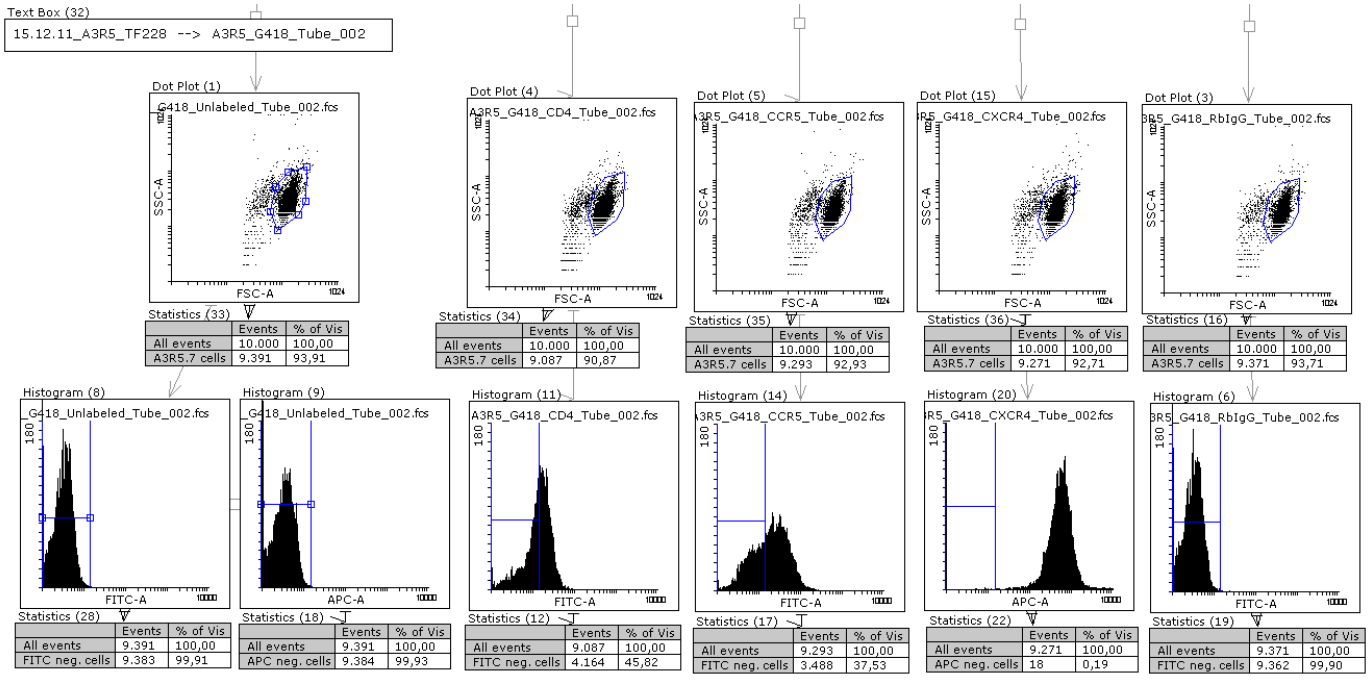

Figure 3: A3R5.7 cells, cultured in the presence of geneticin for CCR5 induction.

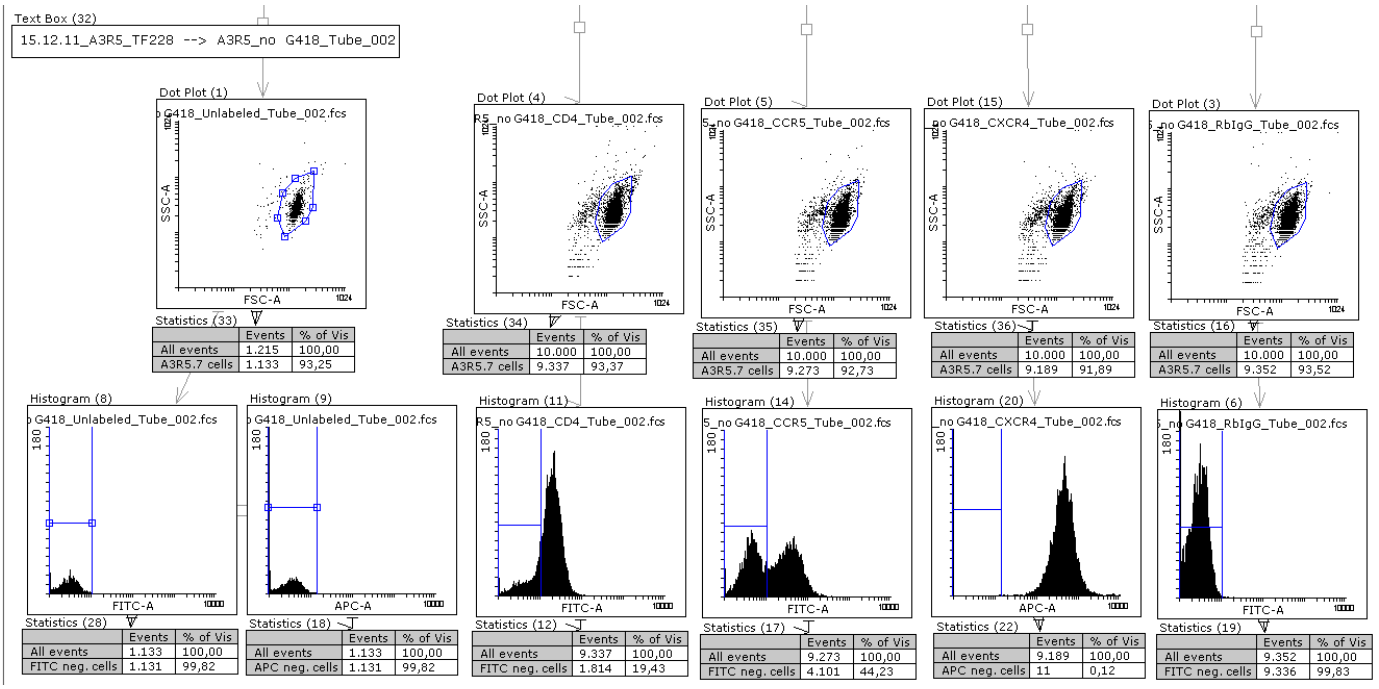

Figure 4: A3R5.7 cells, cultured without geneticin.

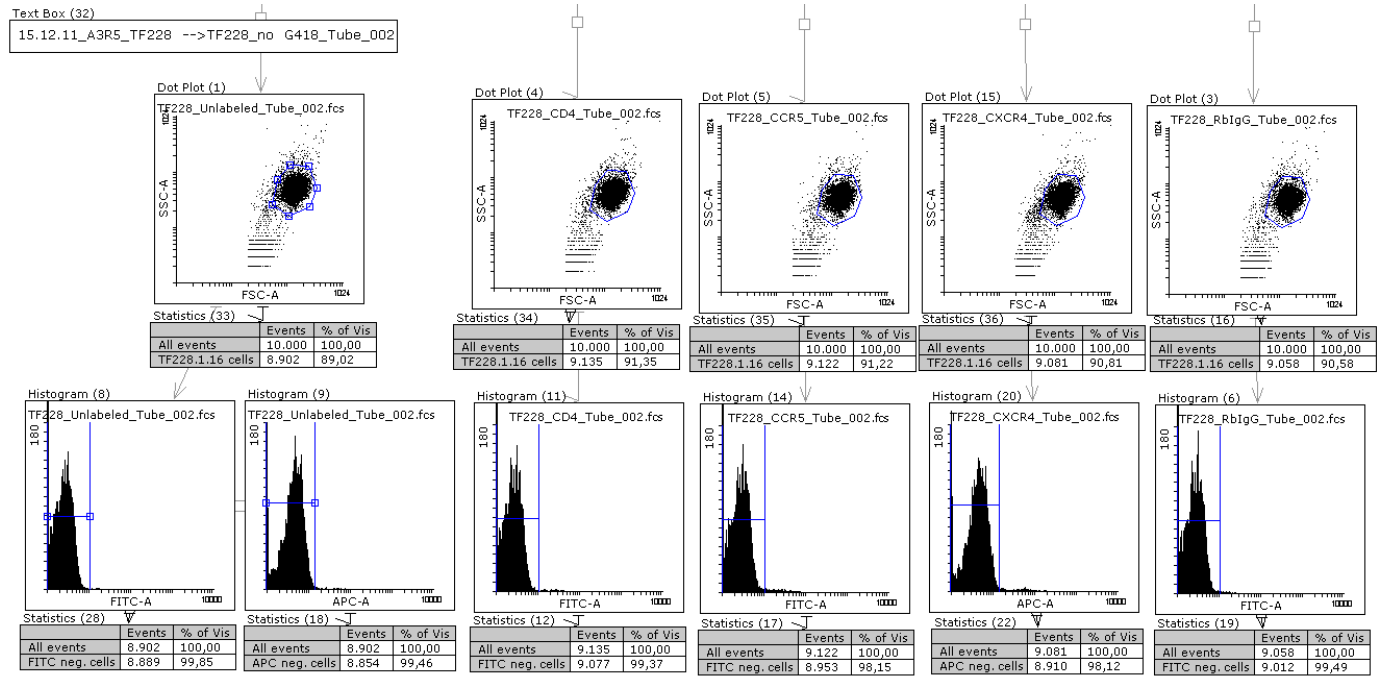

Figure 5: TF228.1.16 cells.

8.2 Flow cytometry data for TF228.1.16 and CHO cell characterization (Fig. 16)

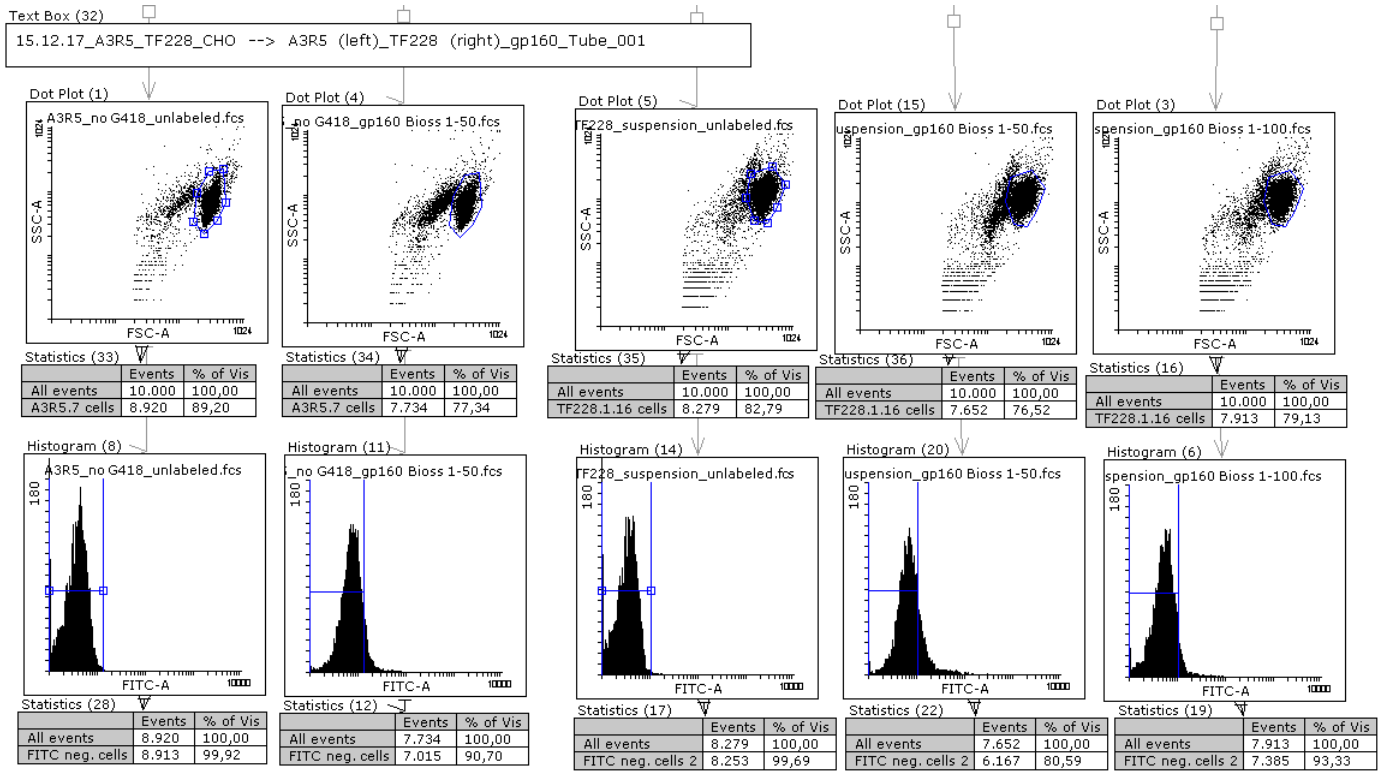

Figure 6: A3R5.7 cells were used as negative control when TF228.1.16 was probed for gp160.

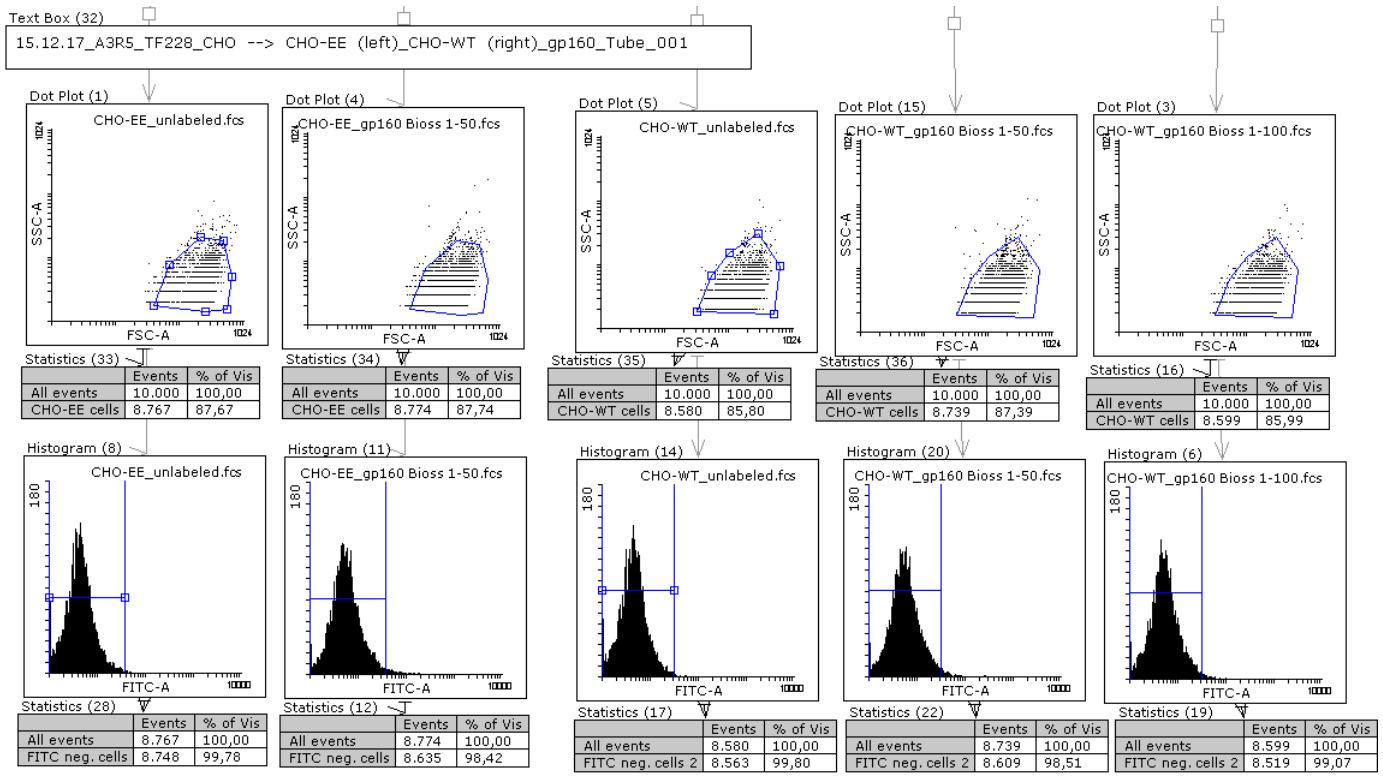

Figure 7: CHO-EE was used as negative control when CHO-WT was probed for gp160.

8.3 Flow cytometry data for standard deviation determination (Fig. 17)

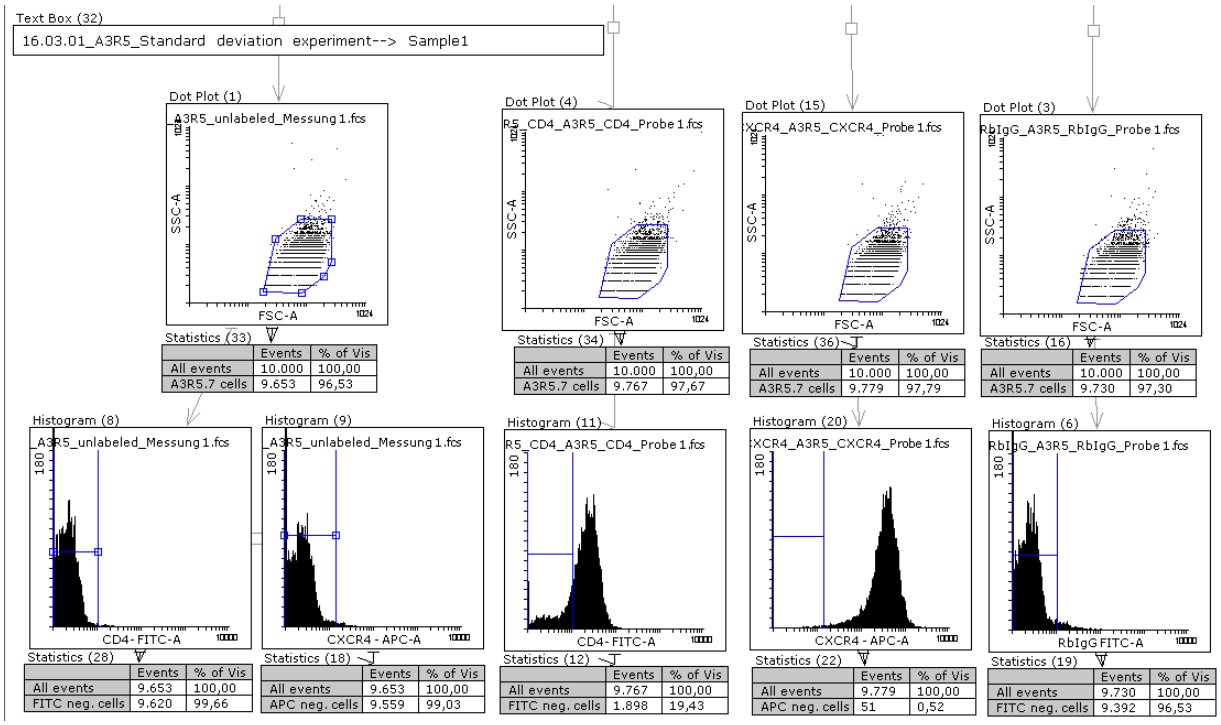

Figure 8: A3R5.7 cells were labelled with anti-CD4-FITC and anti-CXCR4-APC antibodies. This is sample 1.

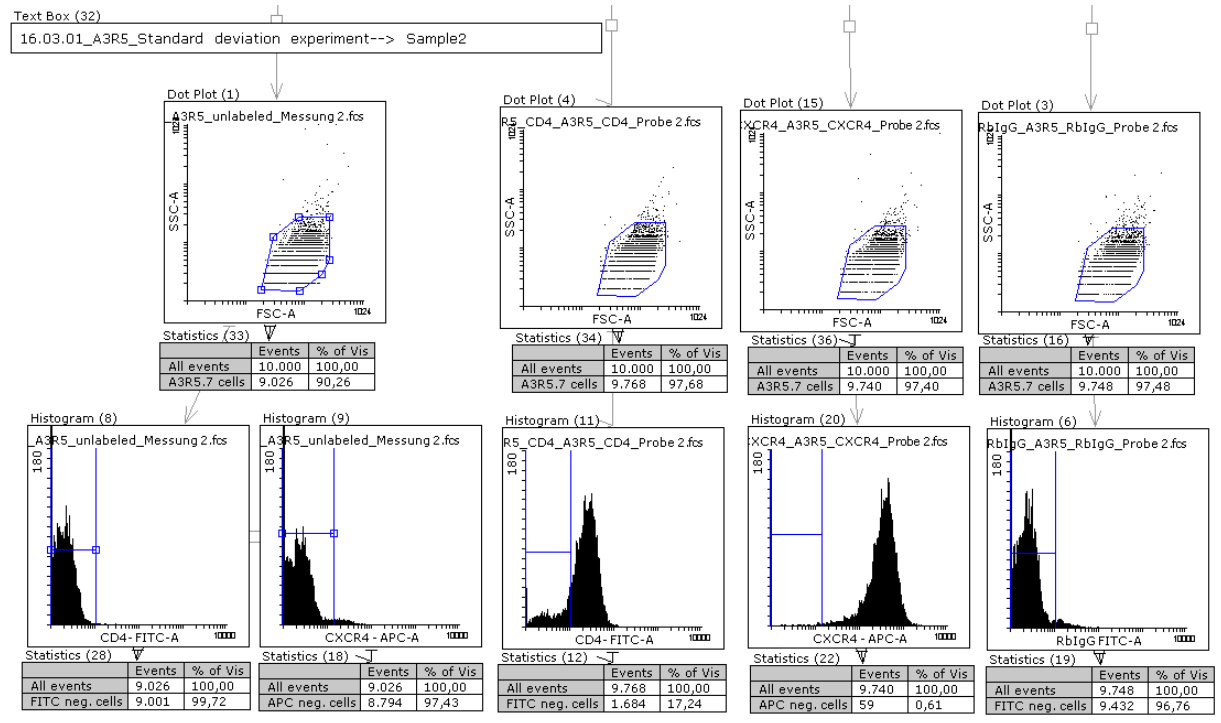

Figure 9: A3R5.7 cells were labelled with anti-CD4-FITC and anti-CXCR4-APC antibodies. This is sample 2.

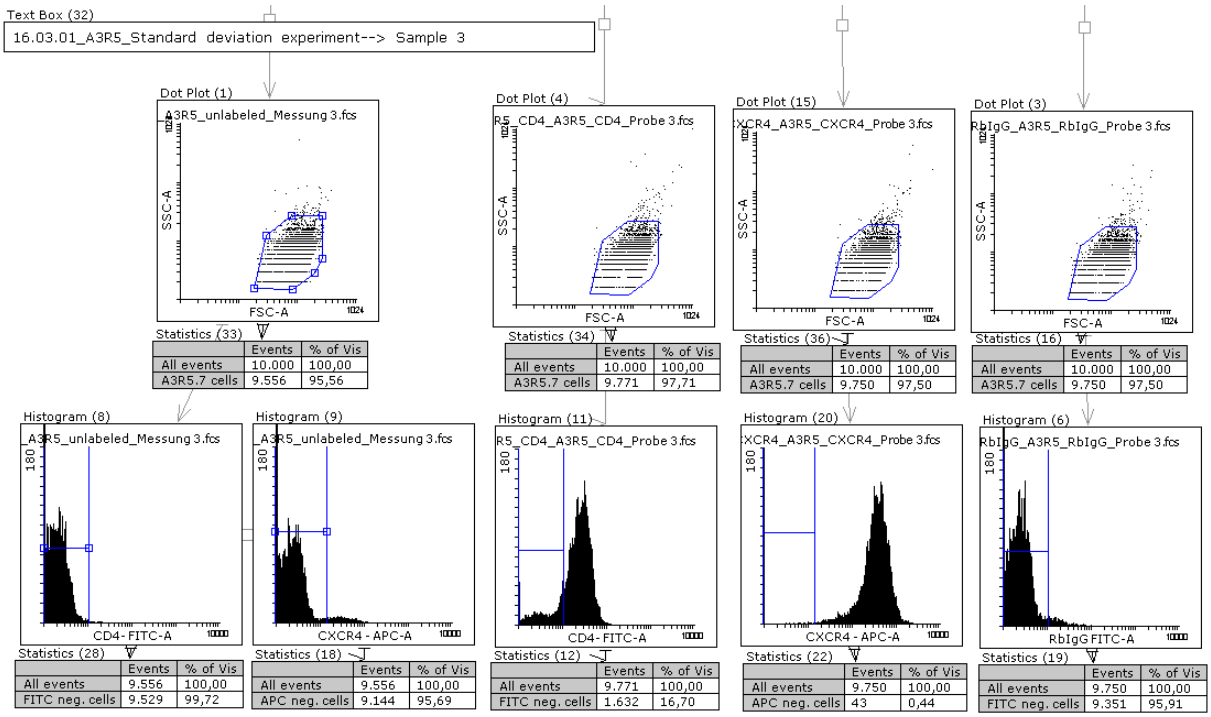

Figure 10: A3R5.7 cells were labelled with anti-CD4-FITC and anti-CXCR4-APC antibodies. This is sample 3.

8.4 Flow cytometry data for A3R5.7 and TF228.1.16 liposome characterization (Fig. 26)

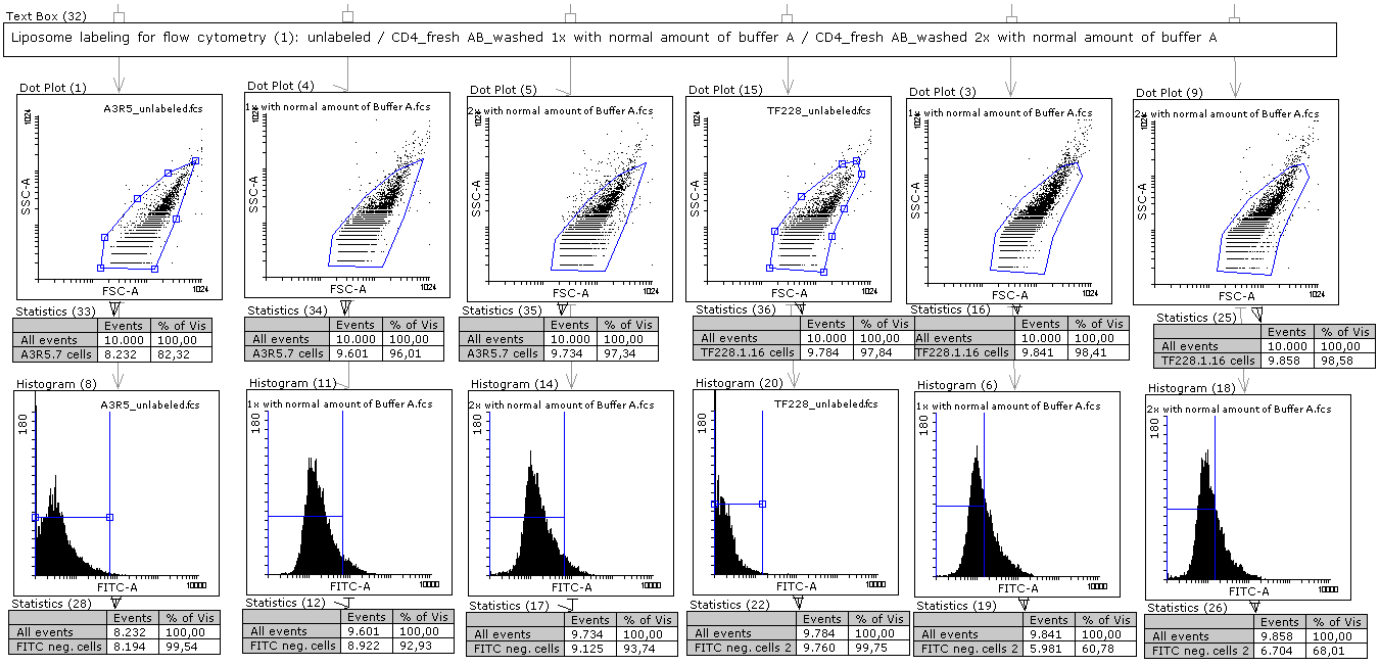

Figure 11: A3R5.7 and TF228.1.16 liposomes were labelled with anti-CD4-FITC antibodies. Samples were washed up to two times to remove unbound antibodies.

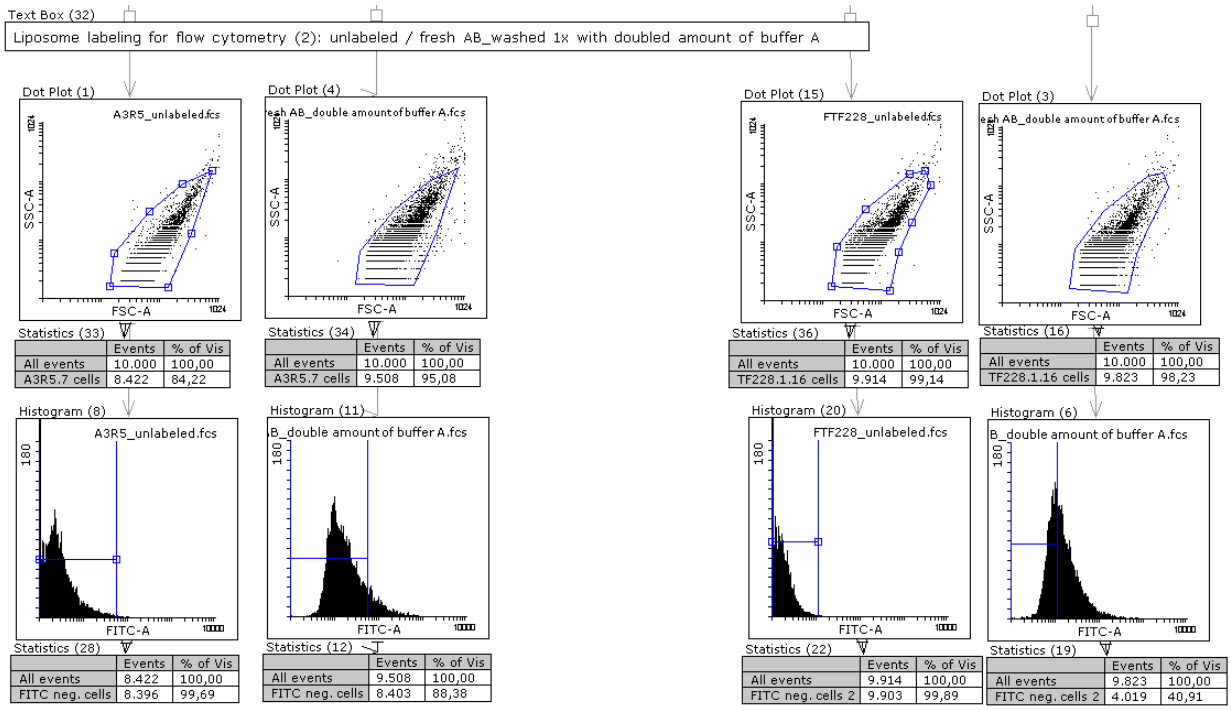

Figure 12: A3R5.7 and TF228.1.16 liposomes purified using the Exo-spin™ Exosome Purification Kit were labelled with anti-CD4-FITC antibodies. Samples were washed once to remove unbound antibodies. The volume of Exo-spin™ Exosome Purification Kit Buffer A that was used was equal to the sample volume.

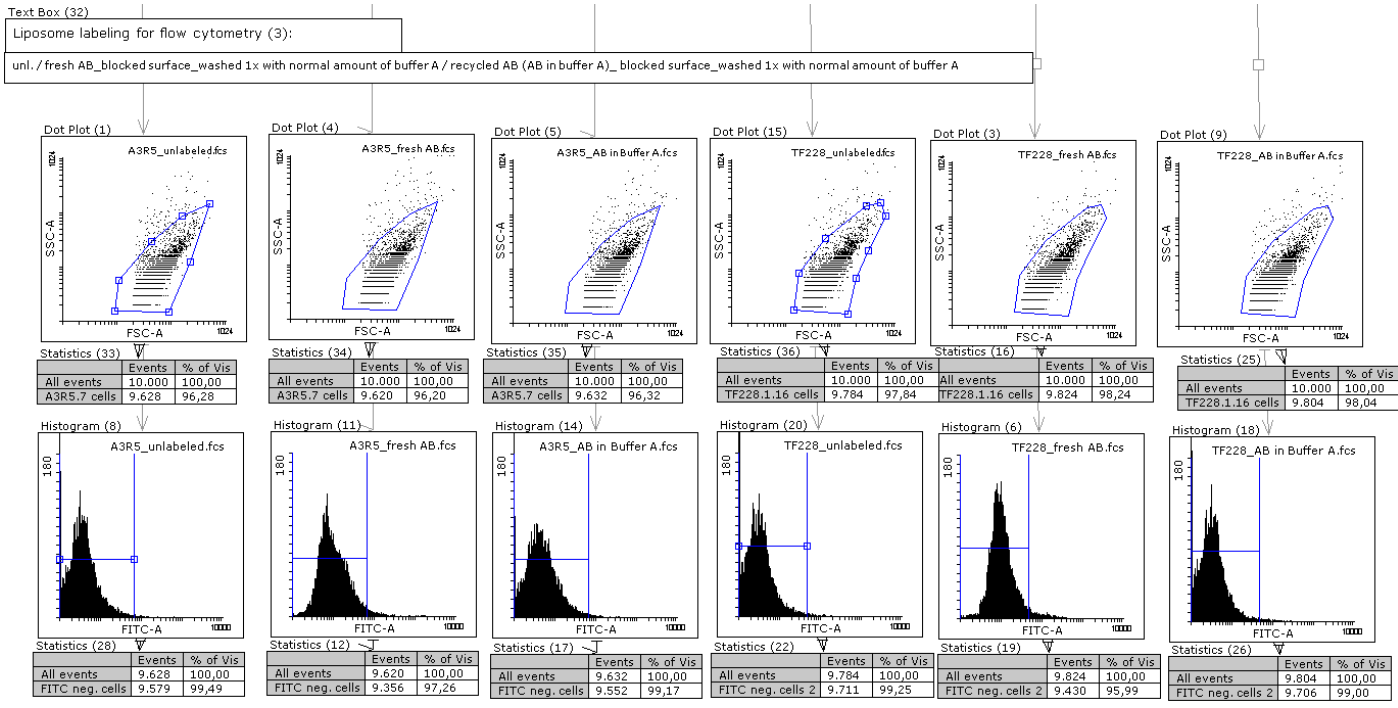

Figure 13: A3R5.7 and TF228.1.16 liposome surfaces were blocked before they were immunostained with anti-CD4-FITC antibodies.

8.5 Flow cytometry data for A3R5.7 and TF228.1.16 live and ghost cell characterization (Fig. 32)

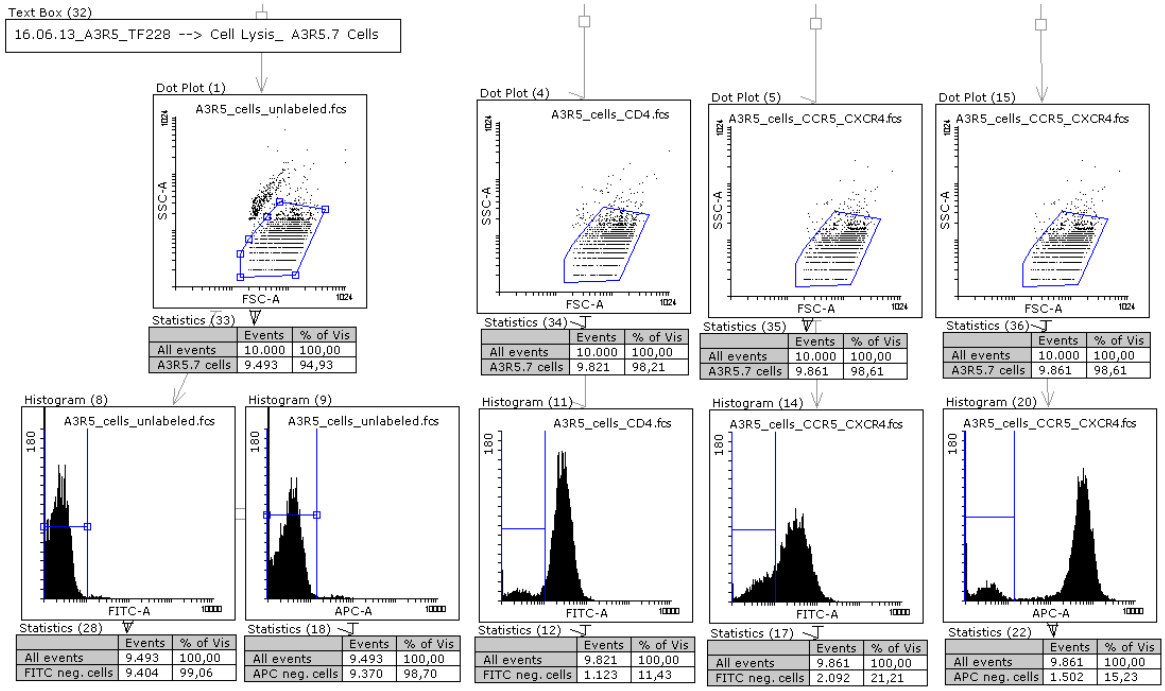

Figure 14: A3R5.7 cells, labelled with anti-CD4-FITC, anti-CCR5-FITC and anti-CXCR4-APC antibodies.

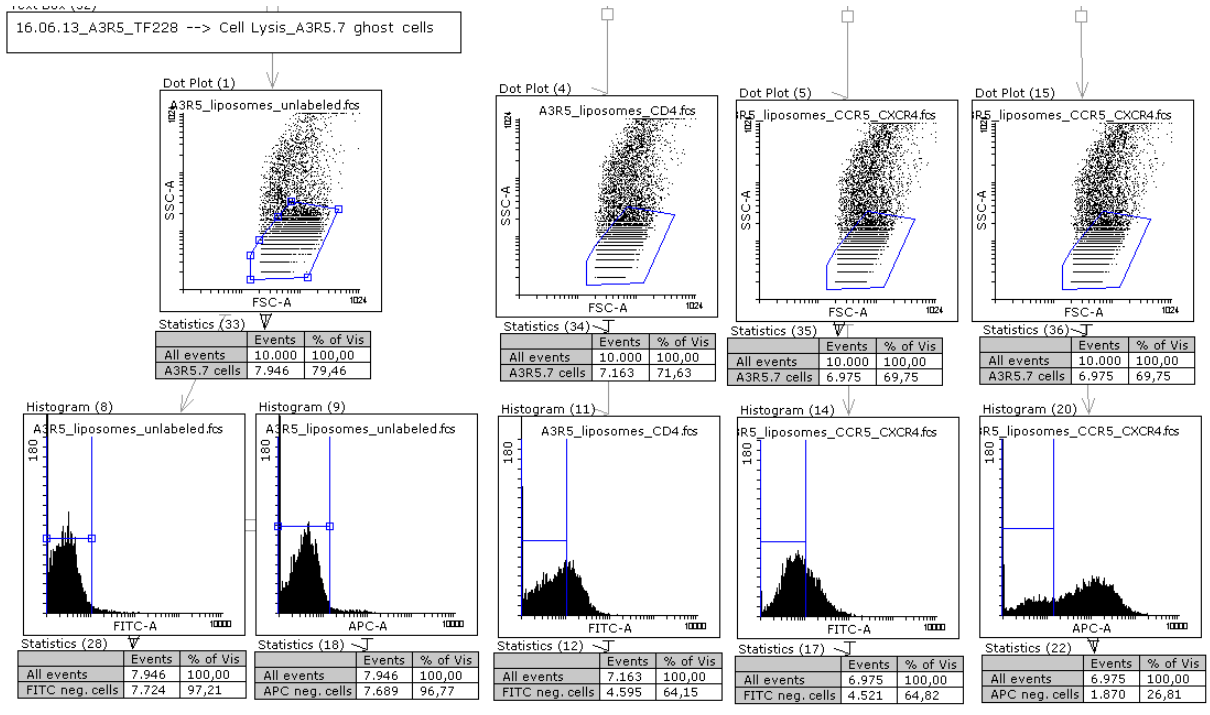

Figure 15: A3R5.7 ghost cells, labelled with anti-CD4-FITC, anti-CCR5-FITC and anti-CXCR4-APC antibodies.

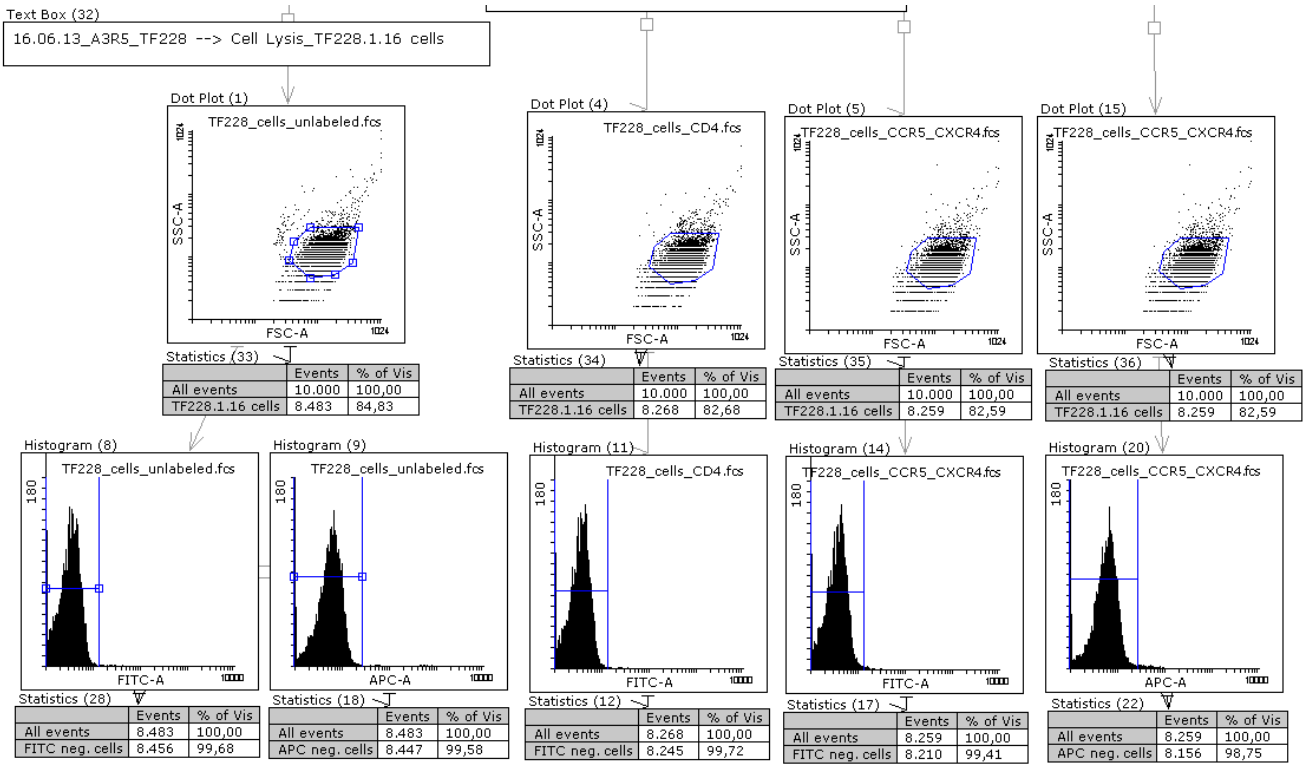

Figure 16: TF228.1.16 cells, labelled with anti-CD4-FITC, anti-CCR5-FITC and anti-CXCR4-APC antibodies.

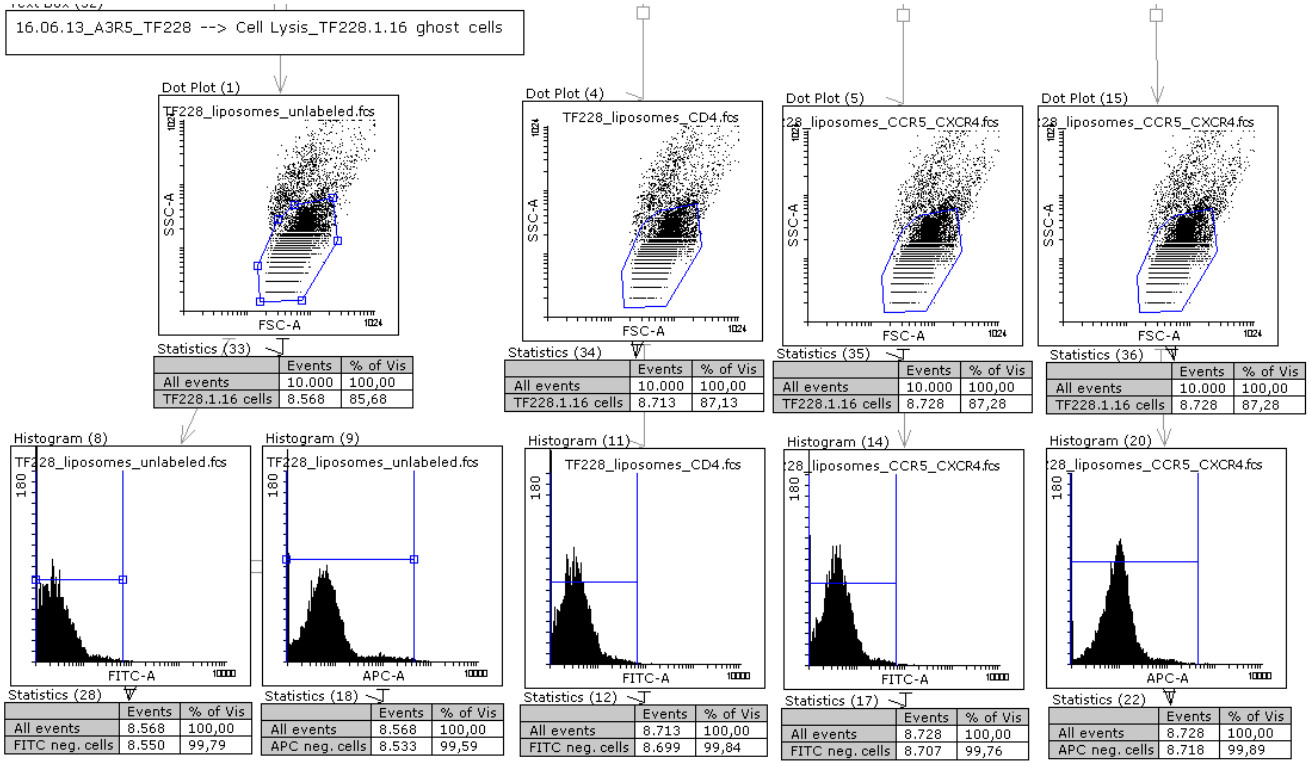

Figure 17:TF228.1.16 ghost cells, labelled with anti-CD4-FITC, anti-CCR5-FITC and anti-CXCR4-APC antibodies.

9 Abbreviations

AIDS	acquired immune deficiency syndrome
APC	allophycocyanin
AZT	azidothymidine
CA	capsid protein
CCR5	CC chemokine receptor type 5
CCR5-FITC antibody	FITC Mouse Anti Human CD195 Antibody
CD4	cluster of differentiation 4
CD4-FITC antibody	FITC Mouse Anti-Human CD4 Antibody
CXCR4	CXC chemokine receptor type 4
CXCR4-APC antibody	APC Mouse Anti Human CD184 Antibody
DMEM	Dulbecco’s Modified Eagle’s Medium
DNA	deoxyribonucleic acid
DPBS	Dulbecco's Phosphate-Buffered Saline
EDTA	ethylene diamine tetraacetic acid
FACS	Fluorescence-activated Cell Sorting
FBS	fetal bovine serum
FITC	fluorescein isothiocyanate
FSC	forward-scatter
G418	geneticin
gag	group-specific antigen
GDP	guanosine diphosphate
gp120/41	glycoprotein with a molecular weight of 120 kDa / 41 kDa
gp160 antibody	anti-HIV gp160 Antibody
GTP	guanosine triphosphate
HAART	ighly active anti-retroviral therapy
HIV	human immune deficiency virus
IN	integrase
kDa	kilo Dalton
MA	matrix protein
MHC	major histocompatibility complex
mRNA	messenger RNA

NC	nucleocapsid protein
NIH	National Institutes of Health
PBS	phosphate-buffered saline
PerCP	peridinin-chlorophyll-protein complex
PI	proteinase Inhibitor
PR	protease
RbIgG-FITC antibody	Anti-Rabbit IgG (whole molecule)–FITC antibody produced in goat
RNA	ribonucleic acid
rpm	revolutions per minute
RPMI	Roswell Park Memorial Institute
RT	reverse transcriptase
SiO_2	silicon dioxide
SSC	side-scatter
STD	standard deviation
TEM	transmission electron microscope